

# DOCTORAL THESIS

## Fibre Bragg gratings in polymer optical fibre for applications in sensing

Chi Zhang

If you have discovered material in AURA which is unlawful e.g. breaches copyright, (either yours or that of a third party) or any other law, including but not limited to those relating to patent, trademark, confidentiality, data protection, obscenity, defamation, libel, then please read our takedown policy at <http://www1.aston.ac.uk/research/aura/aura-take-down-policy/> and contact the service immediately [eprints@aston.ac.uk](mailto:eprints@aston.ac.uk).

**FIBRE BRAGG GRATINGS IN POLYMER OPTICAL FIBRE FOR  
APPLICATIONS IN SENSING**

**Chi Zhang**

Doctor of Philosophy

**Aston University**

January 2011

©Chi Zhang, 2011

This copy of the thesis has been supplied on condition that anyone who consults it is understood to recognise that its copyright rests with its author and that no quotation from the thesis and no information derived from it may be published without proper acknowledgement.

**ASTON UNIVERSITY**

**FIBRE BRAGG GRATINGS IN POLYMER OPTICAL FIBRE FOR  
APPLICATIONS IN SENSING**

**Chi Zhang**

Doctor of Philosophy

January 2011

This thesis presents the potential sensing applications of fibre Bragg gratings in polymer optical fibres. Fibre Bragg gratings are fabricated in different kinds of polymer optical fibres, including Poly methyl methacrylate (PMMA) and TOPAS cyclic olefin copolymer based microstructured polymer optical fibres and PMMA based step-index photosensitive polymer optical fibre, using the 325nm continuous wave ultraviolet laser and phase mask technique. The thermal response of fabricated microstructured polymer optical fibre Bragg gratings has been characterized. The PMMA based single mode microstructured polymer optical fibre Bragg gratings exhibit negative non-linear Bragg wavelength shift with temperature, including a quasi-linear region. The thermal sensitivity of such Bragg gratings in the linear region is up to  $-97\text{pm}/^\circ\text{C}$ . A permanent shift in the grating wavelength at room temperature is observed when such gratings are heated above a threshold temperature which can be extended by annealing the fibre before grating inscription. The largest positive Bragg wavelength shift with temperature in transmission is observed in TOPAS based few moded microstructured polymer optical fibre Bragg gratings and the measured

temperature sensitivity is  $250 \pm 0.5 \text{ pm}/^\circ\text{C}$ . Gluing method is developed to maintain stable optical coupling between PMMA based single mode step index polymer optical fibre Bragg gratings and single mode step index silica optical fibre. Being benefit from this success, polymer optical fibre Bragg gratings are able to be characterised for their temperature, humidity and strain sensitivity, which are  $-48.2 \pm 1 \text{ pm}/^\circ\text{C}$ ,  $38.3 \pm 0.5 \text{ pm per \%RH}$  and  $1.33 \pm 0.04 \text{ pm}/\mu\epsilon$  respectively. These sensitivities have been utilised to achieve several applications. The strain sensitivity of step index polymer optical fibre Bragg grating devices has been exploited in the potential application of the strain condition monitoring of heavy textiles and when being attached to textile specimens with certain type of adhesives. These polymer fibre Bragg grating devices show better strain transfer and lower structure reinforcement than silica optical fibre Bragg grating devices. The humidity sensitivity of step index polymer optical fibre Bragg grating devices is applied to detecting water in jet fuel and is proved to be able to measure water content of less than 20 ppm in Jet fuel. A simultaneous temperature and humidity sensor is also made by attaching a polymer fibre Bragg grating to a silica optical fibre Bragg grating and it shows better humidity measurement accuracy than that of electronic competitors.

Keywords: Polymer, Fibre Bragg Grating

## ACKNOWLEDGMENTS

I would like to thank the Photonics Research Group, Aston University, UK, the Engineering and Physical Sciences Research Council (EPSRC) and the European Commission (EU FP7 Project: “Phosfos”) for funding this PhD. I particularly wish to thank my supervisor, Dr. David Webb for his guidance, advice and endless enthusiasm for my research. My warmest thanks go to Dr. Kyriacos Kalli for sharing his experience when collaborating with me and for his support and advice over the last 5 years. Thanks must go to Dr. Karen Carroll, Dr. Xianfeng Chen, Dr. Chengchun Ye and Dr. Wei Zhang for their help to my research in different projects. Thanks also go to Bert Biggs for supplying a wide variety of equipment.

Thanks have to be made to Dr. G.D. Peng, Dr. M.C.J. Large and Dr. Ole Bang for providing step index and microstructured polymer optical fibres, respectively without which this thesis would not have been as successful.

To my parents who, constantly support me. Without their love and understanding, no achievement in my research work can be reality.

Finally, special thanks are given to my wife, Qing Li for her unending encouragement and patience, especially for restoring my determination to finish.

# Table of Contents

<b>1 THESIS OVERVIEW</b> .....	<b>9</b>
REFERENCES .....	13
<b>2 THEORY OF FIBRE BRAGG GRATING</b> .....	<b>15</b>
2.1 OPTICAL FIBRE.....	15
2.2 FIBRE BRAGG GRATING.....	16
2.3 COUPLED MODE THEORY .....	18
2.4 METHODS FOR BRAGG GRATING FABRICATION .....	22
2.4.1 <i>Amplitude-Splitting Interferometer</i> .....	22
2.4.2 <i>Wavefront-Splitting Interferometer</i> .....	24
2.4.3 <i>Phase Mask Technique</i> .....	25
2.4.4 <i>Point-by-Point Inscription</i> .....	27
2.5 GENERAL SENSING APPLICATIONS.....	28
2.5.1 <i>Temperature Sensitivity</i> .....	28
2.5.2 <i>Strain Sensitivity</i> .....	29
2.6 SUMMARY .....	29
REFERENCES .....	30
<b>3 POLYMER OPTICAL FIBRE BACKGROUND</b> .....	<b>32</b>
3.1 INTRODUCTION TO POLYMER OPTICAL FIBRES AND ITS APPLICATIONS.....	32
3.2 PROPERTIES OF POLYMER OPTICAL FIBRE.....	36
3.2.1 <i>Chemical and Physical Properties of Polymer Optical Fibre</i> .....	36
3.2.2 <i>Optical Loss Properties of Polymer Optical Fibre</i> .....	43
3.3 CONCLUSION.....	47
REFERENCES .....	49
<b>4 PHOTONSENSITIVITY OF PMMA BASED POLYMER OPTICAL FIBRE</b> .....	<b>57</b>

4.1 INTRODUCTION .....	57
4.2 FUNDAMENTAL CONCEPTS OF PHOTOCHEMISTRY .....	58
4.3 PHOTSENSITIVITY OF PMMA BASED BULK MATERIALS .....	60
4.3.1 <i>Photosensitivity of Undoped PMMA Materials</i> .....	61
4.3.1.1 193nm and 248nm UV Irradiation .....	61
4.3.1.2 325nm UV Irradiation .....	63
4.3.1.3 Femtosecond Laser Induced Photosensitivity .....	64
4.3.2 <i>Photosensitivity of PMMA With Photo-chemically Active Dopants</i> .....	66
4.4 PHOTSENSITIVITY OF PMMA BASED POLYMER OPTICAL FIBRES .....	67
4.5 CONCLUSION .....	70
REFERENCES .....	73
<b>5 BRAGG GRATING INSCRIPTION IN POLYMER OPTICAL FIBRE .....</b>	<b>76</b>
5.1 INTRODUCTION .....	76
5.2 POLYMER OPTICAL FIBRE BRAGG GRATING INSCRIPTION SETUP .....	77
5.3 FABRICATED POLYMER OPTICAL FIBRE BRAGG GRATINGS .....	81
5.3.1 <i>Microstructured Polymer Optical Fibre Bragg Gratings</i> .....	81
5.3.1.1 PMMA Based Single Mode Microstructured Polymer Optical Fibre Bragg Gratings .....	81
5.3.1.2 TOPAS Based Single Mode Microstructured Polymer Optical Fibre Bragg Grating .....	85
5.3.2 <i>Step Index Polymer Optical Fibre Bragg Gratings</i> .....	89
5.4 EXPLANATION OF THE OBSERVED ABNORMAL GRATING PERIOD .....	92
5.5 CONCLUSION .....	98
REFERENCES .....	100
<b>6 POLYMER OPTICAL FIBRE BRAGG GRATING SENSITIVITY CHARACTERISATION .....</b>	<b>102</b>
6.1 HUMIDITY SENSITIVITY .....	102
6.1.1 <i>Introduction</i> .....	102
6.1.2 <i>Calibration Setup</i> .....	103
6.1.2.1 The Environmental Chamber .....	103
6.1.2.2 Connecting POF with Silica Optical Fibre .....	103

6.1.3 Humidity Sensitivity of Step-index POFBG .....	111
6.2 TEMPERATURE SENSITIVITY .....	115
6.2.1 Introduction .....	115
6.2.2 Thermal Response of PMMA and TOPAS mPOF Gratings .....	115
6.2.2.1 Experiment Set-up .....	115
6.2.1.2 Thermal Properties of mPOFBGs in PMMA .....	117
6.2.1.3 Thermal Properties of mPOFBGs in TOPAS .....	122
6.2.1.4 Discussion of Results .....	123
6.2.3 Thermal Response of Step-index POFBGs .....	124
6.3 STRAIN SENSITIVITY OF STEP-INDEX POFBGs .....	125
6.3.1 Introduction .....	125
6.3.2 Experimental Arrangement .....	126
6.3.3 Strain Sensitivity and Tunability of Step-index POFBG .....	127
6.4 CONCLUSION .....	131
REFERENCES .....	133

**7 APPLICATION OF POLYMER OPTICAL FIBRE BRAGG GRATING SENSORS TO  
CONDITION MONITORING OF TEXTILES .....135**

7.1 INTRODUCTION .....	136
7.2 THE TENSILE STRAIN MEASUREMENT OF TEXTILE .....	137
7.2.1 Textile Specimen Preparation .....	137
7.2.2 Quasi-static Tensile Test .....	139
7.2.2.1 Testing Setup .....	139
7.2.2.2 Experiment Results .....	143
7.2.2.3 Calculation and Discussion of Structural Reinforcement and Strain Transfer .....	148
7.2.3 Long Term Tensile Test .....	152
7.2.3.1 Experiment Setup .....	152
7.2.3.2 Results and Discussion .....	155
7.3 CONCLUSION .....	163
REFERENCES .....	166

<b>8 APPLICATION OF POLYMER OPTICAL FIBRE BRAGG GRATING SENSORS IN</b>	
<b>DETECTING WATER .....</b>	<b>168</b>
8.1 DETECTING WATER IN JET FUEL.....	169
8.1.1 <i>Background Introduction</i> .....	169
8.1.2 <i>Experiment Setup and Fuel Sample Preparation</i> .....	170
8.1.3 <i>Proof of Principal Experiment</i> .....	171
8.1.4 <i>Discussion</i> .....	173
8.2 SIMULTANEOUS TEMPERATURE AND HUMIDITY SENSOR.....	174
8.2.1 <i>Introduction</i> .....	174
8.2.2 <i>Experiment and Result</i> .....	174
8.2.3 <i>Discussion</i> .....	177
8.3 CONCLUSION.....	178
REFERENCES .....	180
<b>9 THESIS CONCLUSION .....</b>	<b>181</b>
<b>PUBLICATION LIST .....</b>	<b>188</b>

# 1

## Thesis Overview

The fibre Bragg grating was firstly discovered by Hill et al [1] in 1978. Since then, the special properties and the potential applications of the fibre Bragg gratings were widely investigated [2-4]. The primary applications are in optical communication systems [5-6], sensing systems [7-9] and optical fibre lasers [10-12]. Initially, the investigation of fibre Bragg gratings were based on the device fabricated in silica optical fibres with numerous geometries. In recently years, this research has been extended to the fibre Bragg gratings inscribed in polymer optical fibres: Xiong et al [13] successfully wrote the first Bragg grating in step index polymer optical fibre and Dobb et al [14] in microstructured polymer optical fibres thereafter. Compared to its silica counter parts, polymer optical fibre has several advantages, including easier handling, better inherent material biocompatibility, higher thermal sensitivity, the ability to survive much higher strain levels, and so on. Thanks to these advantages, Bragg gratings in polymer optical

fibres may have better performance in some sensing areas than that of silica counter parts, or may be implemented in sensing applications that silica fibre Bragg gratings cannot. This thesis is concerned about the enhanced or special sensitivities of the fabricated Bragg gratings in several POF with different geometries and their potential applications.

The subsequent chapters in this thesis are listed as follows.

Chapter 2 introduces the background knowledge relating to fibre Bragg gratings, including the theorems of gratings, grating fabrication techniques and the sensing characteristics of gratings.

Polymer optical fibres are attracting more interest in its application in telecommunication and even in sensing. Chapter 3 briefly introduces the development path of the polymer optical fibre. This chapter also introduces several kinds of optical polymers and their properties, especially the optical polymer related to the content of this thesis.

Chapter 4 explains the basic concepts of photochemistry at the beginning and review the articles related to the photosensitivity of PMMA based bulk materials and polymer optical fibres.

Chapter 5 introduces the fibre Bragg grating inscription arrangement and successful inscription in several different kind of polymer optical fibres are detailed. The effects of the zeroth-order diffraction of a phase mask on the creation of

Bragg gratings in polymer optical fibres using the mask technique is also discussed at the end of this chapter.

Chapter 6 is concerned about the research of humidity, temperature and strain sensitivities of polymer optical fibre Bragg gratings. In this chapter, to enable the polymer optical fibre Bragg grating working away from the optical bench, the gluing coupling between polymer optical fibre and silica optical fibre is also investigated

In Chapter 7, a collaboration work with researchers from University of Southampton is detailed. Polymer optical fibre Bragg gratings are used to measured strain in textile specimens. The quasi static tensile strain measurement together with the long term tensile strain test of the specimen bonded with polymer optical fibre Bragg gratings is conducted.

Chapter 8 gives the details of two more potential applications based on the water sensitivity of polymer optical fibre Bragg gratings. A polymer optical fibre Bragg grating device is proved to be able to detect realistic levels of dispersed water in jet fuel; a compact silica and polymer FBG based dual parameter sensor element shows well-conditioned response to humidity and temperature.

Chapter 9 is the summary of the thesis and proposes some suggestions for further work.

This thesis is including a list of the author's publications arising during the progression of this PhD.

## References

- [1] K. O. Hill, Y. Fujii, D. C. Johnson, and B. S. Kawasaki, "Photosensitivity in optical fibre waveguides: Application to reflection filter fabrication," *Appl. Phys. Lett.* 62, 1035 (1993).
- [2] A. Othonos and K. Kalli, *Fiber Bragg gratings: fundamentals and applications in telecommunications and sensing*, (Boston: Artech House, 1999)
- [3] K. O. Hill and G. Meltz, "Fiber Bragg grating technology fundamentals and overview," *J. Lightwave Technol.* 15, 1263–1267 (1997).
- [4] T. Erdogan, "Fiber Grating Spectra," *J. Lightwave Technol.* 15, 1277-1294 (1997).
- [5] C. R. Giles, "Lightwave applications of fiber Bragg gratings," *J. Lightwave Technol.* 15, 1391–1404 (1997).
- [6] F. Bilodeau, D. C. Johnson, S. Theriault, B. Malo, J. Albert, and K. O. Hill, "An all-fiber dense wavelength division multiplexer using photoimprinted Bragg gratings," *IEEE Photon. Technol. Lett.* 7, 388–390 (1995).
- [7] A. D. Kersey, M. A. Davis, H. J. Patrick, M. LeBlanc, K. P. Koo, C. G. Askins, M. A. Putnam, and E. J. Friebele, "Fiber grating sensors," *J. Lightwave Technol.* 15, 1442 (1997).
- [8] Y.-J. Rao, "In-fibre Bragg grating sensors," *Meas. Sci. Technol.* 8, 355–375 (1997).
- [9] S. W. James, M. L. Dockney, and R. P. Tatam, "Simultaneous independent temperature and strain measurement using in-fibre Bragg grating sensors," *Electron. Lett.* 32, 1133 (1996).
- [10] G. A. Ball and W. W. Morey, "Compression-tuned single-frequency Bragg grating fiber laser," *Opt. Lett.* 19, 1979-1981 (1994).
- [11] J. Chow, G. Town, B. Eggleton, M. Ibsen, K. Sugden, I. Bennion, "Multiwavelength generation in an erbium-doped fiber laser using in-fiber comb filters," *IEEE Photon. Technol.* 8, 60-62 (1996).
- [12] G. A. Ball and W. W. Morey, "Continuously tunable single-mode erbium fiber laser," *Opt. Lett.* 17, 420 (1992).
- [13] Z. Xiong, G.D. Peng, B. Wu and P.L. Chu, "Highly tunable Bragg gratings in single-mode polymer optical fibers." *IEEE Photon. Technol.* 11, 352-354, (1999).

[14] H. Dobb, D. J. Webb, K. Kalli, A. Argyros, M. C. J. Large, and M. A. van Eijkelenborg, "Continuous wave ultraviolet light-induced fiber Bragg gratings in few- and single-mode microstructured polymer optical fibers," *Opt. Lett.* 30(24), 3296–3298 (2005).

# 2

## Theory of Fibre Bragg Grating

This chapter provides a background introduction to theorems related to optical fibre Bragg gratings. A brief introduction of the FBG fabrication techniques is also given. Finally, the sensing characteristics of FBG are discussed.

### 2.1 Optical Fibre

An optical fibre is a cylindrical dielectric waveguide. It consists of a core which is surrounded by a cladding layer. To confine the light guiding in the core, the refractive index of the core  $n_{core}$  is greater than that of the cladding  $n_{clad}$  to form the total internal reflection at the core cladding boundary.

One of the key parameters of optical fibres is Numerical Aperture which is determined by the two indices [1],

$$NA = n \sin \theta_{max} = \sqrt{n_{core}^2 - n_{clad}^2} \quad (2.1)$$

where  $\theta_{max}$  is the acceptance angle. The larger the value of  $NA$ , hence, the greater acceptance angle, the more amount of light the fibre can collect and also the wider the output beam will expand from the fibre end.

Another widely used key parameter is the V-parameter [2] which defines the mode volume of the core region in step index fibre:

$$V = \frac{2\pi a}{\lambda_c} \sqrt{n_{core}^2 - n_{clad}^2} = 2\pi a NA \quad (2.2)$$

where  $a$  is the radius of the core region and  $\lambda_c$  is the wavelength in vacuum. For single mode optical fibre, the value of the V-parameter should fulfil  $V \leq 2.405$ .

## 2.2 Fibre Bragg Grating

Fibre Bragg gratings (FBGs) consist of a periodic variation of the refractive index in the core of an optical fibre, which is normally produced by exposing the fibre to a spatially varying pattern of ultraviolet (UV) light. The periodic structure, shown in Figure 2-1 can couple a portion of light from the forward propagating core mode to the backward propagating core mode. In 1978, K. O. Hill et al first demonstrated the internal inscription of an FBG in silica fibre [2] and Z. Xiong et al were the first to report inscribing FBG in polymer optical fibre (POF) in 1999 [3].

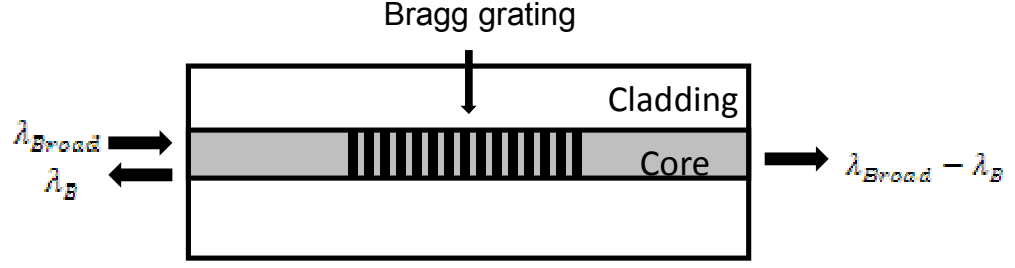


Figure 2- 1: Illustration of the diffraction effect of fibre Bragg grating.

For simplicity, the FBG can be taken as a perturbation to the effective refractive index of the fibre core, which can be expressed as [4]:

$$\partial n_{eff}(z) = \overline{\partial n_{eff}}(z) \left[ 1 + v \cos \left( \frac{2\pi}{\Lambda} z + \phi(z) \right) \right] \quad (2.3)$$

where  $\overline{\partial n_{eff}}(z)$  is the “dc” index change spatially averaged over a grating period,  $v$  is the fringe visibility of the index change,  $\Lambda$  is the nominal period, and  $\phi(z)$  describes grating chirp.

The fibre grating is simply an optical diffraction grating. The equation 2.4 demonstrates the effect of the grating on an incident light wave at an angle  $\theta_1$ : [5]

$$n \sin \theta_2 = n \sin \theta_1 + m \frac{\lambda}{\Lambda} \quad (2.4)$$

where  $\theta_2$  is the angle of diffracted wave and  $m$  is the diffraction order. In an FBG, the coupling is between modes travelling in opposite directions and so the relationship between the two angles is  $\theta_2 = -\theta_1$ .

The core mode propagation constant equation

$$\beta = \frac{2\pi}{\lambda} n_{eff} = \frac{2\pi}{\lambda} n_{co} \sin \theta_1 \quad (2.5)$$

was substituted into equation 2.4, where  $n_{co}$  is the core index, allowing the grating equation for guided modes to be rewritten as:

$$\beta_2 = \beta_1 + m \frac{2\pi}{\Lambda} \quad (2.6)$$

where for the dominant first order diffraction in FBG,  $m = -1$ . Furthermore, when the propagation constants of the co and counter propagation core modes are identical in value and opposite in sign, from equation 2.6, the familiar result for Bragg reflection can be getting:

$$\lambda = 2n_{eff}\Lambda \quad (2.7)$$

## 2.3 Coupled Mode Theory

The coupled mode theory is a quantitative model to describe the diffraction efficiency and deduce the spectra of the optical fibre gratings. It simply and accurately models the optical properties of most optical fibre gratings. The derivation of such theory has been given in detail by many researchers. [6, 7] In this section, the coupled mode theory will be used to explain the behaviour of uniform fibre Bragg gratings and the derivation will closely follow Erdogan's work. [8]

The transverse component of the electric field in the ideal-mode approximation to coupled-mode theory can be written as a superposition of the idea modes, which are the modes in an ideal waveguide with no grating perturbation:

$$E^T(x, y, z, t) = \sum_n [A_n(z) \exp(i\beta_n z) + B_n(z) \exp(-i\beta_n z)] e_n^T(x, y) \exp(-i\omega t) \quad (2.8)$$

Where  $n$  is the label of modes,  $A_n(z)$  and  $B_n(z)$  represent the slowly varying amplitudes of the  $n$ th mode travelling along the fibre axis direction (+ $z$  and  $-z$  directions). In the case of a fibre containing a grating, the dielectric perturbation

induced by the grating causes the coupling between the modes. The amplitudes  $A_n(z)$  and  $B_n(z)$  will evolve along the axis direction according to the following two equations [8]:

$$\frac{dA_n}{dz} = i \sum_j A_j (D_{jn}^t + D_{jn}^z) \exp[i(\beta_j - \beta_n)z] + i \sum_j B_j (D_{jn}^t - D_{jn}^z) \exp[-i(\beta_j + \beta_n)z] \quad (2.9)$$

$$\frac{dB_n}{dz} = -i \sum_j A_j (D_{jn}^t - D_{jn}^z) \exp[i(\beta_j + \beta_n)z] - i \sum_j B_j (D_{jn}^t + D_{jn}^z) \exp[-i(\beta_j - \beta_n)z] \quad (2.10)$$

where  $D_{jn}^t$  is the transverse coupling coefficient between the  $j^{\text{th}}$  and  $n^{\text{th}}$  modes.

In a Bragg grating, equations 2.9 and 2.10 can be simplified [7,8], as the dominant interaction is the coupling between the two modes near the wavelength, for which reflection from a mode of amplitude  $A(z)$  into an identical counter propagating mode of  $B(z)$  occurs. This simplification can be expressed as:

$$\frac{dA'}{dz} = i\hat{\sigma}A'(z) + ikB'(z) \quad (2.11)$$

$$\frac{dB'}{dz} = -i\hat{\sigma}B'(z) - ikA'(z) \quad (2.12)$$

The two amplitudes equations are given by  $A'(z) = A(z)e^{i\Delta\beta z - \frac{\phi}{2}}$ ,  $B'(z) = B(z)e^{i\Delta\beta z + \frac{\phi}{2}}$ , where  $\Delta\beta$  is the detuning, defined as:

$$\Delta\beta = \beta - \frac{\pi}{\Lambda} = 2\pi n_{eff} \left[ \frac{1}{\lambda} - \frac{1}{\lambda_d} \right] \quad (2.13)$$

In equations 2.11 and 2.12,  $k$  is the ac coupling coefficient and  $\hat{\sigma}$  is the dc self-coupling coefficient, defined by:

## 2. Theory of Fibre Bragg Grating

$$\hat{\sigma} = \Delta\beta + \sigma - \frac{1}{2} \frac{d\phi}{dz} \quad (2.14)$$

where  $\Lambda$  is the Bragg grating period,  $\lambda_d = 2n_{eff}\Lambda$  is the design peak reflection wavelength for a grating with infinitesimally weak refractive index modulation. ( $\delta n_{eff} \rightarrow 0$ )

For a uniform single mode fibre Bragg grating,  $\delta n_{eff}$  is constant. Thus,  $k = \frac{\pi}{\lambda} \sqrt{\delta n_{eff}}$ ,  $\sigma = \frac{2\pi}{\lambda} \delta n_{eff}$  [8] and  $\hat{\sigma}$  are all constants. Assuming that the propagation wave is incident from  $z = -\infty$  and there is no backward propagation wave exists from  $z \geq \frac{L}{2}$ , ( $L$  is the length of the grating) the reflectivity can be found and the reflectivity amplitude  $\rho$  of the uniform fibre grating is given by:

$$\rho = \frac{B'(-L/2)}{A'(-L/2)} = \frac{-k \sinh \sqrt{(kL)^2 - (\Delta\beta L)^2}}{\Delta\beta \sinh \sqrt{(kL)^2 - (\Delta\beta L)^2} + i \sqrt{k^2 - (\Delta\beta)^2} \cosh \sqrt{(kL)^2 - (\Delta\beta)^2}} \quad (2.15)$$

The power reflection coefficient is from  $R = |\rho|^2$ :

$$R = \frac{\sinh^2 \sqrt{(kL)^2 - (\Delta\beta L)^2}}{\frac{(\Delta\beta)^2}{k^2} + \cosh^2 \sqrt{(kL)^2 - (\Delta\beta)^2}} \quad (2.16)$$

Using the power reflection coefficient equation, different reflection spectral responses can be plotted with different  $kL$  values, as shown in Figure 2-2. It should be noted here that curves in the figure are plotted against the normalised wavelength

$$\frac{\lambda}{\lambda_{max}} = \frac{1}{1 + \Delta\beta L / \pi N} \quad (2.17)$$

where  $N = L/\Lambda$  is the number of grating planes. For a given  $kL$  value, the bandwidth of a grating will decrease with increasing  $N$ .

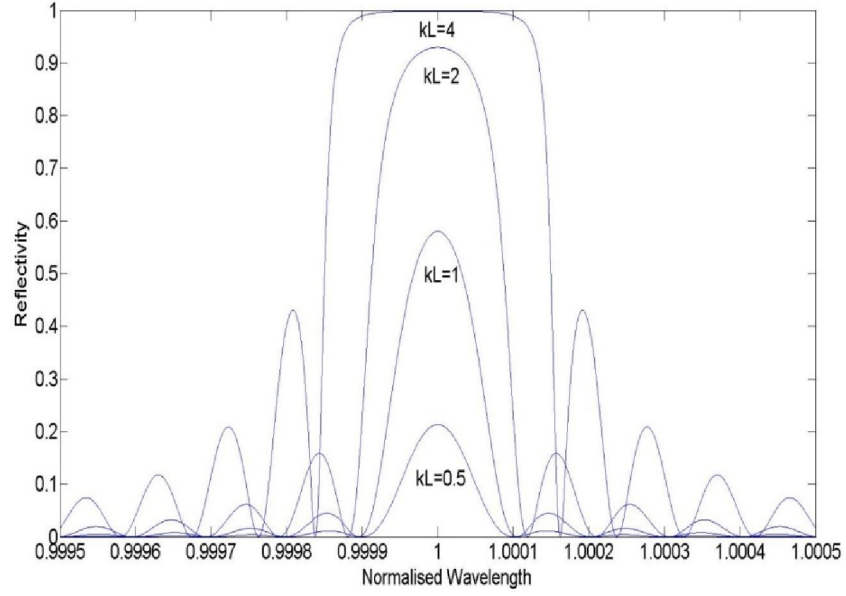


Figure 2- 2: Reflection spectral response versus normalized wavelength ( $\lambda/\lambda_{max}$ ) for a uniform Bragg grating with  $kL = 0.5, 1, 2$  and  $4$ .

Still from equation 2.16, when  $\Delta\beta = 0$ , or at the wavelength  $\lambda_{max} = (1 + \frac{\delta n_{eff}}{n_{eff}})$ , the maximum reflectivity can be achieved, given by:

$$R_{max} = \tanh^2(kL) \quad (2.18)$$

The bandwidth for a uniform Bragg grating is the width between the first zeros on either side of the maximum reflectivity. [8] From equation, it can be found:

$$\frac{\Delta\lambda_0}{\lambda} = \frac{v\delta n_{eff}}{n_{eff}} \sqrt{1 + \left(\frac{\lambda_d}{v\delta n_{eff}L}\right)^2} \quad (1.19)$$

The full width half maximum (FWHM) bandwidth can be approximated by: [9]

$$\Delta\lambda_{FWHM} \approx \lambda_B S \sqrt{\left(\frac{\partial n}{2n_{co}}\right)^2 + \left(\frac{1}{N}\right)^2} \quad (2.20)$$

where  $N$  is the number of the grating planes and for strong gratings  $s \approx 1$  and for weak gratings  $s \approx 0.5$ .

## 2.4 Methods for Bragg Grating Fabrication

Currently, there are four major different techniques for FBGs fabrication in photosensitive optical fibres: Amplitude-Splitting Interferometer, Wavefront-Splitting Interferometer, Phase Mask Technique and Point-by-Point Inscription. The mechanism of the different inscription techniques will be introduced separately.

### 2.4.1 Amplitude-Splitting Interferometer

The interferometer method for side inscription of FBGs was first demonstrated by Meltz et al in 1989. [10] The configuration of a typical amplitude-splitting interferometer for a high coherence UV laser source utilized in fibre Bragg grating fabrication is shown in Figure 2-3 (a). During the inscription, the UV Laser beam is divided into two equal intensity beams by the beam splitter and then these two beams are reflected to intersect at angle  $2\varphi$  from two UV mirrors, while the fibre was held at the intersection of the beams. The Bragg grating period is equal to the interference fringe period, which is given by

$$\Lambda = \frac{\lambda}{2 \sin \varphi} \quad (2.21)$$

where  $\lambda$  is the wavelength of the irradiation laser source.



(a)

(b)

Figure 2- 3: (a) A typical amplitude-splitting interferometer configuration for high coherence UV laser utilized in the fabrication of Bragg gratings in optical fibers; (b) An improved amplitude splitting interferometer for low spatial coherence source. [11]

Sometimes, a low spatial coherence laser source, for example, the excimer laser is used. For this kind of source, the fringe pattern for laser beams produced by the arrangement in Figure 2-3(a) will be in low quality, because there exists different number of reflections in each optical path, leading to one interfering beam acquire lateral orientation compared with the other one. The simplest solution is to introduce another UV mirror in one arm to make the compensation to the beam splitter reflection, as shown in Figure 2-3(b).

The advantage and disadvantage of amplitude-splitting interferometer are both quite clear. The most important advantage of the interferometric method is that by changing the intersection angle, this setup can write a Bragg grating at any desired wavelength. However, like all other interferometers, entirely isolating the optical components in the setup from mechanical vibrations and air flows is very

important and actually is unachievable. Sub-micrometre displacements of the laser beam caused by vibrations and air currents can affect the quality of the interference fringe pattern, which lead to low fringe visibility, thus low strength of the grating.

### **2.4.2 Wavefront-Splitting Interferometer**

There are two typical configuration of the wavefront-splitting interferometer used to fabricate Bragg gratings in optical fibre: the prism interferometer [12] and the Lloyd's mirror interferometer [13]; both interferometers are shown in Figure 2-4. The dominant principle of this interferometric method is that if a collimated UV beam is incident at a reflective surface, for example, a mirror or prism edge, then half of the beam is reflected across the path of the incident beam so that there is interference occurring in the region where the reflected and unreflected beams overlap and the interference fringe pattern is focused to the core of the fibre by a cylindrical lens. With a wavefront-splitting interferometer, the grating quality is less affected by the environment, since the reduction of the optical components together with the optical path in the system. It is easy to write Bragg gratings at tuneable wavelength, however the tuning range is limited by the interferometer arrangement. In addition, the length of the Bragg grating fabricated with this kind of system is restricted to the half of the incident UV beam width.



(a)

(b)

Figure 2- 4: (a) Schematic of a Lloyd's mirror wavefront-splitting interferometer; (b) Schematic of a prism wavefront-splitting interferometer. [11]

### 2.4.3 Phase Mask Technique

The phase mask technique, which was first demonstrated in 1993 [14], may be the most popular and one of the most effective methods for Bragg grating fabrication up to now. This technique makes use of phase mask as a key component of the interferometer to generate the interference pattern.

The phase mask is normally a fused silica plate, possessing an etched periodic surface-relief pattern with period  $\Lambda_{\text{pm}}$  and etching depth  $d$ , as shown in Figure 2-5.



Figure 2- 5: Schematic of Phase mask. [13]

With anormally incident UV radiation, the phase mask diffracts the incident beam into several orders,  $m=0,\pm 1,\pm 2\dots$  and the diffraction angle of the positive and negative orders are equal. The plus and minus orders form an inference pattern, which can be used to inscribe Bragg gratings in optical fibres. Normally, the near field interference fringe patter, generated by  $\pm 1$  order diffraction is used. The period of the Bragg grating fabricated by phase mask,  $\Lambda_g$  will be one half of that of the phase mask period,  $\Lambda_{pm}$ :

$$\Lambda_g = \frac{1}{2} \Lambda_{pm} \quad (2.22)$$

To enhance the first order interference fringe visibility, other orders should be suppressed, especially the zeroth order. To achieve the minimisation of the zeroth order diffraction, the etching depth  $d$  of the relief grating in phase mask is controlled to be:

$$d = \frac{\lambda_{UV}}{2} \quad (2.23)$$

where  $\lambda_{UV}$  is the wavelength of UV irradiation. However, in this case, the beam divergence of the laser source was not counted in, in the real world, the zeroth

order cannot be eliminated and is typically less than 3% [15]. From this equation, it can be concluded that in FBG inscription, for each UV laser source working at a different wavelength, a different phase mask needs to be used.

The main advantage of the phase mask technique is that it reduces the complexity of the fibre grating inscription system by using only one optical component. In the whole system, though vibration and air drifts may still be present, the system stability and reproducibility is greatly improved from the interferometric technique. However, the producible wavelength of the grating is fully depended on the period of expensive phase mask, though this main disadvantage of the phase mask technique may be slightly improved by applying strain to the fibre during FBG inscription to enable few nanometres tunability of the inscribed Bragg wavelength [16]. Therefore, several phase masks are required for writing grating at a range of operational wavelengths.

### **2.4.4 Point-by-Point Inscription**

The first demonstration of the point-by-point technique for fabricating Bragg reflectors was reported by Malo et al. [17]. This technique uses a UV pulse laser or femtosecond laser to inscribe individual grating planes one step at a time along the core of the fibre. A single pulse of light passes through a slit and then is focused onto the core of the optical fibre. After the refractive index at the irradiation point is changed, the fibre is translated a distance  $\Lambda$ , which is the grating period, from the original place by a precision translation stage. This procedure is repeated until the desired grating structure is obtained. The main advantage of this technique is that the grating parameters, like period, length, etc

can be adjusted flexibly, however, the accuracy control of the translation stage movement is very crucial.

### 2.5 General Sensing Applications

FBGs are excellent elements in sensing applications, which is the main topic of this thesis. The principle for using FBGs as sensing devices is that the Bragg grating resonance (the central wavelength of back-reflected light from the grating) depends on the effective refractive index of the core of the optical fibre and the grating period. The effective refractive index, as well as the periodicity of the grating, can be affected by changes in external measurands, principally strain and temperature. Thus, the variation of the Bragg grating resonance wavelength is related to the external measurands.

#### 2.5.1 Temperature Sensitivity

The thermal response of the FBG, arising from the thermal expansion of grating spacing and the thermal optic effect, results in a shift in Bragg wavelength. This shift for a temperature change can be written as [18]:

$$\Delta\lambda_B = \lambda_B(\alpha_\Lambda + \alpha_n)\Delta T \quad (2.24)$$

where  $\alpha_\Lambda$  is the thermal expansion coefficient of the optical fibre and  $\alpha_n$  is the thermo optic coefficient of the fibre. These two coefficients can be express as:

$$\alpha_\Lambda = \frac{1}{\Lambda} \frac{\partial \Lambda}{\partial T} \quad (2.25)$$

$$\alpha_n = \frac{1}{n} \frac{\partial n}{\partial T} \quad (2.26)$$

For silica optical fibre, the thermal expansion coefficient is approximately  $0.55 \times 10^{-6}$  and for the germanium doped silica core fibre, the thermo-optic coefficient is approximately  $8.6 \times 10^{-6}$ . Hence, the typical temperature sensitivity of silica optical fibre Bragg gratings at 1550nm is 10pm/°C. [19]

### 2.5.2 Strain Sensitivity

The shift of Bragg resonance wavelength is directly related to a change in the grating period and the strain optic effect. The axial strain induced Bragg wavelength shift is given by [18]:

$$\Delta\lambda_B = \lambda_B \left[ 1 - \frac{n^2}{2} [p_{12} - \nu(p_{11} + p_{11})] \right] \varepsilon_z \quad (2.27)$$

where  $p_{11}$  and  $p_{12}$  are the components of the strain-optic tensor,  $\nu$  is the Poisson ratio, and  $\varepsilon_z$  is the applied longitudinal strain. In a typical single mode silica based optical fibre, the strain sensitivity for 1550nm FBGs is 1.15pm shift in Bragg wavelength when applying  $1\mu\varepsilon$  to the FBG. [19]

## 2.6 Summary

The mechanisms involved in optical fibre Bragg grating has been discussed in detail. Different types of fibre Bragg grating fabrication methods have been introduced. Finally, the temperature and strain sensing characteristics of fibre Bragg gratings are presented.

## References

- [1] A. Ghatak and K. Thyagarajan, Introduction to Fiber Optics. Cambridge University Press, 1998.
- [2] K. O. Hill, Y. Fujii, D. C. Johnson, and B. S. Kawasaki, "Photosensitivity in optical fibre waveguides: Application to reflection filter fabrication," Applied Physics Letters, 32, pp.647-649, 1978.
- [3] Z. Xiong, G.D. Peng, B. Wu and P.L. Chu, "Highly tunable Bragg gratings in single-mode polymer optical fibers." IEEE Photonics Technology Letters, 11 (3), pp. 352-354, 1999.
- [4] V. Mizrahi and J. E. Sipe, "Optical properties of photosensitive fiber phase gratings," J. Lightwave Technol. 11, 1513-1517, 1993.
- [5] M. Born and E. Wolf, Principles of Optics. New York: Pergamon, 1987.
- [6] A. Yariv, "Coupled-mode theory for guided-wave optics," IEEE J.Quantum Electron., vol. QE-9, pp. 919–933, 1973.
- [7] H. Kogelnik, "Theory of optical waveguides," in Guided-Wave Optoelectronics, T. Tamir, Ed. New York: Springer-Verlag, 1990.
- [8] T. Erdogan, "Fibre grating spectra," IEEE J. Lightwave Technol. 15, pp.1277-2194, 1997.
- [9] P. St. J. Russell, J. L. Archambault and L. Reekie, "Fiber gratings," Physics World, October, 41-6, 1993.
- [10] G. Meltz, W. W. Morey, and W. H. Glenn. "Formation of Bragg gratings in optical fibers by a transverse holographic method," Optics Letters, 14(15), pp.823–825, 1989.
- [11] A. Othonos and K. Kalli, Fiber Bragg Gratings: Fundamentals and Applications in Telecommunications and Sensing. Artech House, Nordwood, MA, 1999.
- [12] R.Kashyap, J. R. Armitage, R. W. Wyatt, S. T. Davey, and D. L. Williams, "All-fibre narrow-band reflection gratings at 150 nm," Electron. Lett. 26 (12), pp.730-731, 1990.
- [13] R. Kashyap. Fiber Bragg Gratings. Academic Press, 1999.
- [14] D. Z. Anderson, V.Mizrahi, T.Erdogan and A. E. White, "Phase-mask method for volume manufacturing of fiber phase gratings," Post-deadline paper

PD16, Technical Digest of Post-Deadline Papers Proc. Conf. on Optical Fiber Communications, OFC '93, pp. 68, 1993.

[15] <http://www.phasemasks.com/fbgphasemasks>

[16] Q. Zhang, D. A. Brown, L. Reinhart, T. F. Morsé, J. Q. Wang, and X. Gang, "Tuning Bragg wavelength by writing gratings on prestrained fibers," *IEEE Photon. Technol. Lett.* 6, 839-842, 1994.

[17] B. Malo, K. O. Hill, F. Bilodeau, D. C. Johnson, and J. Albert, "Point-by-point fabrication of micro-Bragg gratings in photosensitive fiber using single excimer pulse refractive index modification techniques," *Electron. Lett.* 29, pp.1668-1669, 1993.

[18] G. Meltz and W. W. Morey, "Bragg grating formation and germanosilicate fiber photosensitivity," in *Photoinduced Self-Organization Effects in Optical Fibers*, F. Ouellette, ed., Proc. SPIE 1516, 185–199, 1991.

[19] A.D. Kersey, M.A. Davis, H.J. Patrick, M. LeBlanc, KP Koo, CG Askins, MA Putnam and E.J. Friebele, "Fibre grating sensors," *IEEE J. Lightwave Technol.* 15, 8, pp.1442-1463, 1997.

# 3

## Polymer Optical Fibre Background

In this chapter, the development path of polymer optical fibres is reviewed. The properties of several kinds of optical polymer used in polymer optical fibre fabrication are introduced. The optical loss properties of polymer optical fibre are discussed at the end of this chapter.

### **3.1 Introduction to Polymer Optical Fibres and Its Applications**

Polymer has attracted more attention as an optimal material for making optical fibre recently [1]. Polymer optical fibre (POF) has exhibited increasing potential in the future short distance moderate bandwidth data communication applications,

for example, local area network [2], Fibre To The Home (FTTH) solutions [3], and high rate data transmission in automotive industry [4], etc.

The first POF, with a step-index (SI) profile was invented by Du Pont in 1966 and Mitsubishi introduce the first commercialized SI POF into the market in 1975, with Asahi Chemical and Toray following thereafter [references]. Since then, the transparency [5-6], the temperature stability [7-9] and the bandwidth [10-11], which is the three key factors of optical fibre, have been greatly improved to be sufficient for the use in the last hundred meters of high speed all optical networks. The typical SI POF is large core multimode fibre made of polymethyl methacrylate (PMMA) with diameter up to approximately 1mm. [2] At this diameter, it can still remain highly flexibility, allowing easy handling and installation, good connectivity to low cost sources, such as light emitting diodes (LED), thanks to its large multimode core. However, the large core SI POF has its limitations of bandwidth, as because of the large multimode core, modal dispersion is increased, extremely degrading bandwidth to about several hundred megahertz over 100 m. One approach to improve this problem is to change the refractive index profile in the core region from step-index to graded index (GI) [12]. The first GI POF was reported by Ohtsuka and Hatanaka in 1976 [13]. As the modal dispersion was controlled, material dispersion of POF becomes none negligible issue that affected the transparency of POF. This is improved by the innovation of prefluorinated (PF) graded index POF, of which the data transmission distance is higher than PMMA SI/GI POF [14]. The PF GI POF has been taken as a good potential replacement of copper cable and already has several successful application cases [15-16], for example, the 1 Gbit/s all PF GI POF based campus LAN network of Keio University [15].

### 3. Polymer Optical Fibre Background

Apart from the application of POF in data communications, its potential application in sensing was also paid more attention by researchers in the past decades [17-19]. Fibre optical sensors are able to offer several significant advantages over conventional electrical sensors, some of which are listed as following: optical fibre sensors are immune from electromagnetic radiation, which would make conventional sensors fail or corrupt the received signal; optical fibre sensors can transmit measurement optical signals a long distance and can be multiplexed in only one optical fibre, driving down the cost of complex network configurations; Optical fibre sensors are light and spark-free, etc. Numerous optical fibre sensors have been demonstrated in many review articles [20-22]. As a type of optical fibre, POF possess its unique advantages in sensing. The majority of POF for sensing to date is based on PMMA materials. As a potentially low cost sensing solution, it has several advantages compared with its silica counterpart, including ease of termination, ease of handling, safe disposability, higher thermal and strain sensitivity, [23] the ability to survive much higher strain levels, which will be discussed in another section, and better inherent material biocompatibility, etc. A huge variety of sensors have been made by utilizing POF, for example, sensor for measuring strain and mechanical deformation [24-26], for structure health monitoring [27-28], for humidity measuring [29-31], for detecting the presence of ozone [32], for respiratory monitoring[33-34], for seat-occupancy recognition [35] and so on.

In addition, FBGs, the favoured element with high sensitivity in temperature, strain and pressure sensing, etc., which were originally developed in silica optical fibre have been duplicated in POF in recent years [36-38], due largely to the expectation that they will open up new applications where FBGs in silica fibres

have not been suitable. They have already been shown to be more sensitive to strain, temperature and humidity than is the case for silica FBGs [39-41] and several practical applications of polymer optical fibre Bragg grating (POFBG) have been developed. [31, 41-43]

In the recent years, the microstructured polymer optical fibre (mPOF) is innovated on the basis of the success of photonic crystal fibres, [44] which utilise a pattern of multiple tiny air holes that run longitudinally through the entire length of the fibre to guide light. This kind of fibre possesses several important advantages over conventional POF. The mPOF can be fabricated from a single polymer. The different types of polymer materials, i.e. PMMA which is highly transparent, low cost and widely used in POF; fluorinated polymers which have lower material absorption [45]; TOPAS cyclic olefin copolymer (COC) which has less water absorption [46]; Polystyrene (PS) which has a higher refractive index [47]; polycarbonate (PC) which has a higher glass transition temperature ( $T_g$ ) [48]; and biodegradable materials [49], etc., gives the potential to change various properties of fibres. This also gets rid of the restrictions related to the high glass-transition temperature normally existed in silica optical fibre, which would allow organic or inorganic dopants, working at low processing temperature, to be added into fibre by various doping methods. For example, solution doping can introduce rhodamine 6G, the organic dye into the polymer matrix and it has been used to produce a microstructured fibre laser [50-51] and also used to increase photosensitivity and the electro-optic coefficient of the fibre [52]. Quantum dots and ferromagnetic cobalt nanoparticles have also been doped into the fibre by powder doping method for the potential application in quantum dot-based fibre lasers [53] and magnetic field sensing respectively [54]. Changing the geometry of

the patterns of holes can easily get different type of fibres: step index/graded index, single mode/multimode, solid core/hollow core, etc. The dispersion of the fibre also depends on the particular geometry used, thus there is the potential for tailoring the dispersion properties in a relatively straightforward way. As an example, such fibre can display endlessly single mode behaviour [55-56]. In the fibre, the holes offer a means of getting materials to be tested in contact with the evanescent wave field in the core and this application is being developed for biological sensing application, for example, the selective detection of fluorophore-labeled antibodies [46]. Upon the successful inscription of FBGs in mPOF few years ago [38, 57], such biosensors can even potentially be made into FBG based label-free sensor. The holes of mPOF can be coated with metal, like silver to enable the fibre work as an absorption polarizer [58] or makes it suitable for surface enhanced Raman scattering (SERS) experiments [59].

## **3.2 Properties of Polymer Optical Fibre**

### **3.2.1 Chemical and Physical Properties of Polymer Optical Fibre**

#### Poly methyl methacrylate (PMMA)

PMMA is the most commonly used material in POF fabrication. The basic monomer of PMMA is methyl methacrylate (MMA). PMMA is constructed by such monomers through polymerization, as shown in Figure 3-1. During polymerization, the splitting of the carbon-carbon double bonds of the MMA allow the small molecules to attach together to form a long chain molecule. The properties of PMMA are listed in Table 3-1.



Figure 3- 1: MMA and PMMA. [2]

Table 3-1: Properties of PMMA. [60-61]

Transmittance (Visible Region, 200 micron thick)	93 %
Refractive Index (589nm)	1.49
Abbe Number	58
Birefringence	< 20
Photoelastic coefficient	-2.8~ -3.9×10 <sup>-12</sup> Pa <sup>-1</sup>
Glass Transition Temperature	105-120°C
Melting Point	iso 160 sys 200°C
Water Absorptivity(23°C /24 h emersion)	0.3%
Linear Thermal Expansion Coefficient	8×10 <sup>-5</sup> K <sup>-1</sup>
thermo-optic coefficient	-1×10 <sup>-4</sup> K <sup>-1</sup>
Young's Modulus	3.3 GPa
Tensile strength	65~73 MPa
Tensile extension ratio	3~5%
Yield strength	65MPa

### 3. Polymer Optical Fibre Background

Apart from the relatively high optical attenuation of PMMA, which will be discussed in a separate section, the high water sorption capability (above 0.3wt% at 23°C) is another major disadvantage [60, 62]. It makes PMMA based optical components, for example, lenses, change their geometry and consequently affects their optical performance. Furthermore, the absorbed water exists as impurities in the core of the fibre, thus increases the attenuation loss in the fibre [63].

Another property worth discussing is the mechanical properties of PMMA. The typical Young's modulus for bulk PMMA is 3.3 GPa, which is much smaller than silica fibres' 73 GPa [64]. For PMMA based optical fibres, the modulus value can vary [23,25,65-66] due to several possibilities: the various kinds of copolymers in the fibre cores, the different processing conditions, the various molecular weight distributions, the addition of plasticizers and so on. In FBG sensing applications, the low value of Young's modulus for POF normally do not give it many advantages against its silica counterparts. However, in some specific applications, the low Young's modulus of POF does have advantages, for example, using POFBG sensor to monitor a material with a low Young's modulus and such application will be detailed in Chapter 7.

The tensile properties of PMMA based POF is complex. The yield strain is reported to be around 6% for PMMA fibre. [65-66] During the fibre drawing process, the alignment of the polymer molecules along the axis occurs and it may lead to inconstant mechanical properties at different drawing tension [67]. The advantage of the tensile property of POF is that extremely high failure strains are achievable. Silica fibres can possess a typical failure strain of 5-10% [68], which is hard to achieve in practice and can be below 1% for cyclic loading over thousands of cycles, while for polymer fibres the failure strain has been reported as high as

### 3. Polymer Optical Fibre Background

over 100% [69]. To achieve such high value, the polymer optical fibre should be drawn under low tension, as it has been proved in a work [69] that the drawing tension could affect the magnitude of molecular alignment along the fibre axis, thus affecting the failure strain and the higher the tension is, the lower the failure strain will be. In addition, the fibre drawing at low tension also possesses low tensile strength and low yield stress. [70] However, the properties of fibre drawn under high tension can approach that of fibre fabricated under low-tension drawing after an annealing process [65].

The main disadvantage of the tensile property of PMMA is that this material exhibits visco-elasticity, leading to tensile properties of PMMA based POF displaying hysteresis and timescale dependence. Yang et al [66] discovered the hysteresis induced by the cyclic strain applied to PMMA based POF. In their experiment, POF is stretched at the speed of 0.5%/minute in several cycles with the same tensile strain and each cycle starts from the point where the stress has released to zero in the previous cycle, as shown in Figure 3-2. The POF can relax back towards its original length, when the sufficient recovery time is given.



Figure 3- 2: The first, second, third and tenth cycles of the cyclic tensile strain testing of PMMA fibre. [71]

### 3. Polymer Optical Fibre Background

Large et al. [72-73] prove that the tensile properties of the PMMA based POF possess timescale dependence. In one of their experiments, strain as high as 3% is applied to the POF in the order of a minute and then released. After such process, the POF can return to its original length quickly without any hysteresis observed. In another experiment, they held the stretched state of a piece of fibre for 10 hours before releasing. After that, they find the relaxation process is much slower. For a strain of 1%, it takes 10 hours for the fibre to relax back to its original length and for a strain of 4%, the fibre even cannot fully relax back in 10 hours. In addition, the visco-elasticity of PMMA based POF may be less of a problem than it seems, especially when POF is attached to a much stiffer structure for monitoring purposes, the structure may well force the POF back to zero when strain is removed.

#### TOPAS

TOPAS, manufactured by Topas Advanced Polymers GmbH is the brand name of the cyclic olefin copolymer which is copolymerized from norbornene and ethylene using a metallocene catalyst (see Figure 3-3) and it is an amorphous transparent copolymer. TOPAS has several grades with different norbornene content.



Figure 3- 3: TOPAS COC. [74]

The highly transparent resin possesses excellent properties in terms of low birefringence, low water absorption (0.01% absorption, 24 hours immersion in water at 23°C), high Abbey number, and high stiffness that are important in optical

components. [74] In addition, it exhibits an improved melt viscosity [75] and high tear strength [76] allowing better conditions for drawing of optical fibre than PMMA. The properties of TOPAS COC are listed in Table 3-2.

Table 3-2: Properties of TOPAS COC. [74]

Transmittance (Visible region, 200 micron thick)	91 %
--	------



#### CYTOP

Cyclic Transparent Optical Polymer (CYTOP), shown in Figure 3-4 is the brand name of the Perfluorinated polymer developed by ASAHI Glass Co. in collaboration with Keio University, which has already been used in POF manufacturing [77]. CYTOP based POF has lower attenuation and lower material

dispersion than PMMA based POF from visible to near infrared region [2], which gives it potential for short haul telecommunication links. Some of the properties of CYTOP are listed in Table 3-3.



Figure 3- 4: CYTOP. [78]

Table 3-3: Properties of CYTOP. [78]

Transmittance (Visible region, 200 micron thick)	95 %
--	------



### 3.2.2 Optical Loss Properties of Polymer Optical Fibre

The attenuation in polymer optical fibres is several magnitudes higher than in silica optical fibres. The various mechanisms contributing to the losses for polymer optical fibre have been examined, which are essentially similar to those for silica optical fibres [79]. The loss factors are clarified into intrinsic and extrinsic, as shown in Table 3-4.

Table 3-4: Loss factors for POFs

Intrinsic		Extrinsic	
Absorption	Scattering	Absorption	Scattering
Higher harmonics of carbon-hydrogen (CH) bonds absorption	Rayleigh Scattering	Transition metals	Dust and microvoids
Electronic transition		Organic Contaminants	Fluctuation of core diameter
			Orientalional birefringence
			Core-cladding boundary imperfections

The intrinsic losses are mainly caused by the absorption and scattering loss of the material itself which constitute the POF, while the extrinsic losses are coming from the absorption and scattering losses due to impurities and defects, which can be minimised by optimising the process conditions in POF fabrication. Hence, the intrinsic losses should be the major loss contribution in polymer optical fibre loss and will be detailed for the case of PMMA in this section.

#### Vibrational Absorption of Core Materials

Molecular vibrational absorption bands exist in polymers, due to the different chemical bonds, like C-H, N-H, and O-H within the material. The strong absorption from higher harmonics of vibration of C-H bonds is the dominant absorption effect in visible to near infrared wavelength region. Figure 3-5 show the high harmonics of C-H absorption from the near-infrared to visible wavelength region in PMMA core polymer optical fibres.



Figure 3- 5: High harmonics of C-H absorption in PMMA. [80]

This graph gives such information that the transmission loss of the PMMA based POF is increasing with the wavelength and indicates that the polymer optical fibres could not be well functioned in medium and long distance communication networks or sensing networks at 1300/1500nm telecommunication window as its glass counterparts does, due to the significantly high attenuation ( $\sim 10^6$  dB/km) at this wavelength. The loss comparison spectrum between several kinds of polymer

optical fibre and silica optical fibre well defend such conclusion, as shown in Figure 3-6.



Figure 3- 6: Transmission loss spectrum of various kinds of fibres. [81]

This graph clearly demonstrated that the attenuation loss in the various polymer optical fibres is significantly larger than that of silica optical fibres through the whole wavelength range, especially at the two normal telecommunication windows (around 1300 and 1500 nm) of standard silica optical fibre. As a result, POF in communication networks have to operate in the visible wavelength region, which is from 550 to 750 nm, with attenuation of approximately 100 dB/km and the length of POF in fibre Bragg grating sensing devices is normally limited to few to tens of centimetres, as to date most of polymer optical fibre Bragg gratings are based on PMMA core POF and working at telecommunication windows.

This graph also shows several effective methods of improving the loss property of POF. As in PMMA materials, hydrogen, which is the lightest atom, causes the fundamental vibration of the C-H vibration at relatively short wavelength of 3.2  $\mu\text{m}$ . Hence, the harmonics can influence the attenuation loss in the visible region. Replacing the hydrogen atoms in such material with more massive deuterium atom can shift the wavelengths of the fundamental vibration and its harmonics to longer wavelength regions, where loss due to Rayleigh scattering is low. This process is called deuteration. Furthermore, if the C-H atom pairs within the polymer are replaced by fluorine compounds with higher mass, like  $\text{CF}_3$  groups, (perfluorination), the fundamental absorptions can shift to longer wavelength region than that is obtained with deuteration resulting in the intrinsic attenuation loss mainly due to a Rayleigh scattering contribution. Therefore, the losses of the perfluorinated polymer, e.g. CYTOP, can be reduced in several orders of magnitude than PMMA. In addition, the penetration of moisture into the polymer, which normally happened in polymer containing hydrogen or deuterium [82], can also be prevented.

#### Rayleigh Scattering

In the core of optical fibres, Rayleigh scattering is caused by structural irregularities on a scale of less than the order of one-tenth of a wavelength. [83] The irregularities are caused by changes in the material composition and fluctuations of the material density. In the case of fully polymerised PMMA, Rayleigh scattering is mainly caused by the fluctuations of the density. The attenuation of the fibre results from Rayleigh scattering can be calculated by: [84]

$$\gamma_R = \frac{8\pi^3}{3\lambda_0^4} n^8 \rho^2 \beta (kT_f) \quad (3.1)$$

where  $n$  is the refractive index,  $\rho$  is the photoelastic constant,  $\beta$  is the isothermal compressibility,  $k$  is Boltzmann's constant,  $\lambda_0$  is the guided wavelength,  $T_f$  is the fictive temperature of the material. It can be conducted from the Equation 3.1 that if the POF is working in the visible wavelength region, the isotropic density of the core polymer is essential to the loss of the POF.

#### Electronic Transition Absorption

Polymers can absorb light in the ultraviolet region of the spectrum. The absorption mechanism depends on transitions between electronic energy levels of the bonds within the materials, caused by the absorption of photon energy which lead to excitation of the electronic state of the materials. Though the electronic transition peaks commonly appear in the ultraviolet wavelength region, their absorption tails can extend into near infrared, hence influence the transmission loss of POFs.

In the case of PMMA core POF, there exists an  $n-\pi^*$  transition due to an ester group in the MMA molecules, an  $n-\sigma^*$  transition of chain transfer agent, and an  $\pi-\pi^*$  transition of an azo group when azo compounds are used as a polymerization initiator. The most significant absorption is attributed to the transition of the  $n-\pi^*$  orbital of the double bond of the monomer [80].

### **3.3 Conclusion**

Firstly, the development history of polymer optical fibres is reviewed at the beginning of this chapter. Secondly, the chemical and physical properties of several optical polymers like PMMA, TOPAS COC and CYTOP based polymer

### 3. Polymer Optical Fibre Background

optical fibres are briefly introduced and listed. The water sorption and tensile properties of PMMA based polymer optical fibre are highlighted and discussed, as these properties are very important to the sensing applications of polymer optical fibre Bragg grating. Finally, the attenuation mechanisms in polymer optical fibres are detailed and the intrinsic losses including vibrational absorption, Rayleigh scattering and electronic transition absorption, which are the major loss contribution in polymer optical fibre are discussed separately for the case of PMMA. From the reviewed works, it is not hard to find the attenuation of the polymer optical fibre is still greatly limiting its role in both telecommunication and sensing applications, as this high attenuation compared to silica fibre results in a practical limitation to the distribution length of a POF-based communication or sensor network. The most reliable solution to improve the transparency of polymer optical fibre should concentrate on discovering and synthesizing novel low loss optical polymer system for fibre fabrication.

## References

- [1] H. S. Nalwa, *Polymer Optical Fibers* (American Scientific, 2004).
- [2] W. Daum, J. Krauser, P. Zamzow, and O. Ziemann, *POF Polymer Optical Fibers for Data Communication* (Springer-Verlag, 2001).
- [3] I. Möllers, D. Jäger, R. Gaudino, A. Nocivelli, H. Kragl, O. Ziemann, N. Weber, A. M. J. Koonen, C. Lezzi, A. Bluschke, and S. Randel, "Plastic optical fiber technology for reliable home networking: overview and results of the EU project POF-ALL," *IEEE Commun. Mag.* 47, 58 (2009).
- [4] T. Kibler, S. Poferl, G. Böck, H.-P. Huber, and E. Zeeb, "Optical data buses for automotive applications," *J. Lightwave Technol.* 22, 2184-2199 (2004).
- [5] T. Kaino, K. Jinguji, and S. Nara, "Low Loss Poly(methylmeth-acrylate-d8) Core Optical Fibers," *Appl. Phys. Lett.* 42, 567 (1983).
- [6] T. Kaino, "Plastic optical fibers for near-infrared transmission," *Appl. Phys. Lett.* 48, 757–758 (1986).
- [7] T. Yamashita, "Quasi-Static and Dynamic Density Fluctuations in the Glassy State IV. Dynamic Thermal Density Fluctuation and Isothermal Compressibility of Glass," *Jpn J. Appl. Phys.* 33, 4025-4031 (1994).
- [8] Y. Yamaki, M. Asai, S. Takahashi and Y. Koike, "Novel Dopant for Graded-Index Polymer Optical Fiber with High-Thermal Stability," *Appl. Phys. Express.* 3, 071601(2010).
- [9] Y. Takezawa, S. Tanno, N. Taketani, S. Ohara, H. Asano, "Plastic optical fibers with fluoroalkyl methacrylate copolymer as their core," *J. App. Polym. Sci.* 42, 3195-3203 (1991).
- [10] S. Takahashi and K. Ichimura, "Time domain measurements of launching-condition-dependent bandwidth of all-plastic optical fibres," *Electron. Lett.* 27, 217–219 (1991).
- [11] R. J. S. Bates and S. D. Walker, "Evaluation of all-plastic optical fibre computer data link dispersion limits," *Electron. Lett.* 28, 996–998 (1992).

- [12] T. Ishigure, E. Nihei, S. Yamazaki, K. Kobayashi, and Y. Koike, "2.5 Gb/s 100 m data transmission using graded index polymer optical fiber and high speed laser diode at 650-nm wavelength," *Electron. Lett.* 31, 467–468 (1995).
- [13] Y. Ohtsuka, Y. Hatanaka, "Preparation of light-focusing plastic fiber by heat-drawing process," *Appl. Phys. Lett.* 29, 735-737 (1976).
- [14] I. T. Monroy, H. P. A. vd Boom, A. M. J. Koonen, G. D. Khoe, Y. Watanabe, Y. Koike, and T. Ishigure, "Data transmission over polymer optical fibers," *Optical Fiber Technology* 9, 159-171 (2003).
- [15] Y. Koike, "Status of POF for Broadband Society," in proceedings of 14th International conference on Plastic Optical Fiber, (Hong Kong, China, 2005).
- [16] Y. Koike, "The Giga House Project," in proceedings of 18th International Conference on Plastic Optical Fibers, (Sydney, Australia, 2009).
- [17] G. D. Peng and P. L. Chu, "Polymer optical fiber sensing," in *Optical Information Processing Technology*, vol. 4929 of Proceedings of SPIE, pp. 303–311, (2002).
- [18] R.J. Bartlett, R.P. Chandy, P. Eldridge, D.F. Merchant, R.Morgan and P.J. Scully, "Plastic optical fibre sensor and devices", *Trans. Inst. Measurement and Control*, 22, 431-457,( 2000).
- [19] J. Zubia and J. Arrue, "Plastic optical fibers: an introduction to their technological processes and applications," *Opt. Fiber Technol.* 7, 101-140 (2001).
- [20] A. D. Kersey, "A review of recent developments in fiber-optic sensor technology," *Opt. Fiber Technol.: Mater. Devices Syst.* 2, 291–317 (1996).
- [21] K. T. V. Grattan and T. Sun, "Fiber optic sensor technology: an overview," *Sens. Actuators* 82, 40–60 (2000).
- [22] B. Lee, "Review of the present status of optical fiber sensors," *Opt. Fiber Technol.* 9, 57-79 (2003).
- [23] M. Silva-López, A. Fender, W. N. MacPherson, J. S. Barton, J. D. C. Jones, D. Zhao, H. Dobb, D. J. Webb, L. Zhang, and I. Bennion, "Strain and temperature

sensitivity of a single-mode polymer optical fiber,” *Opt. Lett.* 30, 3129–3131 (2005).

[24] K. S. C. Kuang, W. J. Cantwell and P. J. Scully, “An evaluation of a novel plastic optical fibre sensor for axial strain and bend measurements,” *Meas. Sci. Technol.* 13, 1523 (2002).

[25] S. Kiesel, K. Peters, T. Hassan, and M. Kowalsky, “Behaviour of intrinsic polymer optical fibre sensor for large-strain applications,” *Meas. Sci. Technol.* 18, 3144-3154 (2007)

[26] S. Kiesel, K. Peters, T. Hassan, and M. Kowalsky, “Large deformation in-fiber polymer optical fiber sensor,” *IEEE Photonics Technol. Lett.* 20, 416-418 (2008).

[27] S. Liehr, P. Lenke, M. Wendt, K. Krebber, M. Seeger, E. Thiele, H. Metschies, B. Gebreselassie, and J. C. Munich, “Polymer Optical Fibre Sensor for Distributed Strain Measurement and Application in Structural Health Monitoring”, *IEEE Sensors J.*, 9 (11), 1330-1338 (2009).

[28] K.S.C. Kuang, S.T. Quek, C.G. Koh, W.J. Cantwel and P.J. Scully, “Plastic optical fibre sensors for structural health monitoring: a review of recent progress,” *J. Sensors*, 312053, (2009).

[29] S. Muto, O. Suzuki, T. Amano, and M. Morisawa, “A plastic optical fibre sensor for real-time humidity monitoring,” *Meas. Sci. Technol.* 14(6), 746–750 (2003).

[30] C. M. Tay, K. M. Tan, S. C. Tjin, C. C. Chan, and H. Rahardjo, "Humidity sensing using plastic optical fibers," *Microwave Opt. Technol. Lett.* 43, 387-390 (2004).

[31] C. Zhang, W. Zhang, D. J. Webb, G.-D. Peng, G.-D, "Optical fibre temperature and humidity sensor," *Electron. Lett.* 46, 643-644 (2010).

[32] O’Keeffe S.; Fitzpatrick C., Lewis E, “ Ozone measurement in the visible region:an optical fiber sensor system”, *Electron.Lett.*, 41, 1317–1319 (2005).

[33] J. Witt, F. Narbonneau, M. Schukar, K. Krebber, J. De Jonckheere, M. Jeanne, D. Kinet, B. Paquet, A. Depre, L. T. D’Angelo, T. Thiel, and R. Logier,

“Smart medical textiles with embedded optical fibre sensors for continuous monitoring of respiratory movements during MRI,” Proc. SPIE 7653, 76533B (2010).

[34] L. Mohanty and K. S. C. Kuang, “breathing rate sensor with plastic optical fiber,” Appl. Phys. Lett. 97, 073703 (2010).

[35] P. Polishuk, “Plastic Optical Fibers Branch Out,” IEEE Commun. Mag. 140 (September 2006).

[36] Z. Xiong, G. D. Peng, B. Wu, and P. L. Chu, ‘Highly tunable Bragg gratings in single-mode polymer optical fibers,’ IEEE Photon. Technol. Lett. 11, 352-354 (1999)

[37] J. M. Yu, X. M. Tao, and H. Y. Tam, “Fabrication of UV sensitive single-mode polymeric optical fiber,” Opt. Lett. 29, 156 (2004).

[38] H. Dobb, D. J. Webb, K. Kalli, A. Argyros, M. C. J. Large, and M. A. van Eijkelenborg, “Continuous wave ultraviolet light-induced fiber Bragg gratings in few- and single-mode microstructured polymer optical fibers,” Opt. Lett. 30(24), 3296–3298 (2005).

[39] H. Y. Liu, G. D. Peng, and P. L. Chu, “Thermal tuning of polymer optical fiber Bragg gratings,” IEEE Photon. Technol. Lett., 13, 824–826 (2001).

[40] H. Y. Liu, H. B. Liu, G. D. Peng, “Tensile strain characterization of polymer optical fibre Bragg gratings,” Opt. Commun. 251, 37-43 (2005).

[41] C. Zhang, X. Chen, D.J. Webb, , and G.-D. Peng, “Water detection in jet fuel using a polymer optical fibre Bragg grating,” Postdeadline paper, 20th Int. Conf. on Optical Fibre Sensors, (Edinburgh, UK, 2009).

[42] H. B. Liu, H. Y. Liu, G. D. Peng, and P. L. Chu, “Strain and temperature sensor using a combination of polymer, and silica fibre bragg gratings,” Opt. Commun. 219(1-6), 139–142 (2003).

[43] K. Kalli, H. L. Dobb, D. J. Webb, K. Carroll, C. Themistos, M. Komodromos, G-D. Peng, Q. Fang and I. W. Boyd, “Development of an electrically tuneable

Bragg grating filter in polymer optical fibre operating at 1.55  $\mu\text{m}$ ," *Meas. Sci. Technol.* 18, 3155 (2007).

[44] P. St. J. Russell, "Photonic crystal fibers", *J. Lightwave. Technol.*, 24 (12), 4729–4749 (2006).

[45] S. Kondo, T. Ishigure, and Y. Koike, "Fabrication of polymer photonic crystal fiber," In *Proc. of the Micro-Optics Conference*, 10, B–7, (Jena, Germany, 2004).

[46] G. Emiliyanov, J. B. Jensen, O. Bang, P. E. Hoiby, L. H. Pedersen, E. M. Kjaer, and L. Lindvold, "Localized biosensing with topas microstructured polymer optical fiber," *Opt. Lett.* 32, 460-462 (2007).

[47] Y. Gao, N. Guo, B. Gauvreau, M. Rajabian, O. Skorobogata, E. Pone, O. Zabeida, L. Martinu, C. Dubois, and M. Skorobogatiy, "Consecutive Solvent Evaporation and Co-Rolling Techniques for Polymer Multilayer Hollow Fiber Preform Fabrication," *J. Mat. Res.* 21, 2246-2254 (2006)

[48] M. A. van Eijkelenborg, A. Argyros, and S. G. Leon-Saval, "Polycarbonate hollow-core microstructured optical fibre," *Opt. Lett.* 33, 2446 (2008).

[49] A. Dupuis, N. Guo, Y. Gao, N. Godbout, S. Lacroix, C. Dubois, and M. Skorobogatiy, "Prospective for biodegradable microstructured optical fibers," *Opt. Lett.* 32, 109 (2007).

[50] A. Argyros, M.A. van Eijkelenborg, S.D. Jackson and R.P. Mildren, "A microstructured polymer fibre laser," *Opt. Lett.*, 29, 1882-1884, (2004).

[51] A. Argyros, M.A. van Eijkelenborg, S.D. Jackson and R.P. Mildren, "Reply to comment on: A microstructured polymer fiber laser," *Opt. Letters*, 30, 1829-1830, (2005).

[52] M. C. J. Large, S. Ponrathnam, A. Argyros, N. S. Pujari, and F. Cox, "Solution doping of microstructured polymer optical fibres," *Opt. Express* 12, 1966 (2004).

[53] H. C. Y. Yu, A. Argyros, G. Barton, M. A. van Eijkelenborg, C. Barbe, K. Finnie, L. Kong, F. Ladouceur, and S. McNiven, "Quantum dot and silica nanoparticle doped polymer optical fibers," *Opt. Express* 15, 9989-9994 (2007).

- [54] H. C. Y. Yu, M. A. van Eijkelenborg, S. G. Leon-Saval, A. Argyros, and G. W. Barton, "Enhanced magneto-optical effect in cobalt nanoparticle-doped optical fiber," *Appl. Opt.* 47(35), 6497–6501 (2008).
- [55] M. A. van Eijkelenborg, M. C. J. Large, A. Argyros, J. Zagari, S. Manos, N. Issa, I. Bassett, S. Fleming, R. C. McPhedran, C. M. de Sterke, and N. A. P. Nicorovici, "Microstructured polymer optical fibre," *Opt. Express* 9, 319 - 327 (2001).
- [56] J. Zagari, A. Argyros, N. A. Issa, G. Barton, G. Henry, M. C. J. Large, L. Poladian, and M. A. van Eijkelenborg, "Small-core single-mode microstructured polymer optical fiber with large external diameter," *Opt. Lett.* 29, 818-820 (2004).
- [57] C. Zhang, D. J. Webb, K. Kalli, G. Emiliyanov, O. Bang, and E. Kjær, "Bragg grating inscription in TOPAS microstructured polymer optical fibre," in *Proc. 16th Int. Conf. Polymer Opt. Fiber*, paper SEN-I-1 (Turin, Italy, 2007).
- [58] X. Zhang, R. Wang, F. M. Cox, B. T. Kuhlmeier, and M. C. J. Large, "Selective coating of holes in microstructured optical fiber and its application to in-fiber absorptive polarizers," *Opt. Express* 15, 16270-16278, (2007).
- [59] X. Yang and L. Wang, "Silver nanocrystals modified microstructured polymer optical fibres for chemical and optical sensing," *Opt. Comm.* 280, 368-373, (2007).
- [60] J. Brandrup, E. H. Immergut, and E. A. Grulke, eds., *Polymer Handbook* (Wiley, 1999).
- [61] S. Bäumer, *Handbook of Plastic Optics* (Wiley-VCH, 2005).
- [62] P. P. Rousis, "Diffusion of water vapor in polymethyl methacrylate," *J. Membr. Sci.* 15, 141–155(1983).
- [63] T. Kaino, "Influence of water absorption on plastic optical fibers," *Appl. Opt.* 24, 4192–4195 (1985).
- [64] G. W. C. Kaye and T. H. Laby, *Tables of Physical and Chemical Constants*, 16th ed. (Longman, 1995).

- [65] C. Jiang, M. G. Kuzyk, J.-L. Ding, W. E. John, and D. J. Welker, "Fabrication and mechanical behavior of dye-doped polymer optical fiber," *J. Appl. Phys.* 92, 4-12 (2002).
- [66] D. X. Yang, J. Yu, X. Tao and H. Tam, "Structural and mechanical properties of polymeric optical fiber," *Mater. Sci. Eng., A* 364, 256-259 (2004).
- [67] T. Ishigure, M. Hirai, M. Sato, and Y. Koike, "Graded-index plastic optical fibre with high mechanical properties enabling easy network installations I" *J. Appl. Polym. Sci.* 91, 404-409 (2004).
- [68] C. R. Kurkjian, J. T. Krause, and M. J. Matthewson, "Strength and fatigue of silica optical fibers," *J. Lightwave Technol.* 7, 1360 (1989).
- [69] M. Aressy. *Drawing and Mechanical Properties of Plastic Optical Fibres*. MPhil Thesis. University of Birmingham; 2007.
- [70] T. Ishigure, M. Hirai, M. Sato, Y. Koike, "Graded-index plastic optical fiber with high mechanical properties enabling easy network installations. II," *J. Appl. Polym. Sci.* 91, 410-416 (2004).
- [71] D. J. Webb, and K. Kalli, "Polymer fiber Bragg gratings," IN: *Fiber Bragg Gratings Sensors: Thirty Years from Research to Market*. Cusano, Andrea; Cutolo, Antonello and Albert, Jacques (eds) Bentham eBooks, (2010). (In Press)
- [72] M. C. J. Large, L. Poladian, G. W. Barton, and M. A. van Eijkelenborg, *Microstructured polymer optical fibres* (Springer, Berlin, 2007).
- [73] M. C. J. Large, J. Moran, and L. Ye, "The role of viscoelastic properties in strain testing using microstructured polymer optical fibres," *Meas. Sci. Technol.* 20, 034014 (2009).
- [74] Topas® cyclic olefin copolymer Product Specification Document (Ticona Inc.).
- [75] M. J. Brekner, H. Deckers, and H. Osan, "Cycloolefin copolymers having low melt viscosity and low optical attenuation," U.S. patent 5,637,400 (June 10, 1997).
- [76] M. J. Brekner, H. Deckers, and H. Osan, "Cycloolefin copolymers having high tear strength and low optical attenuation," U.S. patent 6,214,951 (April 10, 2001).

[77] Asahi Glass Perfluorinated GIPOF Lucina Product Information, available online at [http://www.lucina.jp/eg\\_lucina/productsengf2.htm](http://www.lucina.jp/eg_lucina/productsengf2.htm)

[78] Asahi Glass CYTOP data sheet, available online at <http://www.agc.com/english/chemicals/shinsei/cytop/about.html>

[79] T. Kaino, M. Fujiki, and K. Jinguji, "Preparation of plastic optical fibers," *Rev. Electr. Commun. Lab.* 32, 478-488 (1984).

[80] T. Kaino, "Polymer optical fibers," in *Polymers for Lightwave and Integrated Optics: Technology and Applications*, L. A. Hornak, ed. (Marcel Dekker, New York, 1992).

[81] H. P. A. van den Boom, W. Li, P. K. van Bennekom, I. T. Monroy, and G.-D. Khoe, "High-capacity transmission over polymer optical fiber," *IEEE J. Sel. Top. Quantum Electron.* 7, 461 (2001).

[82] T. Kaino, "Influence of water absorption on plastic optical fibers," *Appl. Opt.* 24, 4192-4195 (1985).

[83] M.B. Reidenbach and F. Bodem, "Investigation of Various Transmission Properties and Launching Techniques of Plastic Optical Fibres Suitable for Transmission of High Optical Powers," *Opt. and Quantum Electronics.* 7, 355-360 (1975).

[84] J.M. Senior, *Optical fiber communications, Principles and Practice* (Prentice Hall Europe, 1992).

# 4

## **Photosensitivity of PMMA Based Polymer Optical Fibre**

In this chapter, several basic concepts of photochemistry are explained. The literature review of the photosensitivity of PMMA based bulk materials and polymer optical fibres are then conducted.

### **4.1 Introduction**

PMMA is the most important material in this work, as the POF used for FBG fabrication is mainly based on this kind of material. It is necessary to explain the

## 4. Photosensitivity of PMMA Based Polymer Optical Fibre

UV photosensitivity of PMMA, which is a very important property of the material for writing Bragg gratings. UV Photosensitivity is the ability of the UV light to induce refractive index change to the material. In this chapter, several basic photochemistry concepts will be explained. A brief introduction to the mechanisms of photorefractive effect of PMMA based bulk materials and fibres will be given in category of doped and undoped materials.

### 4.2 Fundamental Concepts of Photochemistry

Before starting over the introduction, several concepts relating to polymer chemistry which are the prerequisites to understand the whole chapter need to be briefly introduced:

#### Photo-degradation

Photo-degradation of polymer is kind of primary structure change due to irradiation of light. For polymers with chromophore, which is the light-absorbing group, backbone scission results predominantly from this direct absorption of light energy. [1] For polymers with impurities, which can absorb energy from light, scission of a chemical bond induce by light gives free radicals and is followed by reaction of these highly reactive free radicals with atmospheric oxygen. [1]

#### Photo-polymerization

In polymer chemistry, polymerization is the process of linking monomer molecules together in a chemical reaction to form three-dimensional networks or long polymer chains (macromolecules). [2] Polymerizations can be classified into step

#### 4. Photosensitivity of PMMA Based Polymer Optical Fibre

and chain polymerizations. Step polymerizations proceed by the stepwise reaction between the functional groups of reactants as in reactions, which occurs between any of the different-sized species present in the reaction system. In chain polymerization, an initiator is used to produce an initiator species with a reactive centre, which may be a free radical, or ion. Polymerization occurs by the propagation of the reactive centre by the successive additions of large numbers of monomer molecules in a chain reaction. [2] The growth of the polymer chain can be terminated, when the reactive centre is destroyed by one or more of a number of possible termination reactions.

Photo-polymerization is a kind of chain polymerization. With this technique, the syntheses of polymers by chain reactions are initiated upon the absorption of light by a polymerizable system or the polymerization of the small amounts of photoinitiators which is added into the formulation. Both radical and ionic chain polymerizations can be photoinitiated, depending on the appropriate type of initiators and monomers being used. In the case of already polymerized materials residual monomers in the polymer matrix can be photo-polymerized or lead cross-links between macromolecules. [1]

##### Photo-crosslinking

In polymer material system, the formation of intermolecular cross-links, for example, the covalent bond or ionic bonds between different polymer chains, combines all of the macromolecules to form a three-dimensional network structure. [3] Polymer chains are restricted from sliding by cross-linking, so that the average molecular mass, thus, the density of the material therefore increase. The cross-linking reactions in polymeric system can be performed by different

#### 4. Photosensitivity of PMMA Based Polymer Optical Fibre

methods, which rely on reactions of electronically excited pendant groups on the polymer chains or on reaction of various kinds of reactive species in the ground state that are photo-generated. [1]

Photo cross-linking is usually considered as a radical chain reaction where the initiation step is produced by a photochemical effect. Such photoinitiated cross-linking can be achieved through different pathways: an attack on macromolecules by free radicals, or the reaction of electronically excited photoinitiator molecules with lateral functional groups, or the reaction through pendant photofunctional groups (i.e. acrylate) [3] of the polymer, etc.

##### Photo-isomerisation

In chemistry, isomerisation is the process that one molecule is transformed into another molecule, which has exactly the same chemical formula but different arrangement of the atoms within the molecules, leading to different properties (i.e. refractive index modulation). Such molecules with this ability are called isomers. Most of the isomers that will be mentioned in this chapter are *trans-cis* isomers. Isomerisation of optical isomers can be activated by irradiation, leading to so called photo-isomerisation. The polymer doped with optical isomers will become photosensitive, as these isomers exhibit different refractive indices in their different isomer states.

### **4.3 Photosensitivity of PMMA Based Bulk Materials**

Before looking at the photosensitivity of PMMA based POF, the historical review of photosensitivity in such bulk materials is necessary.

### 4.3.1 Photosensitivity of Undoped PMMA Materials

#### 4.3.1.1 193nm and 248nm UV Irradiation

The refractive index modification of PMMA by UV laser light at 193nm and 248nm was reported by Wochnowski et al in 1999. [4] The PMMA samples were irradiated in a vacuum chamber, where a mass spectrometer was integrated to examine the defragmentation products ablated. After irradiation, the PMMA samples were studied by XPS and FTIR spectroscopy. In addition, the refractive index modification information was measured. In this experiment, the laser induced photochemical reaction in PMMA is photodegradation, as shown in Figure 3-1.



Figure 4- 1: Degradation scheme of irradiated PMMA [4]

#### 4. Photosensitivity of PMMA Based Polymer Optical Fibre

##### 248nm

The PMMA sample was initially irradiated by UV radiation at 248 nm and a low fluence of  $15\text{mJ}/\text{cm}^2$ . After this process, being able to detect a free methyl formate radical indicated that the complete side chain scission was observed. Furthermore, after continues irradiation at a fluence of  $30\text{mJ}/\text{cm}^2$  or higher, the degradation of free ester radical either into methane and  $\text{CO}_2$  or into CO and methanol was detectable by means of mass spectrometry and spectroscopy. Finally, during the period of the prolonged exposure at 248nm, a radical electron forms due to the complete separation of the side chain of PMMA and it destabilized the polymer main chain leading to its scission.

##### 193nm

Irradiation by 193nm can only cause a partial separation of the side chain. No radical electron was created and hence, no main chain scission occurred, during the degradation process.

Refractive index of the PMMA samples after irradiation at either wavelength increased, due to the side chain separation, as shown in Figure 4-2. Following the removal of side chains, molecules in PMMA are contracted by Van der Waals forces, [5] leading to local mechanical density increasing. Figure 2 also gives the following information: Firstly, by comparing between the refractive index variation of 248nm and 193nm irradiated samples, the more side chains are separated, the more the refractive index will be increased; Secondly, the falling of the refractive index at high irradiation may be explained by the degradation of the main polymer backbone. Conducted from the graph, the main chain stability of the 193nm UV

#### 4. Photosensitivity of PMMA Based Polymer Optical Fibre

irradiated sample do better than that of 248nm one, which is consistent with the previous observation.



Figure 4- 2: Refractive index modification of irradiated PMMA [4]

##### 4.3.1.2 325nm UV Irradiation

In 1970, Tomlinson et al. reported a photosensitivity of PMMA materials at 325nm UV radiation. [6] In their experiment, to achieve the significant increase of the refractive index of the irradiated sample, the correct preparation process of the PMMA was essential. This involved a pre-process of oxidation of the monomer methylmethacrylate (MMA), before the PMMA was prepared with distilled monomer at 40°C in an oxygen free environment and the polymerisation was initiated by a 254nm mercury (Hg) lamp or using chemical imitator azobisisobutyronitrile (AIBN), in the concentrations of 50-200 mg/liter. The oxidation was done at different levels, for low levels by auto oxidation in the dark environment, or for higher levels by stirring the distilled monomer with presence of air, for 48 hours while irradiating the sample with a 5 W low pressure Hg lamp. No photosensitivity on UV irradiation was observed from the freshly distilled liquid monomer without pre-oxidation step. To be noted here, the grating fabricated in

#### 4. Photosensitivity of PMMA Based Polymer Optical Fibre

this way required around 200 hours for self-developing, before reaching a constant refractive index state and during the developing period, heating the sample at certain temperature can increase the final refractive index change. [7] Index changes of up to  $3 \times 10^{-3}$  along with a recording spatial resolution better than 200 nm were observed by Tomlinson et al, accompanied by a density increase of 0.8%. They claimed that the dominant effect arouse the change of refractive index was mainly due to density increase, as no evidence of growth in molecular polarizability was observed, and they also speculated that the density increase was due to cross-linking as peroxide products were working as cross-linking agents. The density increasing on irradiation was also confirmed by Bowden et al. [8]. They found that weakly photosensitive samples had higher densities than those strongly photosensitive ones and heating samples to 100°C can also cause an increase in density and removing the photosensitivity at the same time. They concluded that the mechanism responsible may be induced by the polymerization of unreacted monomer in the sample, photoinitiated by the peroxide. They proved such mechanism by using electron spin resonance, and the experimental results indicated that the concentration of free radicals increased more than an order of magnitude after irradiation.

##### **4.3.1.3 Femtosecond Laser Induced Photosensitivity**

When the sufficiently high intensity femtosecond (fs) laser beam is focused into the PMMA material, which is transparent to the fundamental wavelength of the fs laser, the absorption of the radiation by PMMA at the focus will occur via effects like multiphoton ionization. This significant optical absorption leads to irreversible modification of the composition of the PMMA and consequently, it alters the

#### 4. Photosensitivity of PMMA Based Polymer Optical Fibre

refractive index inside the material. Up to now, the modification mechanism of PMMA irradiated by the fs laser is still not fully discovered. Recently, almost all the studies on the fs laser irradiation induced photosensitivity in PMMA are reported according to the refractive index change of the material ( $\Delta n$ ). Zoubir et al demonstrated that tubular waveguides with negative  $\Delta n = 2 \times 10^{-3}$  were fabricated inside in a slab of PMMA using a Ti:sapphire (800nm, 30fs, 20-nJ/pulse) laser with high repetition rate of 25MHz. [9] However, Sowa et al fabricated the first symmetric waveguides in PMMA with positive  $\Delta n = 4.6 \times 10^{-4}$  by fs laser (85 fs, 800 nm, 1 kHz, 27-nJ/pulse). [10] To be noted here, the different plus-minus sign of  $\Delta n$  could be due to different repetition rate of fs laser, PMMA composition or other undisclosed reasons.

The mechanism of the refractive index change has been studied and discussed in many works. Sowa et al explained the mechanism merely as chain scission causing volume contraction. [10] Moreover, in another work, they explain the volume contraction as being due to the thermal expansion causing tensile stress to the surrounding area [11] Wochnowski et al wrote volume gratings in PMMA with a fs laser (140 fs, 775 nm, 1 kHz, 800  $\mu$ J/pulse) and claim the multiphoton process raised by fs laser may be similar to the one-photon modification process induced by ns UV-excimer laser radiation, [4] in which the exposure dose determines a combination of crosslinking and degradation. [12] Recently, upon the success of their previous work in discovery of fs laser induced depolymerisation modification of pure grade PMMA, [13] Baum et al presented a detail investigation of the modification mechanism. [14] They confirmed the positive  $\Delta n$  was due to a combination of depolymerization and crosslinking. They tried to determine the contributions of detected photochemical changes

#### 4. Photosensitivity of PMMA Based Polymer Optical Fibre

corresponding to the observed  $\Delta n$  by using various analytical techniques and their results indicated that both depolymerization and crosslinking contribute to the index change with similar magnitude ( $\Delta n = 5 \times 10^{-5}$  for each component), however the sum of the two magnitudes were unable to explain their previous presented total measured refractive index change, which was up to  $\Delta n = 4 \times 10^{-3}$  [13]. This suggested that other undisclosed effects related to the modification might exist.

##### **4.3.2 Photosensitivity of PMMA With Photo-chemically Active Dopants**

PMMA materials doped with some photochemically active compounds will show photorefractive effect under UV irradiation, thus photosensitivity will be introduced into PMMA. The photochromic compounds, Azo dyes were doped into PMMA to induce photosensitivity. Azo dyes exist in two spatial forms, the trans and cis configuration. A trans-cis isomerization can be photoinitiated by interaction of the photoactive azobenzene with light. This results in a change of the molecular polarizability, leading to a change in refractive index. [15] Tanio et al studied the photo-induced refractive index change of azobenzene doped PMMA films. [16] Azobenzene has an intensive absorption at 320nm due to pi-pi\* transition and when azobenzene was exposed to UV light at higher wavelength (350-410nm), the absorption decreased. Along with the decrease in absorption, the refractive index of the film decreased. In addition, the refractive index change correlated well with the amount of the isomerization of azobenezene. Other compounds, like stilbene can also be used to induce photosensitivity in PPMA. Imamura et al investigated the trans- to cis photoisomerisation of 313nm polarised UV light

#### 4. Photosensitivity of PMMA Based Polymer Optical Fibre

irradiated PMMA material, containing the stilbene compound, 4-methoxystilbene. [17] The optical nonlinearity increases with the isomerization from trans- to cis- structure, hence it causes the decrease of refractive index of PMMA material matrix containing the stilbene derivative side chain in the main chain backbone, [18] as the refractive index of stilbene compounds at trans- structure is higher than that of cis- structure.

### **4.4 Photosensitivity of PMMA Based Polymer Optical Fibres**

Since 1990s, FBGs have been fabricated on PMMA based POF by several research groups, most of which use UV laser at 325nm. During the inscription process, unlike the long self-developing period of grating inscribed in PMMA bulk sample, grating in POF usually appears in a few minutes to an hour, depending on the chemical constituent of fibre core material.

Xiong et al reported the first POFBG in their home made step-index POF in 1999. [19] At the fibre preform preparing stage, to increase the photosensitivity of the core of their fibre, the core monomer, which contain methyl methacrylate(MMA), ethyl methacrylate (EMA) and benzyl methacrylate (BzMA), was prepared with low level lauryl peroxide (initiator) and low chain transfer agent and polymerized at the temperature lower than glass transition temperature of the polymer preform. POF Grating with approximate reflectivity of 80% was written on the fibre by using 325nm light from a frequency-doubled MOPO pumped by a frequency-tripled Nd:YAG pulse laser and an interferometer setup. The magnitude of estimated

#### 4. Photosensitivity of PMMA Based Polymer Optical Fibre

refractive index change was  $10^{-4}$ . No evidence of the index alteration mechanism was given by the authors, who only mentioned that the index increase might be due to cross linking or polymerization initiated by the UV light.

To understand the POFBG formation dynamics, a further study of the grating inscription process was carried out by people from the same group. [20] In this experiment, FBG was fabricated in the fibre with BzMA doped PMMA core and PMMA cladding by using 325nm light from the same pulse laser with intensity of  $60 \text{ mw/cm}^2$  as before (pulse width: 5 ns, repetition rate: 10 Hz). In the first 62 minutes, the refractive index modulation increase approximately linearly to  $0.2 \times 10^{-3}$  in a slow process. The authors claim that the grating formed at this stage was Type I POF grating, by analogy with silica FBGs [ref]. During the fabrication process at this stage, the reflection spectra and transmission spectra were complimentary, indicating low losses were induced by the Type I POF grating and in addition, the blue Bragg wavelength shift was observed, which indicated that the index change induced by Type I grating is negative. After 62 minutes, the index increased rapidly into  $2 \times 10^{-3}$ . The authors took the grating at this stage as Type II grating. Comparing with the spectra of Type I POF grating, the spectra of the Type II grating possesses broader bandwidth and larger losses at short wavelength region. After the fabrication finished, the Type II POF grating was then observed under microscope and the apparent damage at the core-cladding interface was observed, indicating that the Type II POF grating and the Type II silica grating have similar characteristics. Apart from this work, authors also observed another totally different growth behaviour at lower power UV exposure ( $45 \text{mw/cm}^2$ ) by using the same experiment set-up. [21] During the inscription period, the reflection power of the grating spectra grew continuously in the first 28

#### 4. Photosensitivity of PMMA Based Polymer Optical Fibre

minutes and kept roughly constant in the next 20 minutes. After these two stages, the reflection started decreasing and at 88 minutes, the reflection peak of the grating spectra was near disappeared. Meanwhile, the UV illumination was stopped at this point, with the grating spectra monitoring system still working and the authors found that the POFBG gradually regenerated to the constant maximum reflection in 8 hours. They could not explain this growth behaviour with proof and only speculated the regrowing phenomena of the POFBG might be due to the relaxation of the thermal stress with time, which might induce refractive index change.

The discovery of the photosensitivity of commercially available single mode step index POF was achieved by Harbach et al recently. [22] The core of this kind of fibre was doped with polystyrene to increase the refractive index and FBGs were fabricated in the core of the fibre by using a 308nm pulse laser. They speculated that the photosensitivity is induced by the doped polystyrene copolymer, which acted as absorption centres that then lead to photo-thermal degradation. [23]

Furthermore, nominally pure PMMA based POF even shows photosensitivity, which up to the date, still cannot be entirely explained. Dobb et al [24] first presented the FBG fabrication in this kind of single material (pure PMMA) based single mode microstructured POF by using a 30mW 325nm CW He-Cd laser and phase mask technology. During inscription, the grating normally takes 30-60 minutes to reach saturation and the grating strength is quite stable in a long period after irradiation. The mechanism of this observed photosensitivity need more research as it looks quite different from that of observed in bulk PMMA by Tomlinson etc., which requires a long time for auto-development.

#### 4. Photosensitivity of PMMA Based Polymer Optical Fibre

In recent years, people also attempted to add photo reactive dopants into the core of the fibre to improve the photosensitivity of POF and have already achieved success: Luo et al [25] doped the photosensitive dye, benzildimethylketal (BDK) [26-27] into the core of the PMMA POF and fabricated FBGs in such fibre with a 355nm frequency-tripled Nd:YAG pulse laser (10 Hz, 6ns pulse width). Yu et al [28] and Zhang et al [29] were able to fabricate FBGs in Trans-4-stilbenemethanol doped POF, which is one member of stilbene derivatives [30] by using frequency doubled 532nm pulse laser pumped, 325nm pulsed dye laser and 325nm CW He-Cd laser respectively.

#### **4.5 Conclusion**

A brief review of the photosensitivity of the PMMA based bulk materials and polymer optical fibres was conducted in this chapter. To start with, several fundamental concepts of photochemistry were introduced, including photo-degradation, photo-polymerization, photo-crosslinking and photo-isomerisation. The photosensitivity of PMMA based bulk materials and PMMA based optical fibres were then reviewed, as shown in Table 4-1.

#### 4. Photosensitivity of PMMA Based Polymer Optical Fibre

Table 4-1: Photosensitivity of PMMA based bulk materials and PMMA based optical fibres

##### Undoped PMMA Bulk Materials

Material Type	Undoped PMMA Bulk		
Light source	193nm and 248nm UV	325nm UV	Femtosecond Laser
Photosensitivity Mechanism	Photo-degradation	Photo-crosslinking, Photo-polymerisation	Photo-crosslinking and Photo-degradation (Not fully discovered)

##### Doped PMMA Bulk Materials

Material Type	Doped PMMA Bulk	
Dopands	Azo dyes	Stillbene compounds
Light source	350-410nm UV	313nm UV
Photosensitivity Mechanism	Photo-isomerisation	

##### PMMA Based Polymer Optical Fibre

Material Type	PMMA Based Polymer Optical Fibre			
Dopands	BzMA	Polystyrene	N/A	Trans-4-stillbene methanol
Light Source	325nm Pulse	308 Pulsed	325nm CW	325nm Pulse
Photosensitivity Mechanism	Photo-crosslinking, Photo-polymerisation	Photo-thermal degradation	Not fully discovered	Photo-isomerisation

#### 4. Photosensitivity of PMMA Based Polymer Optical Fibre

In conclusion, some of the mechanisms that induced photosensitivity to PMMA have been explained, however, there is clearly still a lot of research to be done to disclose those complicated cases.

## References

- [1] W. Schnabel. *Polymers and Light: Fundamentals and Technical Applications*, WILEY-VCH: Weinheim, 2007
- [2] G. G. Odian. *Principles of Polymerization*, 4th ed.; Wiley-Interscience: Hoboken, NJ, 2004.
- [3] A. Bhattacharya, J. M. Rawlins, P. Ray, *Polymer Grafting and Crosslinking*; Wiley: Hoboken NJ, 2008.
- [4] C. Wochnowski, S. Metev, and G. Sepold, "UV-laser-assisted modification of the optical properties of polymethylmethacrylate," *Appl. Surf. Sci.* 154-155, pp.706-711, 2000.
- [5] A. Schmoldt, Dissertation, TU Berlin, 1994.
- [6] W. J. Tomlinson, I. P. Kaminow, E. A. Chandross, R. L. Fork, W. T. Silfvast, "Photoinduced refractive index increase in poly(ethylmethacrylate) and its applications," *Appl. Phys. Lett.* 1970; 16(12): 486-9.
- [7] J. M. Moran, I. P. Kaminow, "Properties of holographic gratings photoinduced in polymethyl methacrylate," *Appl. Opt.* 12,1964-70, (1973).
- [8] M. J. Bowden, E. A. Chandross, I. P. Kaminow, "Mechanism of the photoinduced refractive index increase in polymethyl methacrylate," *Appl. Opt.* 13, 112-7, (1974).
- [9] A. Zoubir, C. Lopez, M. Richardson, and K. Richardson, "Femtosecond laser fabrication of tubular waveguides in PMMA," *Opt. Lett.* 29, 1840–1842 (2004).
- [10] S. Sowa, W. Watanabe, T. Tamaki, J. Nishii, and K. Itoh, "Symmetric waveguides in PMMA fabricated by femtosecond laser pulses," *Opt. Express* 14, 291–297, (2006).
- [11] W. Watanabe, S. Sowa, T. Tamaki, K. Itoh, and J. Nishii, "Three-dimensional waveguides fabricated in PMMA by a femtosecond laser," *Jpn. J. Appl. Phys.* 45, L765–L767, (2006).

#### 4. Photosensitivity of PMMA Based Polymer Optical Fibre

- [12] C. Wochnowski, Y. Cheng, K. Meteva, K. Sugioka, K. Midorikawa, and S. Metev, "Femtosecond-laser induced formation of grating structures in planar polymer substrates," *J. Opt. A, Pure Appl. Opt.* 7, 493–501, (2005).
- [13] A. Baum, P. J. Scully, M. Basanta, C. L. P. Thomas, P. R. Fielden, N. J. Goddard, W. Perrie, and P. R. Chalker, "Photochemistry of refractive index structures in PMMA by femtosecond laser irradiation," *Opt. Lett.* 32, 190–192, (2007).
- [14] A. Baum, P. J. Scully, W. Perrie, D. Liu, and V. Lucarini, "Mechanisms of femtosecond laser-induced refractive index modification of poly(methyl methacrylate)," *J. Opt. Soc. Am. B* 27, 107–111 (2010).
- [15] W. J. Tomlinson and E. A. Chandross, "Organic photochemical refractive index image recording systems," in *Advanced Photochemistry* (Wiley Interscience, New York, 1980)
- [16] N. Tanio and M. Irie, "Refractive index of organic photochromic dye-amorphous polymer composites," *Jpn. J. Appl. Phys.* 33, p3942-3946, (1994).
- [17] Y. Imamura, Y. Yamaguchi and Q. Tran-Cong. "Polarized light-induced photoisomerization in glassy poly(methyl methacrylate) and local relaxation processes of the polymer matrix," *J. Polym. Sci, Part B: Polym. Phys.* 38, pp. 682–690, (2000).
- [18] T. Zyung, W. Y. Hwang, and J. J. Kim, "Photochemically formed refractive index profiles in nonlinear optical polymer thin films," *Appl. Phys. Lett.* 64, 3527 (1994) .
- [19] Z. Xiong, G. D. Peng, B. Wu, P.L. Chu, "Highly tunable Bragg gratings in single-mode polymer optical fibers," *IEEE Photon. Technol. Lett.* 11, 352-4, (1999).
- [20] H. Y. Liu, H. B. Liu, G. D. Peng, P. L. Chu, "Observation of type I and type II gratings behaviour in polymer optical fiber," *Opt. Commun.*, 220, 337-43, (2003)
- [21] H. B. Liu, H. Y. Liu, Peng GD, G. D. Peng, P. L. Chu, "Novel growth behaviors of fiber Bragg gratings in polymer optical fiber under UV irradiation with low power," *IEEE Photon. Technol. Lett.* 16, 159-61, (2004)

#### 4. Photosensitivity of PMMA Based Polymer Optical Fibre

- [22] G. N. Harbach, H. G. Limberger, and R. P. Salathé, "Influence of Humidity and Temperature on Polymer Optical Fiber Bragg Gratings," in Bragg Gratings, Photosensitivity, and Poling in Glass Waveguides, OSA Technical Digest (CD) (Optical Society of America, 2010), paper BTuB2.
- [23] N. G. Harbach, "Fiber bragg gratings in polymer optical fibers." PhD thesis Lausanne: EPFL, 2008.
- [24] H. Dobb, D. J. Webb, K. Kalli, A. Argyros, M. C. J. Large, and M. A. van Eijkelenborg, "Continuous wave ultraviolet light-induced fiber Bragg gratings in few- and single-mode microstructured polymer optical fibers," *Opt. Lett.* 30(24), 3296–3298 (2005).
- [25] Y.H. Luo, Q.J. Zhang, H.Y. Liu, and G.D. Peng, "Gratings fabrication in benzildimethylketal doped photosensitive polymer optical fibers using 355 nm nanosecond pulsed laser," *Opt. Lett.* 35, 751-753, (2010).
- [26] H. Franke, "Optical recording of refractive-index patterns in doped poly-(methyl methacrylate) films," *Appl. Opt.* 23, 2729-2733, (1984).
- [27] O. H. Park, J. I. Jung, and B. S. Bae, "Photoinduced condensation of sol-gel hybrid glass films doped with benzil dimethyl ketal," *J. Mater. Res.* 16, 2143, 2001.
- [28] J. M. Yu, X. M. Tao, and H. Y. Tam, "Fabrication of UV sensitive single-mode polymeric optical fiber," *Opt. Lett.* 29, 156 (2004).
- [29] Z.F. Zhang, C. Zhang, X.M. Tao, G.F. Wang, "Inscription of Polymer Optical Fiber Bragg Grating at 962 nm and Its Potential in Strain Sensing," *IEEE Photon. Technol. Lett.* 22, 1562 – 1564, (2010).
- [30] G. H. Brown. *Photochromism*, Wiley: New York, 1971.

# 5

## **Bragg Grating Inscription in Polymer Optical Fibre**

This chapter introduces the set-up for fibre Bragg grating inscription and then give details of the several different kinds of polymer optical fibre Bragg gratings fabricated with this arrangement. In the end, the effect of the zeroth-order diffraction of a phase mask on the creation of Bragg gratings in polymer optical fibres is discussed.

### **5.1 Introduction**

Bragg gratings have been inscribed in polymer optical fibres using conventional techniques that have been utilised for the inscription of gratings in silica optical

## 5. Bragg Grating Inscription in Polymer Optical Fibre

fibres, for example, POFBG has been fabricated using the phase mask technique [1] or a ring interferometer arrangement [2], with grating inscription undertaken using continuous wave or pulsed laser sources operating at either 325 nm [1] or 355 nm [2]. Up to date, the strongest POFBG achieved is with 28 dB transmission rejection and a linewidth less than 0.5 nm [3]. The inscription time can vary from a few minutes [4] to over one hour [5], depending on the different photosensitivity induced into the core of the fibre. Upon those successful experiences, FBGs are successfully inscribed in several kinds of POF in this thesis, i.e. PMMA based mPOF, TOPAS mPOF and PMMA based doped single mode step index POF.

### 5.2 Polymer Optical Fibre Bragg Grating Inscription Setup

The experimental arrangement for POFBG inscription is shown in Figure 5-1, based on phase mask technique.

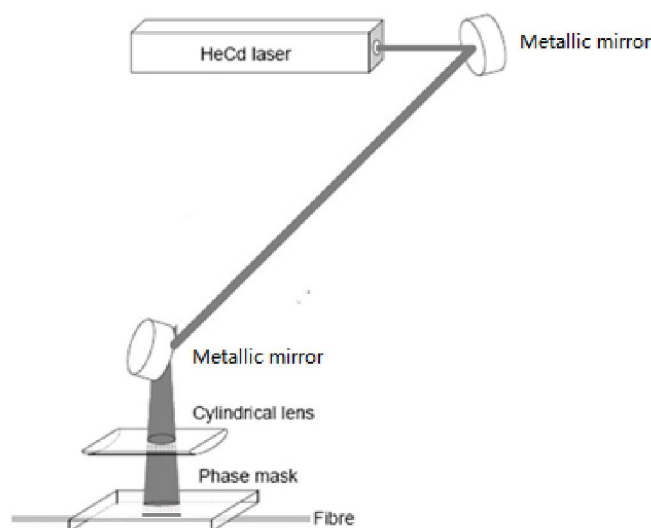


Figure 5- 1: Experimental arrangement for FBG inscription.

## 5. Bragg Grating Inscription in Polymer Optical Fibre

A continued-wave helium cadmium laser (KIMMON IK5652R-G) operating at 325nm and ~30mW of laser power is used in the system. The reflection mirror stands by the laser is controlled by a motorised linear stage (Newport MTM100CC.1) and a motion controller (Newport MM4006), enabling both static and scanning inscription of the gratings. After cleaving of the fibre, POF is mounted into v-grooves (Mellis Griot), thereby supported along its length in order to minimize the effects of air currents and laser-induced heating on the fibre position. The v-grooves are attached to a three-axis translation stage (Mellis Griot). The O/E Land phasemask for 325nm UV source (mask period = 1057.2nm), which is capable for grating fabrication up to 6mm long is placed on two pieces of polyimide tape stuck on the V-groove which is used to provide minimum distance between the fibre and phasemask to avoid the contact between them and the thickness of tape can be adjusted with the variation of the diameter of the POFs by using different numbers of layers. A static laser beam (beam width = 1.2mm) is focused vertically onto the fibre by a cylindrical lens (focus length = 10cm) through the phase mask. Therefore, the laser intensity irradiated on the fibre is approximately  $200\text{mW}/\text{mm}^2$  and the grating length is therefore equal to the beam width.

With this set-up, the gratings can be monitored in reflection during inscription using broadband ASE light source (Thorlabs ASE-FL7002-C4, 5 mW output power, and operating wavelength range of 1530–1610nm, shown in Figure 5-2) and optical spectrum analyser (OSA, HP70004A), as illustrated in Figure 5-3.

## 5. Bragg Grating Inscription in Polymer Optical Fibre



Figure 5- 2: Output spectrum of the Thorlabs ASE-FL7002 broadband light source. [6]

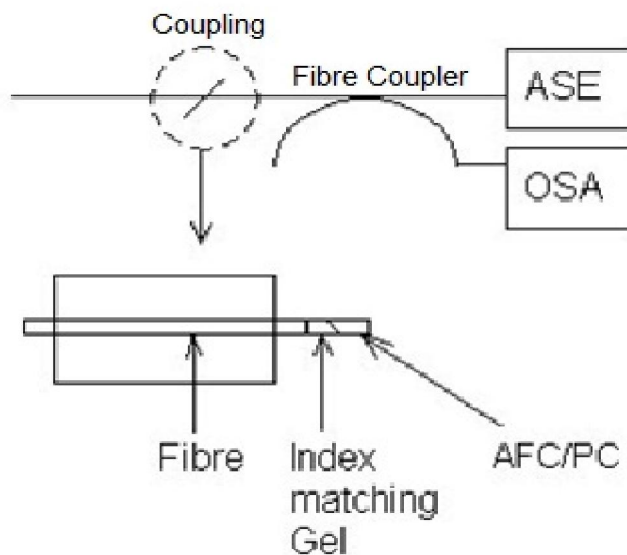


Figure 5- 3: Diagram of grating monitoring setup.

A C-band 2X2 single mode fibre coupler is used to monitor the grating in reflection. One out arm of the coupler is spliced with single mode AFC/PC pigtail which was used to couple the light into the POF. Between the AFC connector and the POF, a small drop of index matching gel was used to reduce the Fresnel reflections and

## 5. Bragg Grating Inscription in Polymer Optical Fibre

help with coupling the light from connector to fibre. The two input arms of the coupler, spliced with single mode FC/PC pigtails were correspondingly connected to the light source and the OSA. At first, the light source was a He-Ne laser working at 633nm. By adjusting the translation stage, the maximum throughput of POF at 633nm is obtained. Then the light source is switched to the broadband ASE source. This is due to the invisible infra-red Bragg wavelength of the grating. In addition, the gratings can also be monitored in transmission. Instead of using the coupler, light can be directly coupled into one end of the fibre from the broadband light source and out of the fibre from the other end to the OSA by using butt coupling method and FC/PC patch cord.

Before the end of this section, the cleaving of the POF is worth mentioning. POF cannot be cleaved by cleavers for silica fibres but by blade cutting. There are a few studies [7-8] investigating the cleaving of POFs and they claim that the quality of the cutting surface of the fibre is mainly affected by the temperature of the fibre and blade together with the speed of the cut. In this thesis, the PMMA based fibres are found to be well cleaved by hand on a hot plate (Agar Scientific) with a razor blade (Agar Scientific) at approximately 80°C and TOPAS based fibres are found to be easily cleaved by a razor blade at room temperature. The quality of the cut is verified using a microscope (Carl Zeiss Axioscope 2 mot plus) and will be shown in the next section.

## 5.3 Fabricated Polymer Optical Fibre Bragg Gratings

### 5.3.1 Microstructured Polymer Optical Fibre Bragg Gratings

#### 5.3.1.1 PMMA Based Single Mode Microstructured Polymer Optical Fibre Bragg Gratings

The PMMA SMmPOF used in Bragg grating fabrication is supplied by the Optical Fibre Technology Centre, The University of Sydney, Australia. The cross section of the fibre after cleaving is shown in Figure 5-4. The fibre used consisted of pure PMMA and was fabricated using the method described in reference [9]. The sides of the fibre were flattened in order to investigate whether this geometry would aid alignment of the laser beam relative to the holes in the fibre, however no benefit was observed. The fibre has an outside diameter of  $150\mu\text{m}$  (round edges) and  $115\mu\text{m}$  (flat edges) and a core diameter of  $14.6\mu\text{m}$ ; the core being surrounded by 60 air holes with diameters ( $d$ ) of  $2.6\mu\text{m}$  and a separation ( $\Lambda$ ) of  $8.6\mu\text{m}$  [9] giving  $d/\Lambda=0.3$ . Note, this fibre is the unique PMMA mPOF mentioned in the author's experiments within this thesis.

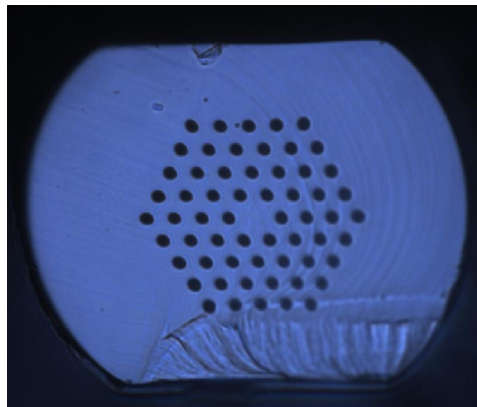


Figure 5- 4: Cross section of PMMA SMmPOF.

## 5. Bragg Grating Inscription in Polymer Optical Fibre

By using the arrangement described in the last section, Bragg gratings were successfully inscribed in a 5cm long PMMA SMmPOF at ambient condition and monitored in reflection during inscription. The exposure time was around 44 minutes until reaching the grating saturation. Such long exposure time indicate that this kind of fibre is not suitable for longer FBG inscription by using scanning inscription method, otherwise the writing process will be time consuming and the requirement for the system stability will be very high. The growth characteristics of the grating inscription process are shown in Figure 5-5, with data collected every 30 seconds. Note the break in the graph is due to the minor re-alignment of the butt coupling during inscription.

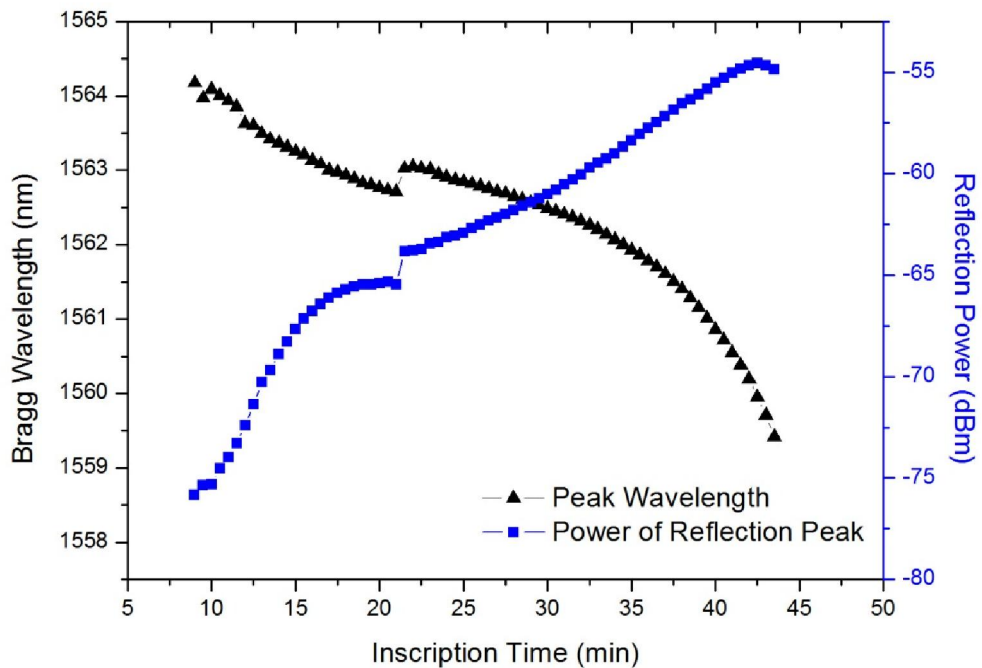


Figure 5- 5: Bragg wavelength shift and reflection power change during grating writing.

The resulting SMmPOFBG spectrum after irradiation stopped, as shown in Figure 5-6 had a wavelength of 1563.4nm, a FWHM of 4.5nm, a length of 1.2mm and a reflection power of 20 dB above the noise level. (OSA resolution bandwidth is

## 5. Bragg Grating Inscription in Polymer Optical Fibre

0.5nm) To be noted here, this Bragg grating was unable to be observed by using a  $\times 100$  oil immersion lens and microscope (Carl Zeiss Axioscope 2 mot plus), which may be due to low visibility of the fringes as the fibre contain many holes so that the observation is affected.

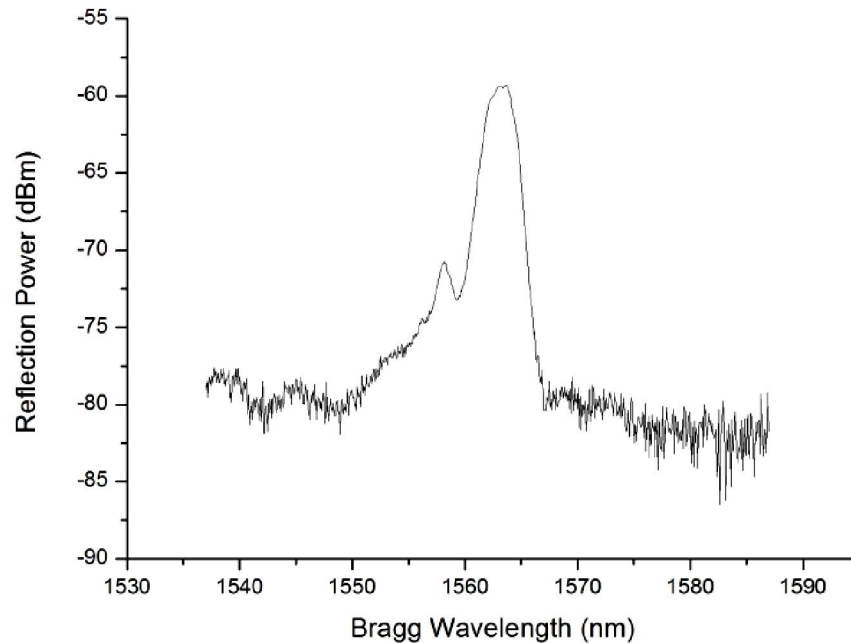


Figure 5- 6: Reflection Spectrum of the SMmPOFBG.

The Bragg wavelength of the grating is chosen purely for convenience in that most of the equipment available in the lab operates in this wavelength range. Attempts were made to observe the grating in transmission, without success, possibly due to the short and weak grating and high attenuation of the fibre at this wavelength region, which is measured to be around 0.82 dB/cm by cut back technique, as shown in Figure 5-7.

## 5. Bragg Grating Inscription in Polymer Optical Fibre

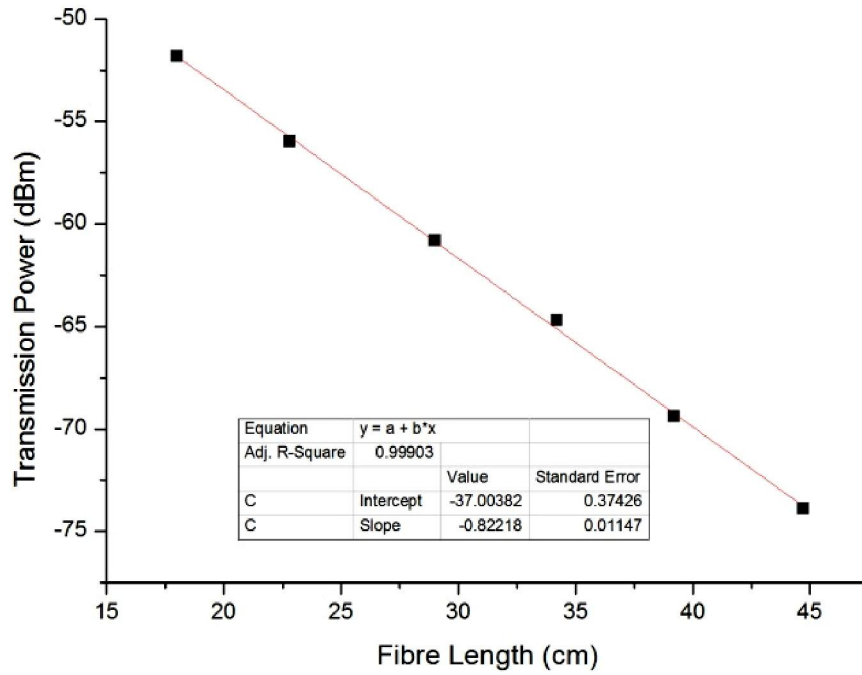


Figure 5- 7: Cut back measurement of the transmission loss of the PMMA mPOF.

Though the reflectivity of the grating is unknown, as the transmission spectrum of the grating is not able to be obtained, the induced dc average refractive index modulation  $\Delta n_{dc}$  is able to be estimated roughly by using the following equation [10]:

$$\Delta n_{dc} = \frac{n_{eff} \Delta \lambda_B}{\eta \lambda_B} = \frac{\Delta \lambda_B}{2\eta \Lambda} \quad (5.1)$$

where  $\Delta \lambda_B$  is the Bragg wavelength shift by the mean refractive index modulation,  $\Lambda$  is the period of the phase mask,  $\eta$  represents the fraction of the integrated fundamental-mode intensity contained in the core and approximately assumed to be 1 here. During the writing process, the Bragg wavelength of the grating shifts to the shorter wavelength and has a total shift of 6nm. This negative wavelength shift is caused by three factors which have been proved by Harbach et al. [11]: 1. The

## 5. Bragg Grating Inscription in Polymer Optical Fibre

negative mean refractive index change  $\Delta n_{dc}$ ; 2. The Bragg wavelength shifts to lower wavelengths with increasing temperature which is induced by the heating effect from laser. (The thermo-optic coefficient of the PMMA is negative); 3. The Bragg wavelength shifts to lower wavelengths due to a reduction of humidity within the fibre, which lead to the grating pitch and mean polarizability changing, when laser irradiate on the fibre [11]. In our case, during inscription the Bragg wavelength shifted -4.6nm, and after writing stopped, the heating effect to the fibre disappear and the Bragg wavelength shift back 4nm, according to the captured final spectrum in Figure 5-6. So the net Bragg wavelength shift is -0.6nm and the mean index modulation is estimated to be  $-0.6/(1057.2/2)=3 \times 10^{-4}$ . To be noted here, the wavelength shift induced by factor 3 is not considered in this case, because after stopping the illuminating of the fibre, the water content in the fibre may return to its previous equilibrium value, due to absorb water from the air. Anyway, the estimation of the mean refractive index modulation here is rough.

### **5.3.1.2 TOPAS Based Single Mode Microstructured Polymer Optical Fibre Bragg Grating**

The few mode TOPAS mPOF used in this thesis is fabricated at COM•DTU at the Technical University of Denmark (DTU), from preforms made at the Danish Polymer Centre at DTU. The preform is made in a vacuum oven from TOPAS COC granules of the grade 8007 and has a diameter of 50mm and a length of 85mm. Three rings of 2mm holes are then drilled into the preform in a triangular structure and a fibre is drawn at about 140°C with no pressure applied to the air holes. The resulting few moded fibre had an outside diameter of 340µm, a core diameter of 60µm and a hole size of 20micron (Figure 5-8). The smaller hole size

## 5. Bragg Grating Inscription in Polymer Optical Fibre

of the third ring is an indication of a non-uniform heat distribution inside the preform during the drawing process.

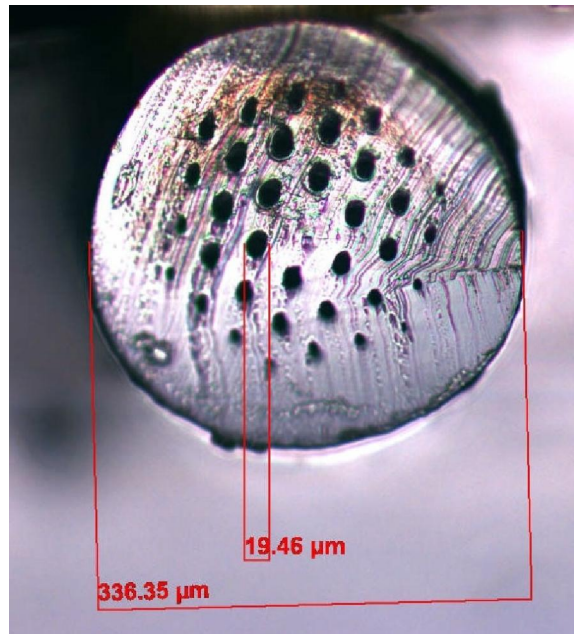


Figure 5- 8: Microscope picture of the end facets of the TOPAS mPOF.

By using the arrangement already described, Bragg gratings are successfully inscribed in TOPAS mPOF at ambient condition and monitored in transmission during inscription. Normally it required around 25 minutes of exposure to approach a maximum grating reflectivity, as shown in Figure 5-9(a); data collected every 30 seconds. After inscription, the butt coupling is slightly optimised and the final transmission spectra of the grating is recorded and revealed a Bragg wavelength around 1596nm, a FWHM of 1.5nm, a length of 1.2mm and a transmission power of 14 dBm, see Figure 5-9(b). (OSA resolution bandwidth is 1nm) From the position of the resonance, the effective refractive index of the propagating mode in the TOPAS mPOF can be deduced by calculation, which is around 1.51 and this value is identical to that of the data sheet. The reflectivity of the grating is can be calculated to be 96% from following equation:

## 5. Bragg Grating Inscription in Polymer Optical Fibre

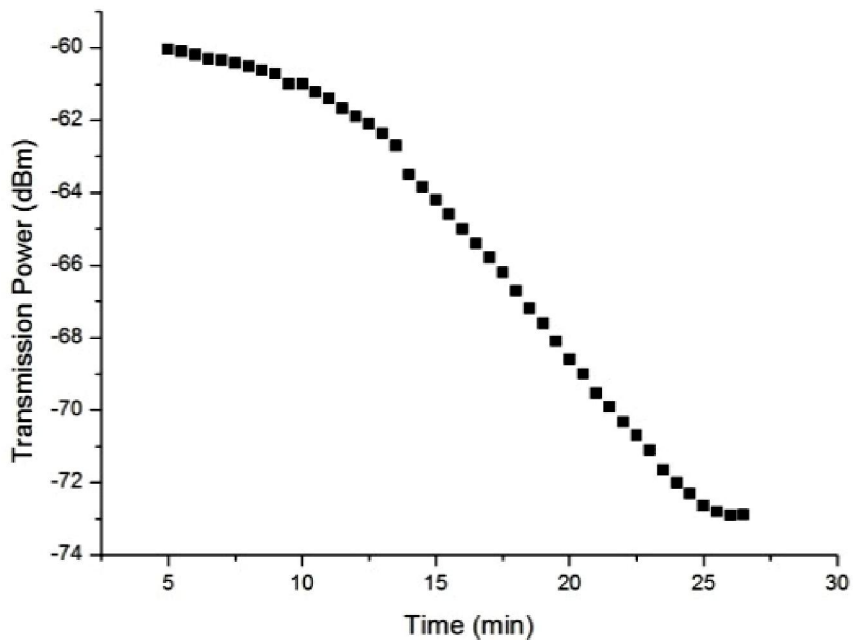
$$\text{dB} = 10\log\left(\frac{1}{1-\frac{\%}{100}}\right) \quad (5.2)$$

Then the refractive index modulation amplitude  $\Delta n_{ac}$  of the grating region can be estimated to be  $2 \times 10^{-4}$  from the following two equations:

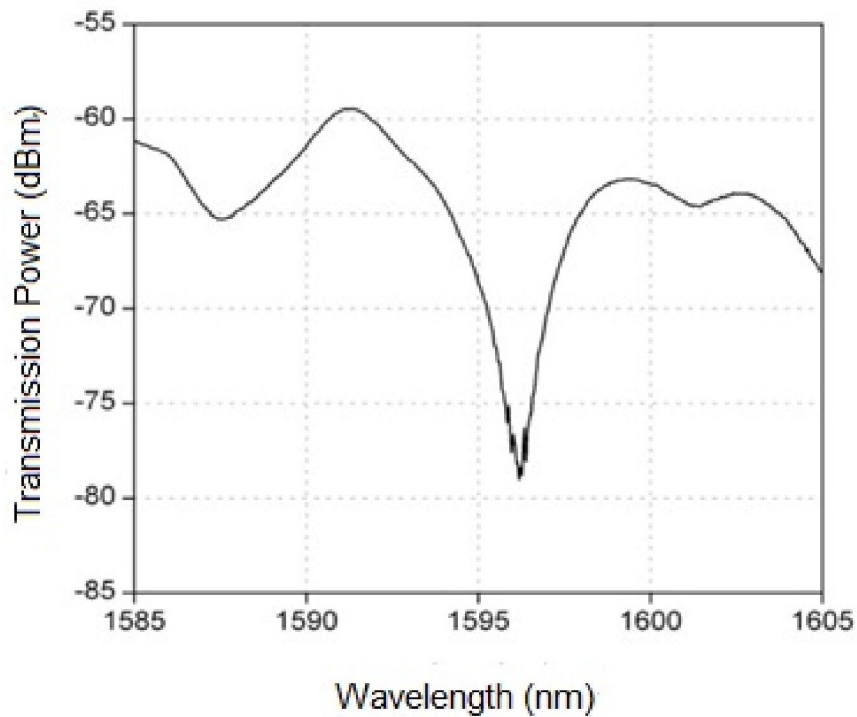
$$R = \tanh^2(\Omega L) \quad (5.3)$$

$$\Omega = \pi \cdot \Delta n_{ac} \cdot \eta / \lambda \quad (5.4)$$

where  $R$  is the reflectivity of the grating,  $L$  is the length of the grating,  $\Omega$  is the coupling coefficient and  $\eta$  represents the fraction of the integrated fundamental-mode intensity contained in the core and approximately assumed to be 1 here.



(a)



(b)

Figure 5- 9: (a) Transmission power change during TOPAS mPOFBG writing; (b) Transmission spectrum of TOPAS mPOFBG.

A microscope picture of the inscribed TOPAS mPOFBG is shown in Figure 5-10. The measured grating period is around 1040nm, which is approximately equal to the period of the phase mask, not half of it as initially expected (refer to Equation 2.22). This can possibly be explained from the effects of the zero-order diffraction of the phase mask on polymer Bragg gratings, due to the imperfect suppression of the phase mask zero order and will be detailed in a separate section in this chapter.

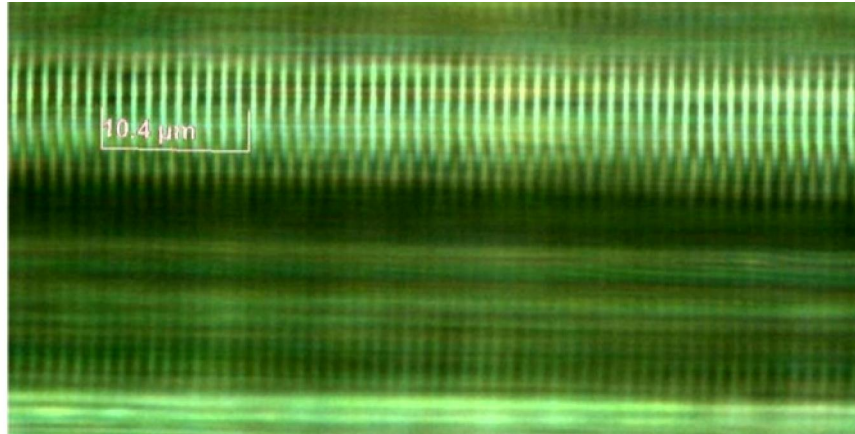


Figure 5- 10: Microscope picture of the TOPAS mPOFBG.

### 5.3.2 Step Index Polymer Optical Fibre Bragg Gratings

The photosensitive single mode step index PMMA polymer optical fibre used in grating fabrication experiments is supplied by University of New South Wales, Australia. The fibre (shown in Figure 5-11) possesses a 200 micron diameter pure PMMA cladding with a 10 micron diameter core based on PMMA but containing dopants (details are not provided by the supplier) to raise the refractive index and enhance the photosensitivity to 325nm UV light so as to enable the faster inscription of the Bragg grating. So for this kind of fibre, the scanning inscription method is chosen for grating fabrication and this will enable a longer grating length, leading to the narrower bandwidth. Upon the FWHM bandwidth equation of a uniform Bragg grating (Equation 2.20), the longer the grating (more grating planes) is, the smaller the bandwidth will be.

## 5. Bragg Grating Inscription in Polymer Optical Fibre

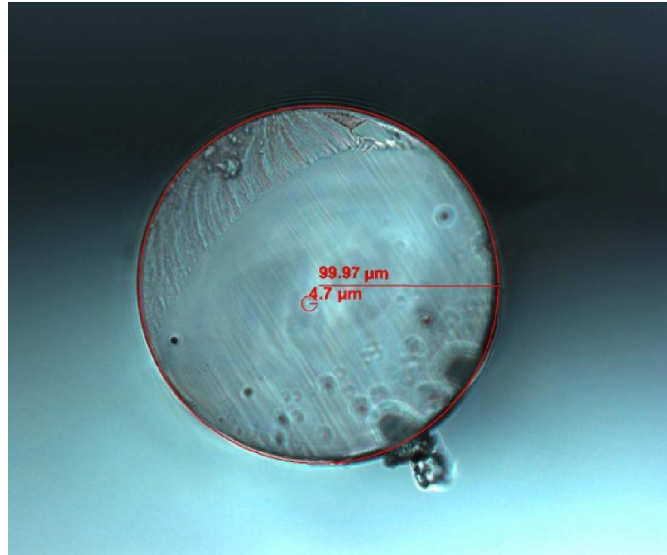
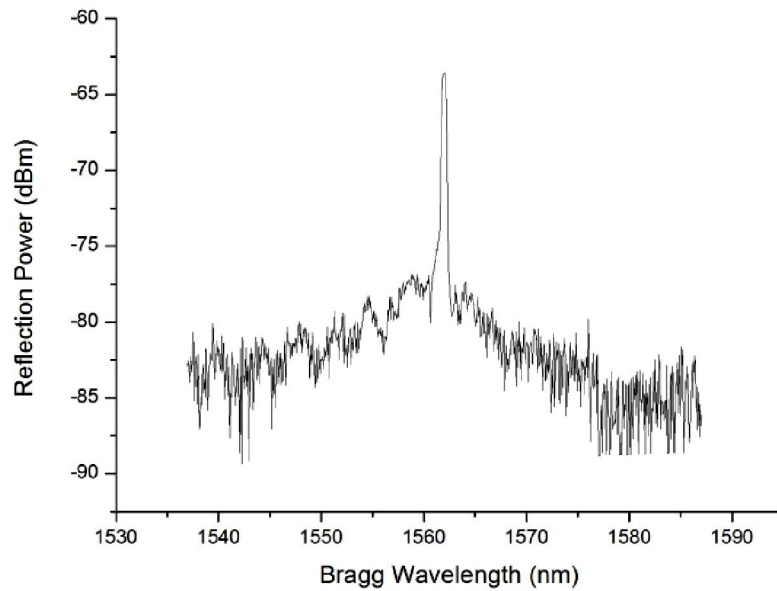
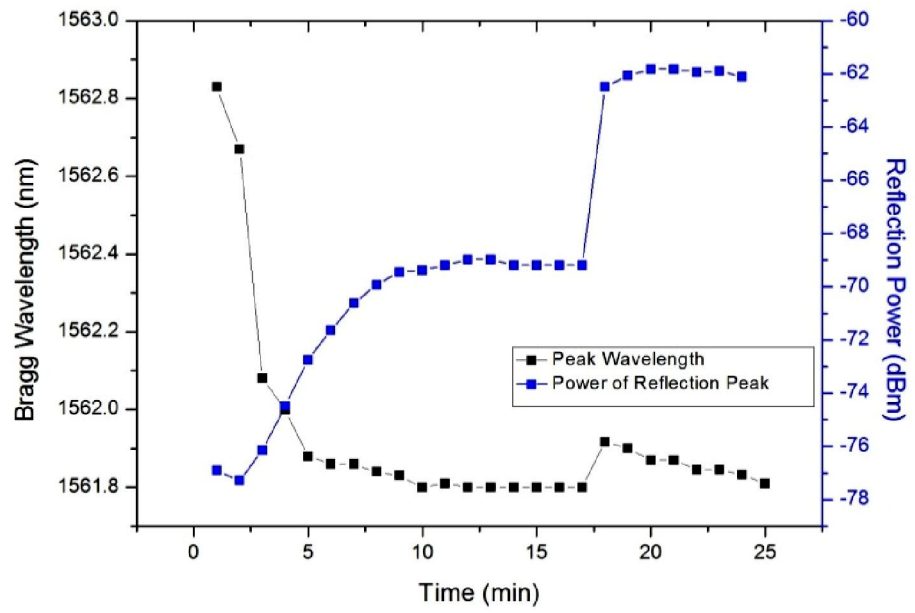


Figure 5- 11: Optical microscope image of the cross-section of the photosensitive single mode step index PMMA POF.

The Bragg grating is inscribed in the doped photosensitive step index PMMA polymer optical fibre with the scanning inscription set-up at ambient condition. The scanning speed is set to be 4 micron per second and the scanning length is 6mm, which is limited by the length of the phase mask, so the whole exposure period of the fibre is around 25 minutes. The growth characteristics of the grating inscription process are shown in Figure 5-12(a) (The break of the curve in the graph is due to the re-alignment of the butt coupling during inscription.); data collected every 60 seconds and the final optimised spectrum of FBG after stopping the laser irradiation is show in Figure 5-12(b). The Bragg wavelength of the grating is around 1562nm, FWHM is around 0.7 nm, and the reflective power above the noise level is around 20dB. (OSA resolution bandwidth is 0.1nm) The grating is also failed to be observed in transmission, possibly due to the high attenuation of the PMMA based fibre at this wavelength. The induced dc average refractive index modulation  $\Delta n_{dc}$  is able to be estimated to be  $-0.83/(1057.2/2)=4 \times 10^{-4}$ .

## 5. Bragg Grating Inscription in Polymer Optical Fibre



(b)

Figure 5- 12: (a) Bragg wavelength shift and reflection power change during grating inscription; (b) Reflection profile of FBG in doped POF.

## 5. Bragg Grating Inscription in Polymer Optical Fibre

After inscription, the grating is observed with the microscope, as shown in Figure 5-13. The measured grating period is around 1050nm, which is also approximately equal to the period of the phase mask, as was observed with the TOPAS mPOFBG.

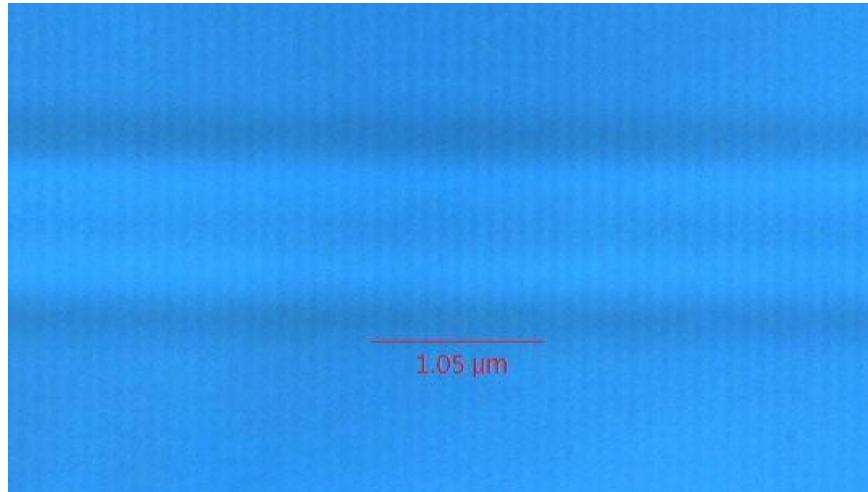


Figure 5- 13: Microscope picture of the photosensitive single mode step index PMMA POF.

### 5.4 Explanation of the Observed Abnormal Grating Period

In previous section, the abnormal grating period is observed, which is approximately equal to the phase mask pitch, not half of it as initially expected. This phenomenon can possibly be explained from the effects of the zeroth-order diffraction of the phase mask on polymer fibre Bragg gratings. The effect of the zeroth-order diffraction on the interference behind the phase mask has been analysed by Dyer et al [13] in silica optical fibres and theoretically and experimentally investigated by Xiong et al [14] in bulk polymer materials. In this section, the mathematical description of the field distribution from the phase mask

## 5. Bragg Grating Inscription in Polymer Optical Fibre

will follow that provided by Xiong et al. In addition, the zeroth-order diffraction effect is also simulated in Matlab (Version 7.0).

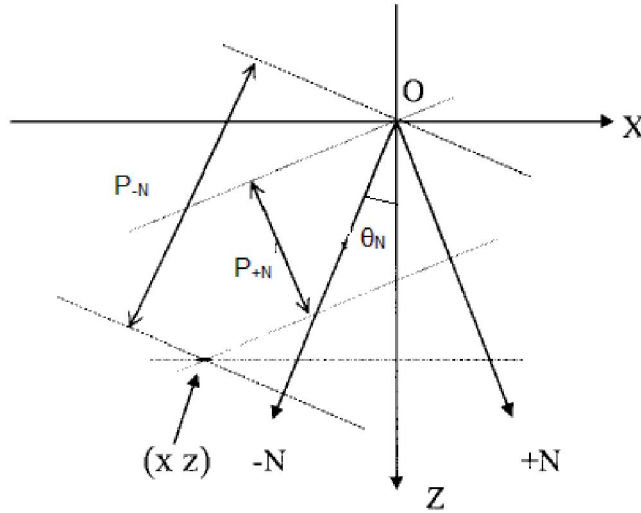


Figure 5- 14: The coordinate system to simulate the three beams interference. X direction is along the length of the grating and Z is the direction of the incident laser beam (normal to the phase mask).

The phase change at point  $(x, z)$  shown in Figure 5-14 behind the phase mask can be expressed as

$$P_{+N} = x \sin \theta_N + z \cos \theta_N, \quad (5.5) [14]$$

where  $\theta_N$  is the diffraction angle of the  $N$  th-order and  $\sin \theta_N = N\lambda_{UV}/\Lambda_{pm}$ , where  $\Lambda_{pm}$  is the phase mask period and  $\lambda_{UV}$  is the wavelength of UV irradiation. The electrical field distribution of the interference from the  $N$ th diffraction behind the phase mask is

$$E = \sum_{k=-N}^N C_k \exp (i2\pi P_k / \lambda_{UV}) \quad (5.6) [14]$$

Where  $C_k$  is the amplitude of the electrical field of the  $k$ th-order diffraction. If we only consider the symmetrical diffraction situation here,  $C_k = C_{-k}$  and the

## 5. Bragg Grating Inscription in Polymer Optical Fibre

zeroth-order amplitude can be replaced with  $2C_0$ . The intensity distribution  $EE^*$  is then provided as following:

$$I = 4 \left\{ \sum_{k=0}^N \left[ C_k^2 \cos^2 \left( \frac{2\pi kx}{\Lambda_{pm}} \right) \right] + \sum_{j \neq k} C_k C_j \cos \left( \frac{2\pi kx}{\Lambda_{pm}} \right) \left( \frac{2\pi jx}{\Lambda_{pm}} \right) \times \cos \left( \frac{2\pi z (\cos \theta_k - \cos \theta_j)}{\lambda_{UV}} \right) \right\} \quad (5.7) [14]$$

To simplify equation 5.7, the diffraction orders higher than  $\pm 1$  will be ignored. For the interference pattern of the zeroth order and two first-order diffraction beams, the intensity distribution is expressed as

$$I_{0,\pm 1} = 4 \left[ C_1^2 \cos^2 \left( \frac{2\pi x}{\Lambda_{pm}} \right) + C_0^2 + 2C_0 C_1 \cos \left( \frac{2\pi x}{\Lambda_{pm}} \right) \times \cos \left( \frac{2\pi z (1 - \sqrt{1 - \left( \frac{\lambda_{UV}}{\Lambda_{pm}} \right)^2})}{\lambda_{UV}} \right) \right] \quad (5.8) [14]$$

When there only exists the two first-order diffraction beams, the intensity distribution is

$$I_{0,\pm 1} = 4C_1^2 \cos^2 \left( \frac{2\pi x}{\Lambda_{pm}} \right), \quad (5.9) [14]$$

The equation which is also the first term of Equation 5.8, demonstrates that the fringe pattern has a sinusoidal intensity distribution along the x direction with a period equal to half of the phase mask's period and possesses uniform intensity along z direction and the grooves of the phase mask (y direction).

The second term  $4C_0^2$  in Equation 5.8 is a constant related to the zeroth-order diffraction, which reduces the contrast of the fringe pattern of the first term.

## 5. Bragg Grating Inscription in Polymer Optical Fibre

The third term of Equation 5.8 represents the interaction between the zeroth order and the two first-order diffraction beams. It create oscillation along x direction and also along z direction with period  $\Lambda_z$ , which can be calculated by

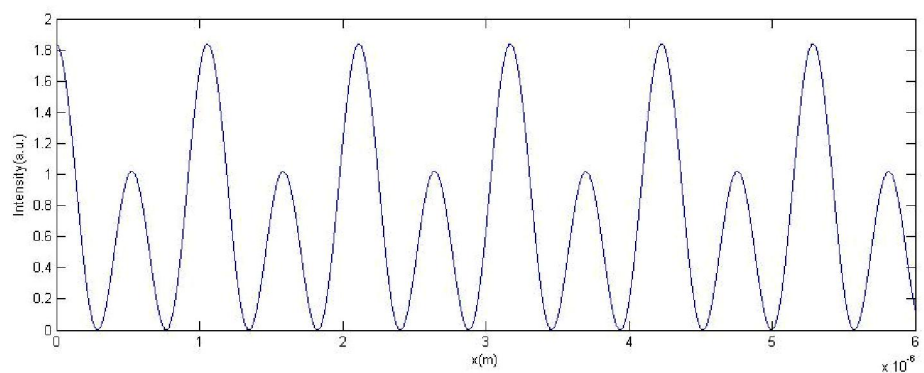
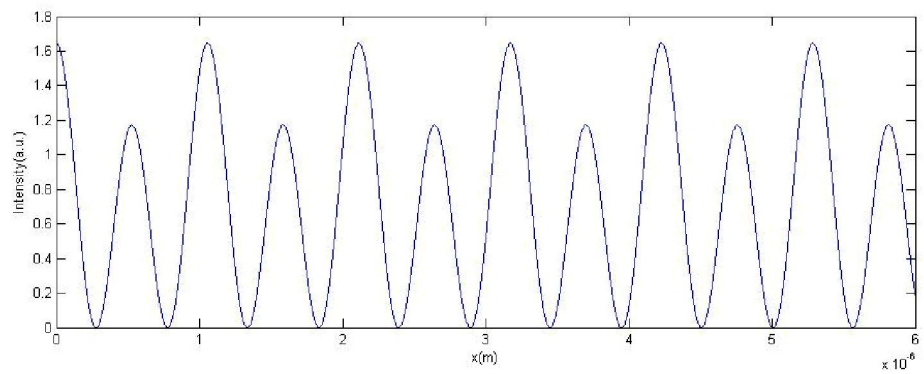
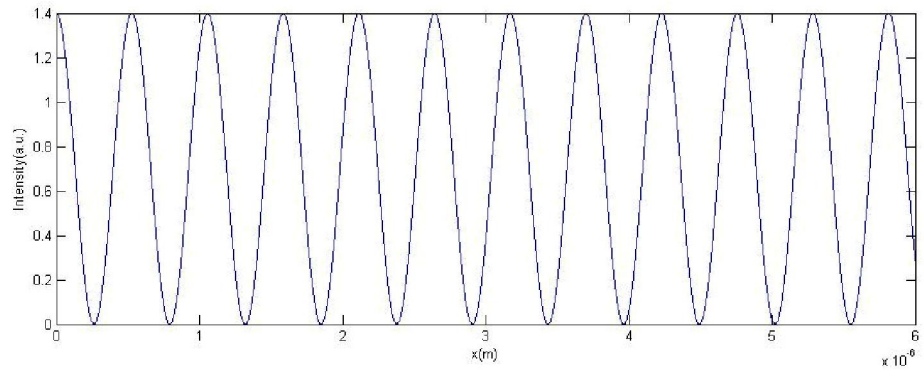
$$\Lambda_z = \frac{\lambda_{UV}}{\sqrt{1 - \left(\frac{\lambda_{UV}}{\Lambda_{pm}}\right)^2}} \quad (5.10)[14]$$

When the values of parameters in Equation 5.10 are set to those used in the inscription experiments, which is  $\lambda_{UV} = 325\text{nm}$ ,  $\Lambda_{pm} = 1057.2\text{nm}$ , the period  $\Lambda_z$  is  $6.6\mu\text{m}$ .

The intensity distributions under different levels of the zeroth-order diffraction contribution  $(2C_0)^2$  of the phase mask are calculated as shown in Figure 5-15(a-e). The  $\pm 1$  order diffraction contribution  $C_1^2$  is set to be 35% at  $\lambda_{UV} = 325\text{nm}$ , which is equal to that of the phase mask used in POFBG fabrication in this thesis. From the simulation results, it can be discovered that the interference pattern changes with the increasing of the zeroth-order diffraction and when the zeroth-order diffraction increase to certain level, for example, Figure 5-15 (d), the period of the fringes are more likely equal to that of the phase mask. Therefore, this calculation well supports the optical microscope observation results of the grating fringes in polymer optical fibres with the same period as the phase mask, as the zeroth-order diffraction contribution of phase mask used for POFBG

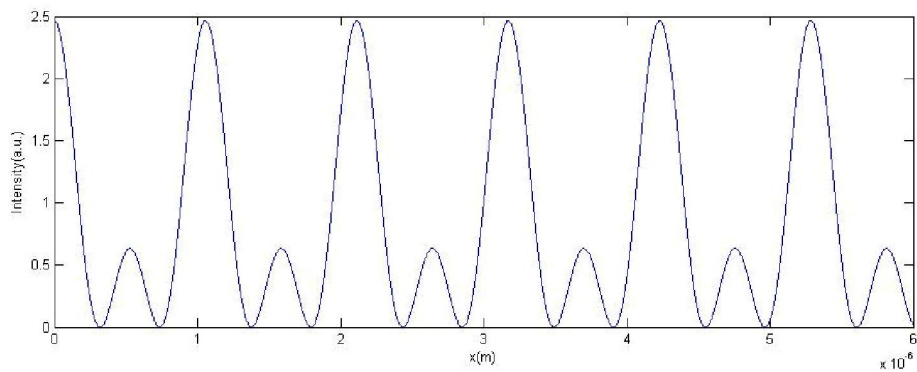
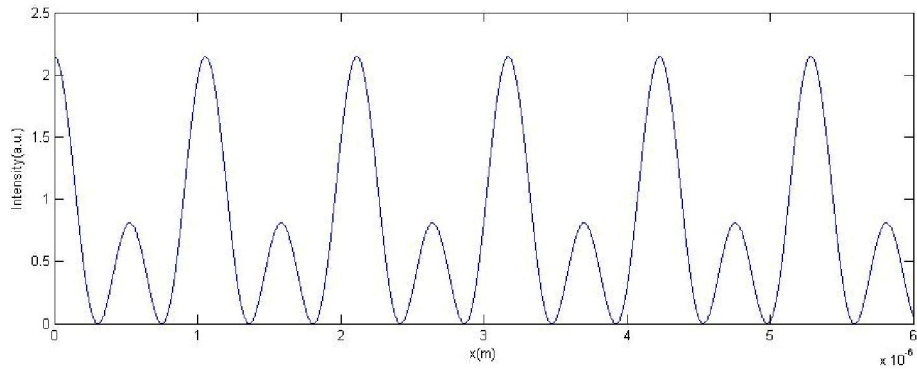
## 5. Bragg Grating Inscription in Polymer Optical Fibre

fabrication in this thesis is as high as around 8% at  $\lambda_{UV} = 325\text{nm}$  .



(c)

## 5. Bragg Grating Inscription in Polymer Optical Fibre



(e)

Figure 5- 15: The interference distribution along the x direction at  $z = 0$  with different levels of the zeroth-order diffraction  $(2C_0)^2$ : (a) 0%; (b)1%; (c)3%; (d)8%; (e) 15%, With experimental parameters:  $\lambda_{UV} = 325\text{nm}$ ,  $\Lambda_{pm} = 1057.2\text{nm}$  and  $C_1^2 = 35\%$ .

In addition, the three dimension diffraction distribution behind the phase mask used for grating inscription is also simulated, as shown in Figure 5-16. It again proves the existing of the periodical oscillation along z direction and illustrates how the grating visibility is destroyed.

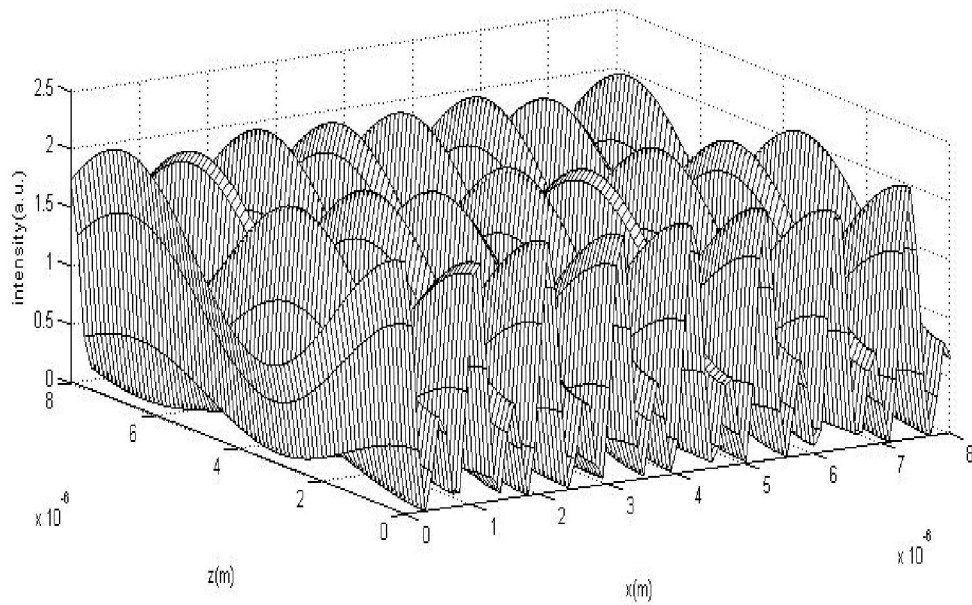


Figure 5- 16: The three dimensional intensity distribution of the three beams Interference with experimental parameters:  $\lambda_{UV} = 325\text{nm}$ ,  $\Lambda_{\text{pm}} = 1057.2\text{nm}$ ,  $(2C_0)^2 = 8\%$  and  $C_1^2 = 35\%$ .

### 5.5 Conclusion

In this chapter, the polymer optical fibre Bragg grating fabrication set-up is detailed and used to inscribe polymer optical fibre Bragg gratings. Several successful cases in different kinds of polymer optical fibres are demonstrated in this chapter, as listed in Table 5-1.

## 5. Bragg Grating Inscription in Polymer Optical Fibre

Table 5-1: Summary of fabricated polymer optical fibre Bragg gratings.

Material	PMMA Based		TOPAS Based
Fibre Type	Microstructured	Step-index	Microstructured
Dopands	None	UV photosensitive	None
Laser Type	325nm CW		
Inscription Period	~44 minutes	~25 minutes	~25 minutes
Grating Reflectivity	Cannot get	~96%	Cannot get
Refractive Index Modulation	$3 \times 10^{-4}$	$2 \times 10^{-4}$	$4 \times 10^{-4}$

Note, in this thesis, the fabricated PMMA based POFBGs are all working at the wavelength region where PMMA exhibits high attenuation and this will limit the length of the fibre used in grating fabrication and in real applications, for example in sensing applications. The further improvement should be concentrated on writing POFBGs at lower wavelength regions by using other phase masks [15] and the ideal region could be the visible wavelength region, though finding a suitable light source could be an issue.

The abnormal grating period which is equal to the period of the phase mask is observed after inscription and it is likely caused by the effect of the zeroth-order diffraction of a phase mask on the creation of Bragg gratings in polymer optical fibres. The simulation results have good agreement with the optical microscope pictures of the grating fringes.

## References

- [1] H. Dobb, D. J. Webb, K. Kalli, A. Argyros, M. C. J. Large, and M. A. van Eijkelenborg, "Continuous wave ultraviolet light-induced fiber Bragg gratings in few- and single-mode microstructured polymer optical fibers," *Opt. Lett.* 30(24), 3296–3298 (2005).
- [2] H. Y. Liu, G. D. Peng, and P. L. Chu, "Thermal tuning of polymer optical fiber Bragg gratings," *IEEE Photon. Technol. Lett.*, 13, 824–826 (2001).
- [3] H. Y. Liu, G. D. Peng, P. L. Chu, "Polymer fiber Bragg gratings with 28 dB transmission rejection," *IEEE Photon. Technol. Lett.* 14, 935-937 (2002).
- [4] J. M. Yu, X. M. Tao, and H. Y. Tam, "Fabrication of UV sensitive single-mode polymeric optical fiber," *Opt. Lett.* 29, 156 (2004).
- [5] G. D. Peng, Z. Xiong, and P. L. Chu, "Photosensitivity and gratings in dye-doped polymer optical fibers," *Opt. Fiber Technol.* 5, 242-251 (1999).
- [6] Thorlabs ASE-FL7002 Product Specification Document. (Thorlabs Inc.)
- [7] S.H.Law, M.A.van Eijkelenborg, G.W.Barton, C.Yan, R.Lwin, and J.Gan, "Cleaved end-face quality of microstructured polymer optical fibres," *Opt. Commun.* 265, 513-520 (2006).
- [8] O. Abdi, K. C. Wong, T. Hassan, K. J. Peters and M. J. Kowalsky, "Cleaving of solid single mode polymer optical fiber for strain sensor applications," *Opt. Commun.* 282, 856–861, (2009).
- [9] G.Barton, M.A.van Eijkelenborg, G.Henry, M.C.J.Large, and J.Zagari, "Fabrication of microstructured polymer optical fibers," *Opt. Fiber Technol.* 10, 325-335 (2004).
- [10] R. Kashyap. *Fiber Bragg Gratings*. Academic Press, 1999.
- [11] G. N. Harbach, H. G. Limberger, and R. P. Salathé, "Influence of Humidity and Temperature on Polymer Optical Fiber Bragg Gratings," in *Bragg Gratings, Photosensitivity, and Poling in Glass Waveguides*, OSA Technical Digest (CD) (Optical Society of America, 2010), paper BTuB2.

## 5. Bragg Grating Inscription in Polymer Optical Fibre

[12] N. G. Harbach, "Fiber bragg gratings in polymer optical fibers." PhD thesis Lausanne: EPFL, 2008.

[13] P. E. Dyer, R. J. Farley, and R. Geidl, "Analysis of grating formation with excimer laser irradiated phase masks," *Opt. Commun.* 115(3–4), 323–334 (1995).

[14] Xiong, G. D. Peng, B. Wu, and P. L. Chu, "Effects of the Zeroth-Order Diffraction of a Phase Mask on Bragg Gratings," *J. Lightwave Technol.* 17, 2361 (1999).

[15] I. P. Johnson, K. Kalli, and D. J. Webb, "827nm Bragg grating sensor in multimode microstructured polymer optical fiber," *Electron. Lett.* 46(17), 1217–1218 (2010).

# 6

## **Polymer Optical Fibre Bragg Grating Sensitivity Characterisation**

In this chapter, firstly, the humidity sensitivity of the step-index POFBGs was calibrated. Secondly, the temperature responses of mPOFBGs and step-index POFBGs were both investigated. Finally, the strain sensitivity of the step-index POFBGs was studied.

### **6.1 Humidity Sensitivity**

#### **6.1.1 Introduction**

PMMA can absorb moisture from its surroundings (up to 2wt% at 23°C), leading to both a swelling of the material and an increase in refractive index with a

## 6. Polymer Optical Fibre Bragg Grating Sensitivity Characterisation

consequent increase in the Bragg wavelength of a grating inscribed in the material [1-3]. Upon this property, PMMA based POFBG may be potentially considered as the element of a humidity sensor, hence, the calibration of such sensitivity of fabricated PMMA based POFBGs is necessary.

### 6.1.2 Calibration Setup

#### 6.1.2.1 The Environmental Chamber

The humidity sensitivity response of PMMA based POFBGs was studied in an environmental chamber (SANYO Gallenkamp plc) so that the environmental temperature and relative humidity (RH) during the tests can be controlled. The internal dimensions of the chamber are 90x90x75 cm. The range of RH varies with the set value of temperature, and is given in Table 6-1. The uncertainty in the RH value is between 3% (at max. RH) and 5% (at min. RH). The uncertainty in temperature is between 0.3 and 1°C. When the temperature or RH was changed, it took more than 15 minutes for the chamber to reach the set value.

Table 6-1: Specifications of the chamber. [4]

Temperature (°C)	20	25	60
Range of RH (%)	50 - 98	30 - 98	15 - 98

#### 6.1.2.2 Connecting POF with Silica Optical Fibre

In the environmental chamber, the butt-coupling arrangement described in Chapter 5 for monitoring POFBGs is unsuitable, due to the vibration which will affect the very sensitive coupling between the POF and single mode step index

## 6. Polymer Optical Fibre Bragg Grating Sensitivity Characterisation

silica optical fibre, and the difficulty to fix the translation stage inside the chamber. Hence, an alternative reliable method for connecting POF with silica fibre is required.

In the initial phase of the research into connectorisation, POF is considered to be glued into ferrule whereas demountable connector forms. However, this idea has encountered practical problems. The single mode POF currently available comes mainly from research groups and no effort has been put into standardising fibre diameters and the quality of fibre, some of which even have acentric core. As pointed out in Chapter 5, the fibre cores need to be aligned to about a micron and consequently the ferrule needs to be very closely matched to the fibre diameter. The only non-standard ferrule discovered from the market is the 152 microns one provided by Coopers needlework Co. Birmingham, which is close to diameter of the mPOF at 150 microns. The problem then encountered was that it seemed impossible to insert the POF into the ferrule. Numerous attempts were made without success. The problem seems to relate to the flexibility of the polymer fibre; when the fibre is fed into the ferrule, at some stage the fibre contacts the inner side of the ferrule and because of the compliant nature of the polymer the frictional forces cause the fibre to expand slightly, which is enough to jam the fibre in the ferrule. Increasing the force pushing the fibre simply causes it to jam more solidly. In general, the attempt in producing demountable connector by using ferrules is unsuccessful.

Instead of using ferrules, POF attempts were made with directly gluing POF to silica fibre to form a monitorable device by using optical glue:

Connecting step index POF with silica fibre

## 6. Polymer Optical Fibre Bragg Grating Sensitivity Characterisation

The choice of glue is very important. Not only does the glue have to provide a rugged bond to the two fibre materials but the refractive index needs to be closely matched to the fibres in order to suppress significant back-reflections from the joint. As an example from early work, one of the candidate glues investigated was Loctite 3525. Figure 6-1 shows one attempt to produce a connection with this glue in which the refractive index mismatch reveals itself as an increase in the background signal level which reduced the signal to noise ratio from 22dB before gluing to 8dB after gluing.

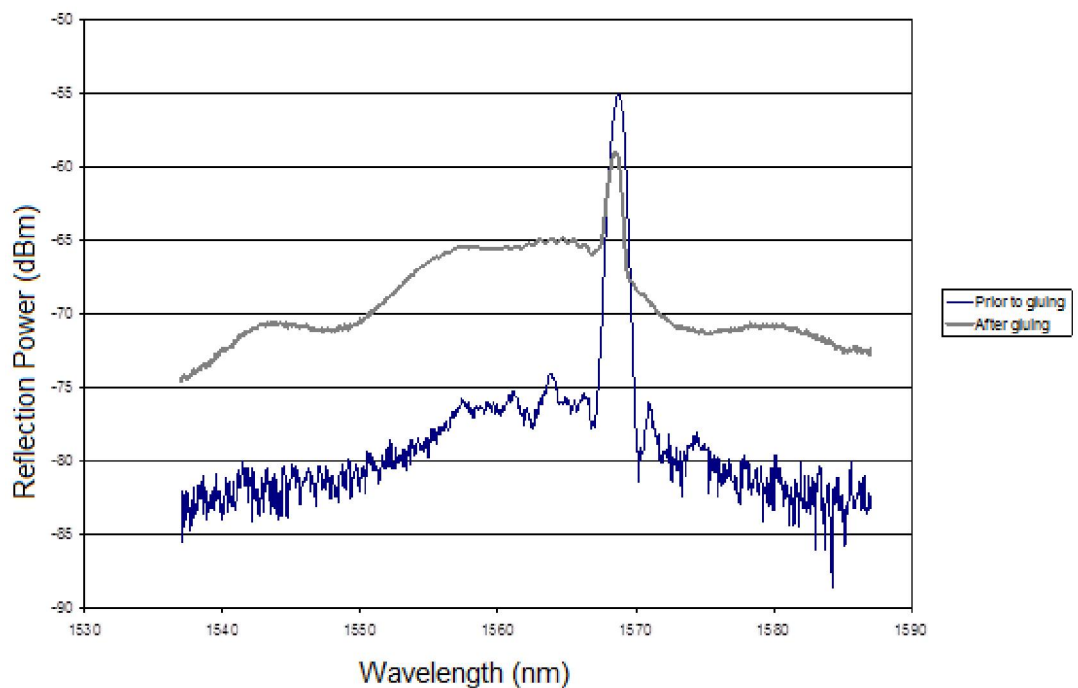


Figure 6- 1: Early attempt with Loctite 3525 showing strong back-reflection from the connection (elevated background spectrum).

It was discovered that careful control of the fibre alignment could result in suppression of the reflected background spectrum, but only at the expense of introducing an unacceptable signal loss of around 5dB each way, see Figure 6-2.

## 6. Polymer Optical Fibre Bragg Grating Sensitivity Characterisation

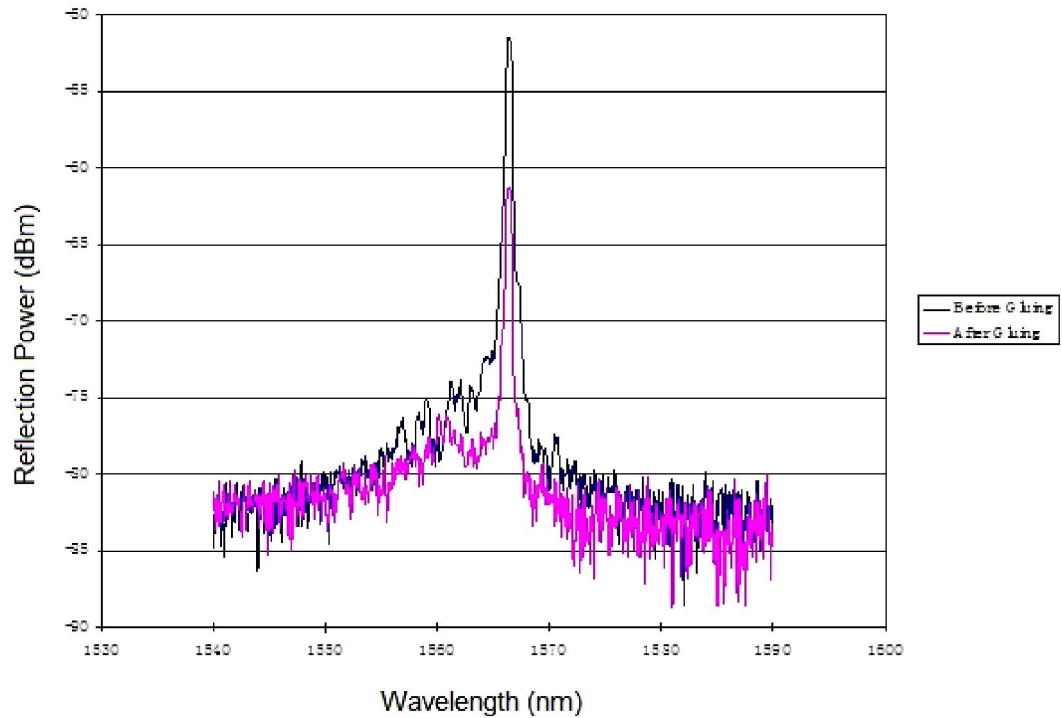


Figure 6- 2: Early attempt with Loctite 3525 showing 10dB round trip loss following gluing.

Table 6-2 lists the comparison of the advantages and disadvantages of different kind of glues which were tried in the gluing experiment.

Table 6-2: The comparison of different optical glues' behavior in gluing experiments.

Glue Type	Typical Loss Induced by Gluing	Problems / Advantages
Dymax OP-4-20639/20647	N/A	Weak connection
Loctite 3525	5-10 dB	Curing fast (Tack Free Time 10-15 seconds, Fixture Time <5 seconds), Solid connection, Unacceptable high loss
Norland 76/78	<0.5 dB	Curing slow(Tack Free Time 10-15 seconds, Fixture Time 5 minutes), Solid connection, Low loss

## 6. Polymer Optical Fibre Bragg Grating Sensitivity Characterisation

After trials with different glues, different alignment procedures and different curing schedules, the following approach is confirmed to be able to provide a means of producing reliable and repeatable connections between silica fibre and POF, and be affected by neither the POF fibre diameter nor the concentricity of the fibre core:

1. The single mode silica optical fibre (SMF28) pigtail is angled-cleaved using an Oxford Fiber HSFC-2001 High Strength Fibre Cleaver. The step-index POF with Bragg grating is flat-cleaved using a new razor blade on a hot plate at 80°C.
2. The cleaved end of the silica fibre has as small a drop of optical glue (Norland 76/78) as possible applied, which should be just cover the cross section of the fibre, using a tooth-pick and is butt-coupled with the step-index POF by using an X-Y-Z translation stage (Melles Griot).
3. The core-to-core alignment is initially aligned by red light source (OZ Optics FODL-23S-635-1) and then optimised by illuminating the POFBG using a broadband light source (Thorlabs ASE-FL7002-C4) via the silica fibre pigtail and observing the reflected signal from the FBG using an optical spectrum analyser (HP70004A), see Figure 6-3.

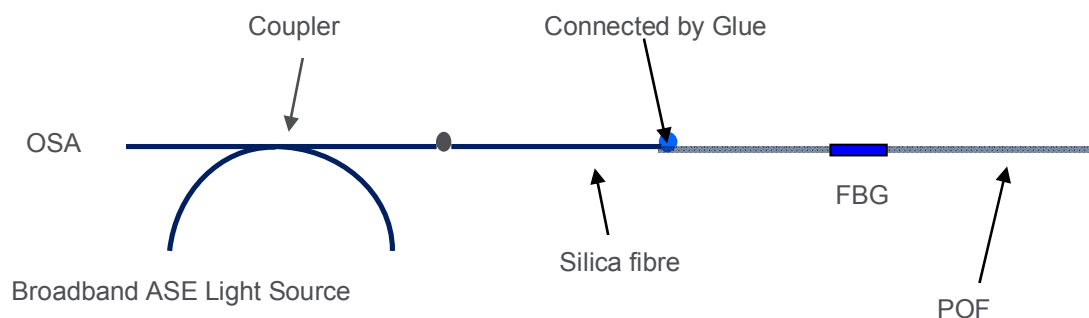


Figure 6- 3: Sketch of the POFBG device.

## 6. Polymer Optical Fibre Bragg Grating Sensitivity Characterisation

4. The glue between the fibres is cured by UV lamp (OmniCure 1000, EXFO) at around 60mW power for 5 minutes. The light guide of the UV lamp was fastened vertically to the gluing point with a distance at around 10mm between them. After that, more glue (Norland 76/78) was put on the connection point in two steps, until a bulb, which can protect the connection point, form at diameter of around 1mm, as shown in Figure 6-4. At each step, the glue should be cured at the same power (60mW) for 15 minutes.

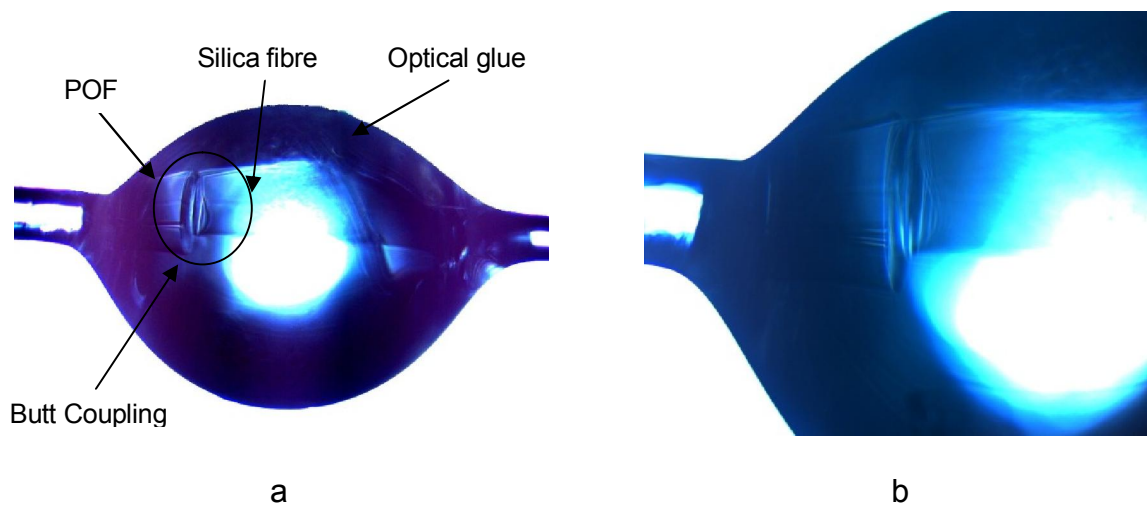


Figure 6- 4: Microscope picture of Connection point (a.5X b.10X). Note the mismatch is due to the eccentric core of the POF.

5. The reflection spectrum of the grating was measured before and after gluing finished, as show in Figure 6-5. The additional loss was less than 0.3dBm in this case.

## 6. Polymer Optical Fibre Bragg Grating Sensitivity Characterisation

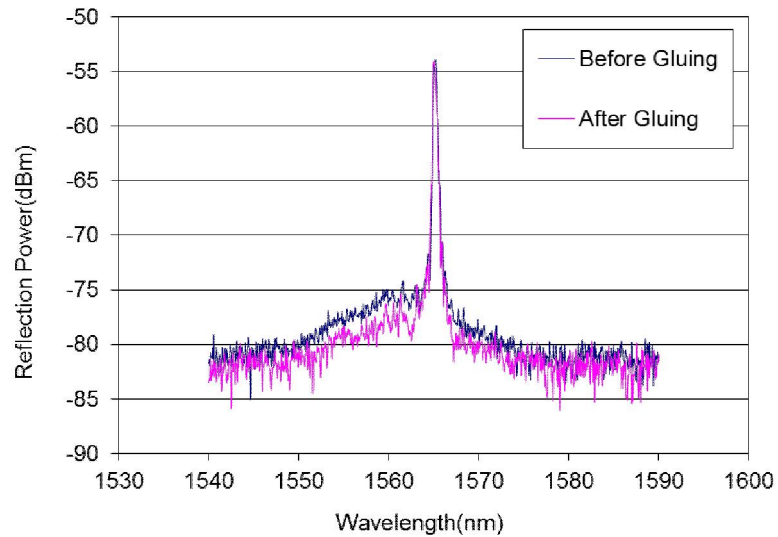


Figure 6- 5: The comparison of POFBG spectrum before and after gluing.

### Connecting mPOF with silica fibre

After the success with step-index POF, connecting mPOF to silica fibre was also investigated. Table 6-3 shows the adhesives tried and their main properties.

Table 6-3: Glues investigated for silica-mPOF connection.

Adhesive	Refractive index, cured	Viscosity (mPa•s)	Tensile Strength (psi)
Loctite 3525	1.51	9500 - 21000	35000
Norland 76	1.51	3500 - 21000	450
Norland 78	1.50	8000 - 11000	694
Dymax OP-4-20725	1.419	5000	420

The initial trial was started with the Loctite glue as it appeared that its high viscosity may help minimise travel of the glue up the holes of the fibre. Testing was undertaken with single mode mPOF containing FBG with a 14µm diameter

## 6. Polymer Optical Fibre Bragg Grating Sensitivity Characterisation

core. Light was launched into the mPOF using silica fibre (SMF28) cleaved at an angle of  $1^\circ$  to reduce back-reflections using an Oxford Fiber HSFC-2001 High Strength Fibre Cleaver; to aid the coupling, a small amount of the uncured Loctite 3525 adhesive was used to reduce the Fresnel reflections from the fibre end surfaces. As the refractive index of the uncured Loctite adhesive is 1.48, it acts as a very good index matching gel, which makes light much easier to be coupled into the mPOF. Once the coupling of the light was adjusted to give the best grating response the adhesive was cured using a UV light source of 60mW for 10 seconds. However once the Loctite adhesive was cured by the UV light the refractive index increased to 1.51, which completely destroyed the light guiding of the fibre causing the reflected signal from the grating to be completely lost in the system noise.

To counter this situation, it was decided to try to use a different adhesive to simply seal the end of the mPOF and prevent the Loctite 3525 adhesive from travelling along the hole structure. Dymax OP-4-20725 was used to accomplish this as it had a lower refractive index of 1.419, and would therefore perturb the light guiding of the mPOF less than the Loctite adhesive. Once the Dymax adhesive had been cured, the input source light was then successfully coupled into the mPOF using a stripped and angle-cleaved SMF28 silica fibre together with Loctite 3525 at the joint. A signal was obtained at the Bragg wavelength and the Loctite was successfully cured, creating a permanent joint between the silica and polymer fibres. Unfortunately as the joint was flexed the signal at the Bragg wavelength varied considerably in strength and could even be lost in the system noise. The explanation of this phenomenon was that the Dymax adhesive had also penetrated far into the holes of the fibre spoiling but not fully destroying the wave

## 6. Polymer Optical Fibre Bragg Grating Sensitivity Characterisation

guiding, thanks to its relatively low refractive index, so any significant bending at the region around the gluing joint can let much of the light travel straight out of the fibre, thus result in the Bragg peak in the spectrum disappearing. The potential solution could be minimising the distance of where the holes were blocked by cleaving, however, it would be quite crucial to control the cleaving length. In summary, the connecting mPOF to silica fibre is not as easy as step index POF and due to the lack of success of this key step, the humidity and strain response of mPOFBGs are not presented in this chapter.

### 6.1.3 Humidity Sensitivity of Step-index POFBG

To initially characterise the response of the POFBG device as illustrated in Figure 6-3 to water, it was placed inside the environmental chamber. Due to the high loss of PMMA at the infrared wavelength region, a short (7 cm) length of the 180 micron diameter doped PMMA based step-index single mode POF containing the grating at 1566nm (measured at ambient condition) as shown in Figure 6-6(a) was used in the device. The Bragg wavelength change by humidity was monitored in reflection by the same arrangement in grating inscription.

Initially the POF FBG was placed in the chamber with both the temperature and humidity held constant at 22°C and 45% RH and the Bragg wavelength allowed to stabilise. With the temperature held constant, the humidity was then increased quickly to 52% and the Bragg wavelength monitored as a function of time, see Figure 6-6(c). In approximately 30 minutes, the water stopped diffusing into the fibre and water equilibrium was achieved inside the fibre. The total wavelength red-shift against 39mins is 0.124nm, shown in Figure 6-6(b). FBG peak's intensity change is negligible during this period, as shown in Figure 6-6(d).

## 6. Polymer Optical Fibre Bragg Grating Sensitivity Characterisation

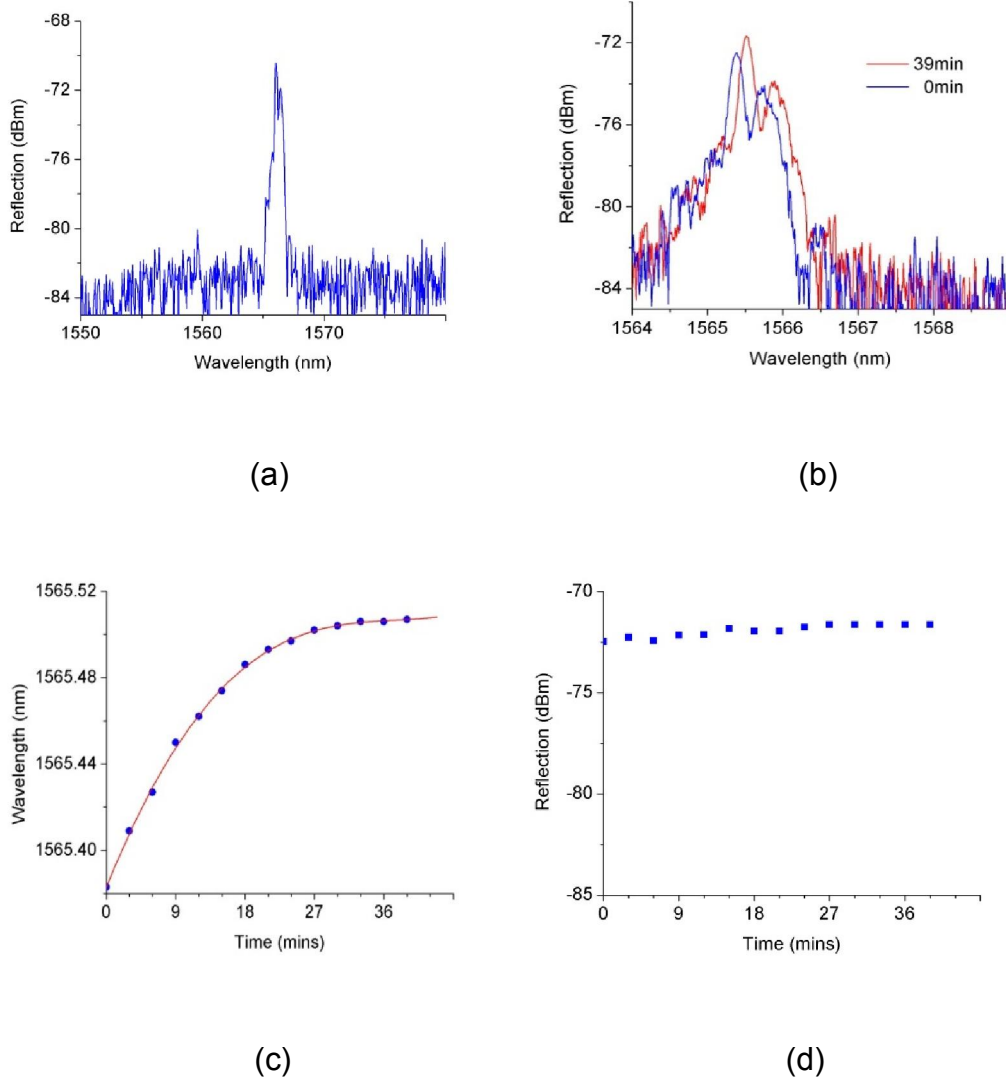


Figure 6- 6: (a) PMMA based POFBG spectrum; (b) Recorded Bragg wavelength of PMMA based POFBG at beginning and end of the experiment; (c) Response of water absorption of PMMA based POFBG in 39 minutes; (d) FBG peak's intensity plot against the time.

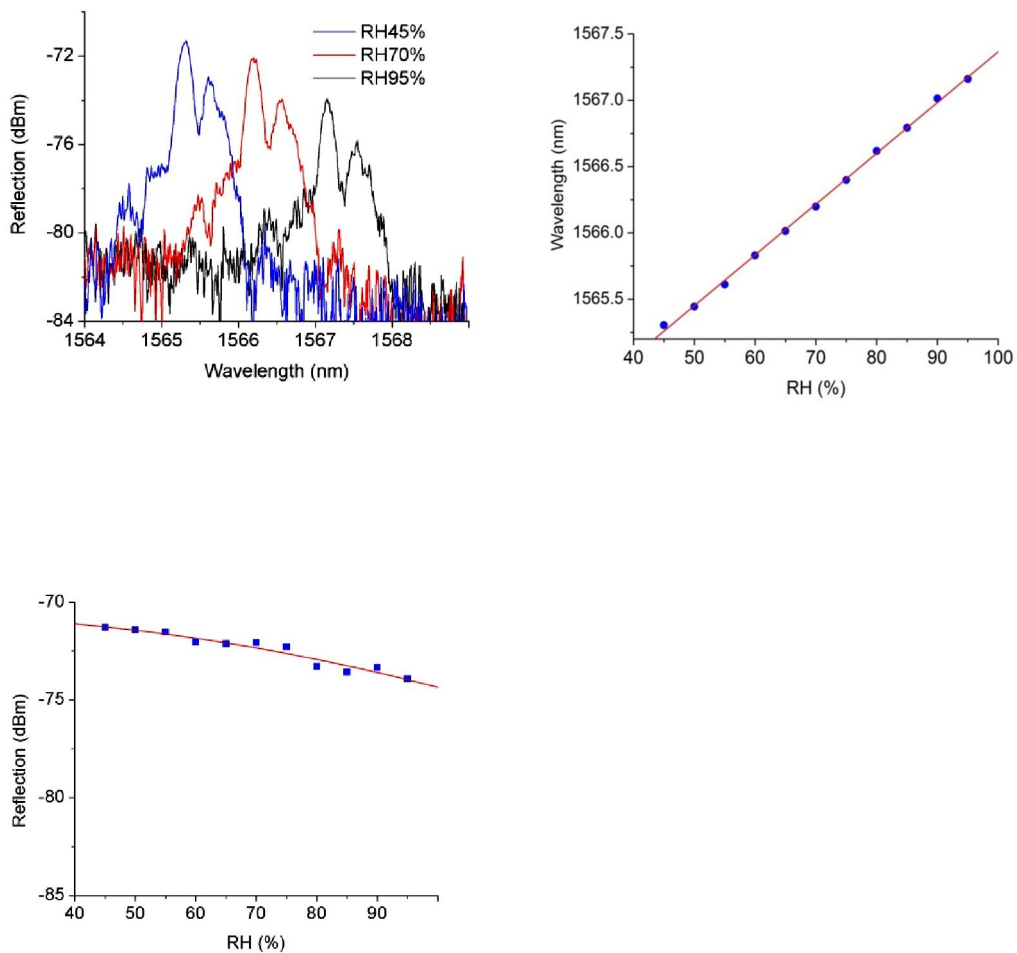
With the temperature still held at 22°C, the relative humidity was then changed in a series of steps from 45% to 90%. (To be noted here, due to the system limitation of the environmental chamber, 45% relative humidity is the lowest value the system can reach at 22°C, thus the response of FBGs to a humidity lower than 45% is not presented.) At each step, 30 minutes was allowed for the humidity to stabilize, which was measured from the previous experiment. The Bragg wavelength of the POFBG reveals a total shift of ~1.857nm, as shown in Figure

## 6. Polymer Optical Fibre Bragg Grating Sensitivity Characterisation

6-7(a). The device exhibits an apparently linear Bragg wavelength shift with increasing humidity with a sensitivity of  $38.3 \pm 0.5 \text{ pm}$  per % RH, see Figure 6-7(b).

Figure 6-7(c) show that the intensity of FBG decreases significantly whilst %RH increases to high value. This behaviour possibly due to the following factors: 1.

The output power of the broadband light source (Thorlabs ASE-FL7002-C4) at wavelength from 1560nm to 1570nm is decreasing 5dB. 2. Water absorption increases the attenuation of the fibre. [5-6]



(c)

Figure 6- 7: (a) Recorded Bragg wavelength of PMMA based POFBG at beginning, middle and end of the experiment; (b) Humidity sensitivity of PMMA based fibre at 22 °C; (c) FBG peak's intensity plot against the time.

## 6. Polymer Optical Fibre Bragg Grating Sensitivity Characterisation

The repeatability of the humidity sensitivity of POFBG was proved by testing the response of a device containing another POFBG with constant temperature at 22°C and a cycle of increasing and decreasing humidity between 45%RH and 85%RH, as shown in Figure 6-8. In the cycling experiments, the device exhibits humidity sensitivity of  $39.8 \pm 0.9 \text{ pm per \% RH}$  and  $40.9 \pm 0.8 \text{ pm per \% RH}$  during the process, which has good agreement with previous result. In addition, there was no humidity hysteresis observed in Figure 6-8 when the cycling experiment finished, therefore the humidity reversibility of the POFBGs is good.

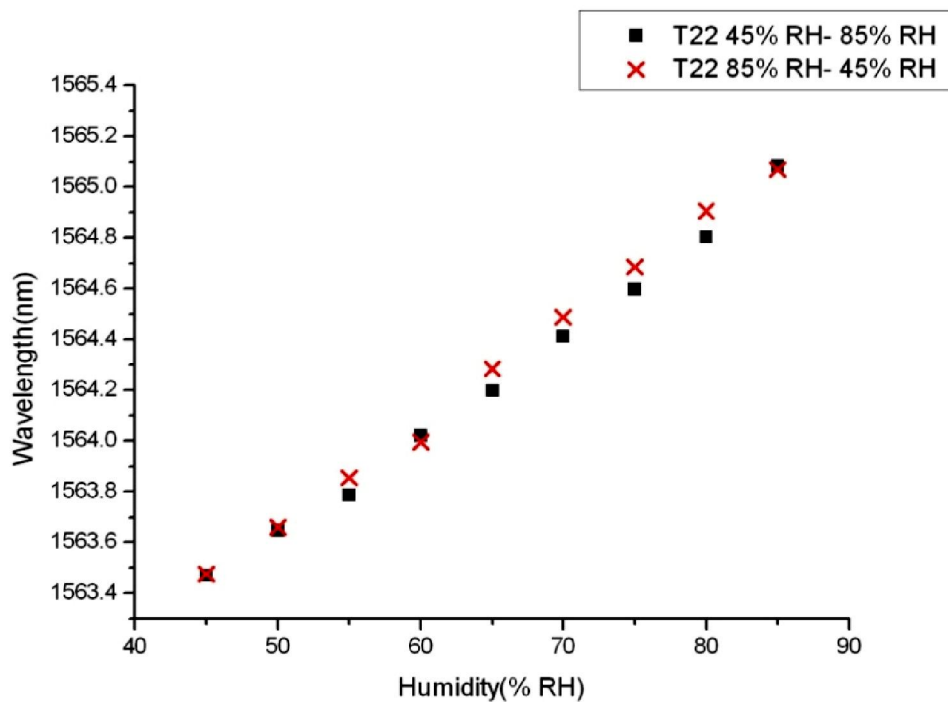


Figure 6- 8: Humidity response of PMMA based fibre in a humidity cycling experiment at 22 °C.

## **6.2 Temperature Sensitivity**

### **6.2.1 Introduction**

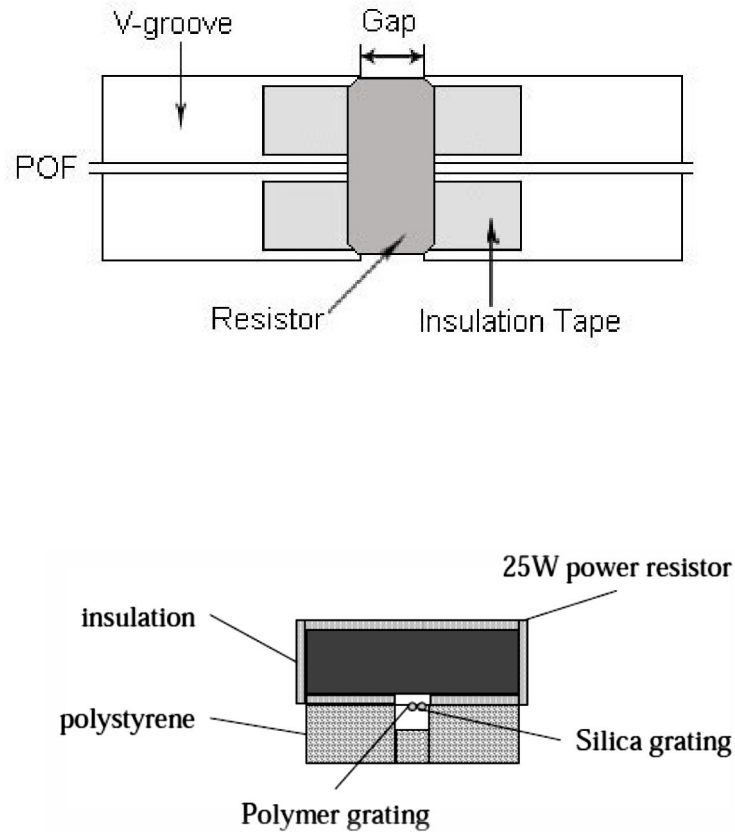
The temperature sensitivity of the gratings in PMMA based step-index POFs has been studied previously, [7-8] which revealed a negative temperature coefficient of between  $-146\text{pm}/^\circ\text{C}$  and  $-360\text{pm}/^\circ\text{C}$ . These results are significantly larger in magnitude than that observed for FBGs in silica optical fibres, which is around  $10\text{pm}/^\circ\text{C}$  [9]. This increased sensitivity means that the thermal properties of gratings in POF are of particular interest. In this section, investigation into the temperature (lower than the glass transition temperature of PMMA) response of gratings in both pure PMMA based mPOF and doped PMMA based step-index POF is performed, revealing a different behaviour than previously reported [7,8]. In addition, the working temperature range of the sensors can be extended using an annealing process.

### **6.2.2 Thermal Response of PMMA and TOPAS mPOF Gratings**

#### **6.2.2.1 Experiment Set-up**

As mPOF is unable to be glued with silica optical fibre, the thermal response of the mPOF gratings cannot be calibrated using the environmental chamber, hence, it had to be investigated using the heating rig in the ambient condition as shown in Figure 6-9.

## 6. Polymer Optical Fibre Bragg Grating Sensitivity Characterisation



(b)

Figure 6- 9: (a) Top view of the heating rig, (b) cross-section view of the heating rig.

In the rig, two V groove blocks (Melles Griot) were fastened on a translation stage leaving a 1cm long air gap between them. The mPOF with FBG was placed in the v-grooves along with a temperature calibrated FBG in silica fibre (see Figure 6-10), which was used to measure the temperature of the heating zone, making sure the two FBGs were closely spaced in the air gap.

## 6. Polymer Optical Fibre Bragg Grating Sensitivity Characterisation

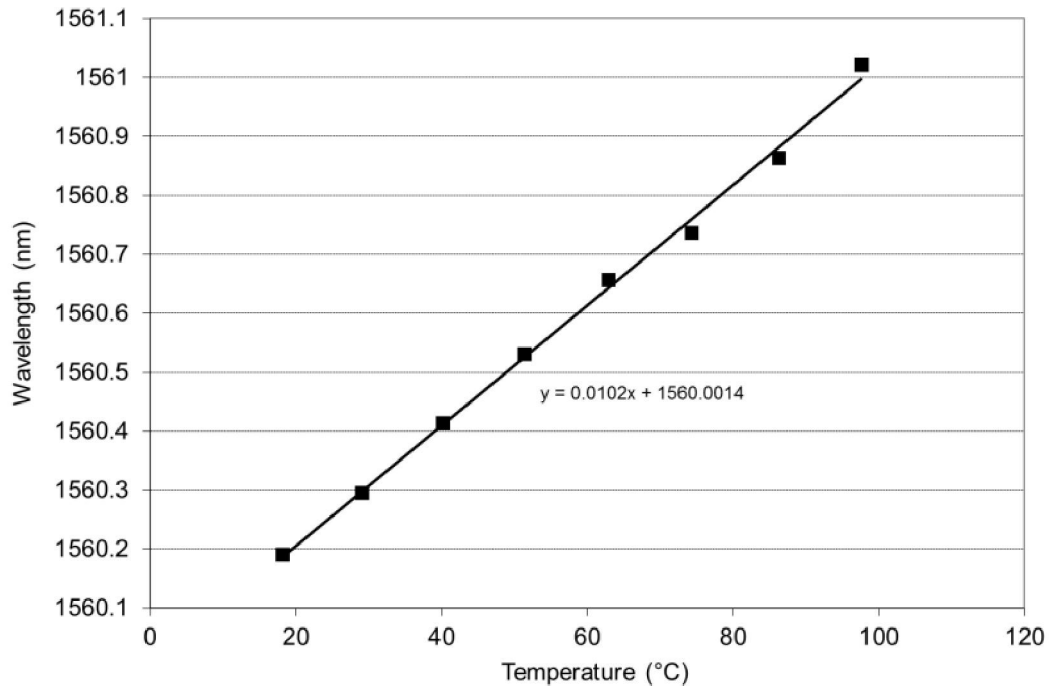


Figure 6- 10: Temperature calibration of silica FBG (18°C -100°C).

A 25W heating resistor (RS Components) was placed over the FBGs to heat the devices and the whole heating zone was insulated by polystyrene pieces. The heating process was monitored by the same arrangement as the grating inscription. The FBG region was generally heated to several temperatures by tuning the voltage value across the resistor. At each new settings, the voltage was held constant for 10 minutes to ensure temperature stabilisation before the value of the shift in the peak of the grating spectrum was recorded from the OSA.

### 6.2.1.2 Thermal Properties of mPOFBGs in PMMA

The first experiment consisted of cycling a single grating, made in non-annealed pure PMMA mPOF, to different temperatures, shown in Figure 6-11. The grating was first taken to a maximum of 77.1°C with each incremental temperature being held for 10 minutes. During this process, the Bragg wavelength of the grating shift gradually to lower wavelength region. The grating was then allowed to cool back

## 6. Polymer Optical Fibre Bragg Grating Sensitivity Characterisation

to room temperature. In the second cycle, the grating was heated to 85.5°C, cooled again, then in the final cycle the maximum temperature was 91.5°C. After each cycle, a permanent shift in the wavelength of the grating was observed; after the first cycle this was -8.7nm and after the second this was a further -10.5nm. The temperature response of each cycle is non-linear and exhibited a quasi-linear region at certain temperatures, which extends to higher temperatures with each progressive cycle due to the annealing that took place during the previous cycle. The sensitivity of the grating in each of these regions is shown on the graph in Figure 6-11, which is -92.4pm/°C, -97pm/°C and -71.8pm/°C respectively.

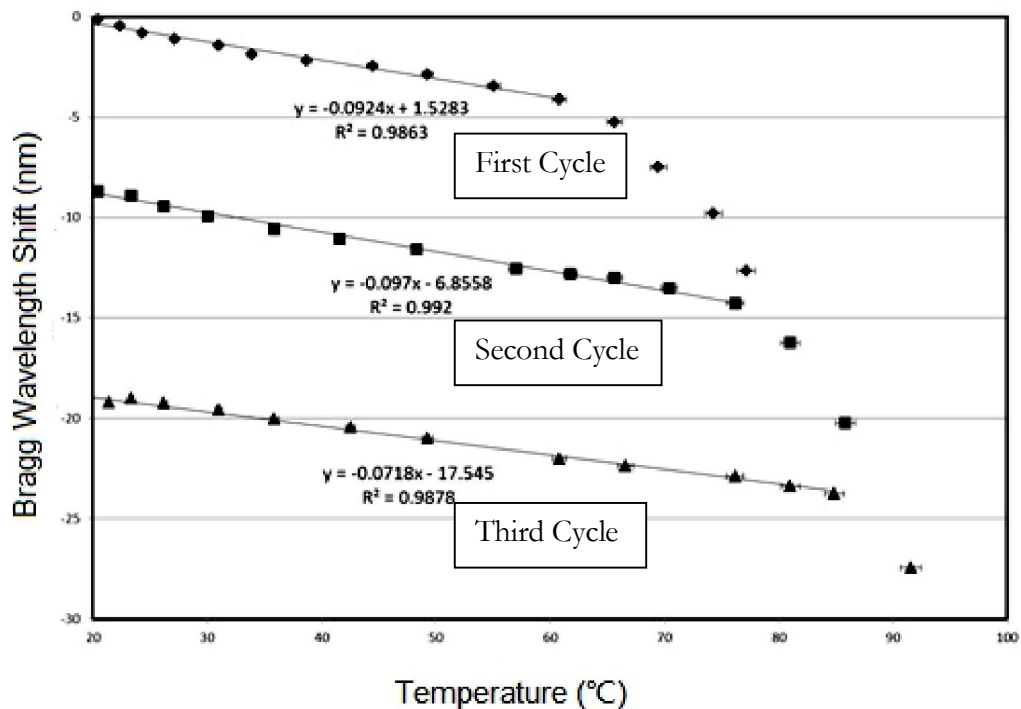


Figure 6- 11: Bragg wavelength shift with temperature for three consecutive heating cycles. ●First cycle, ■second cycle, ▲third cycle.

In order to understand the annealing process, samples of fibre were heated at temperatures ranging from 60°C to 100°C for 7 hours prior to grating inscription in the oven. The length and diameter of the fibre were measured during the heating

## 6. Polymer Optical Fibre Bragg Grating Sensitivity Characterisation

process. Three different samples of fibre (original length = 20cm) were measured at each temperature and the mean length change calculated. The results for the change in length with time for different temperatures are shown in Figure 6-12. At temperatures above 80°C, the decreasing of length increases significantly. Furthermore, the results also show that even after 7 hours, the fibre is still shrinking.

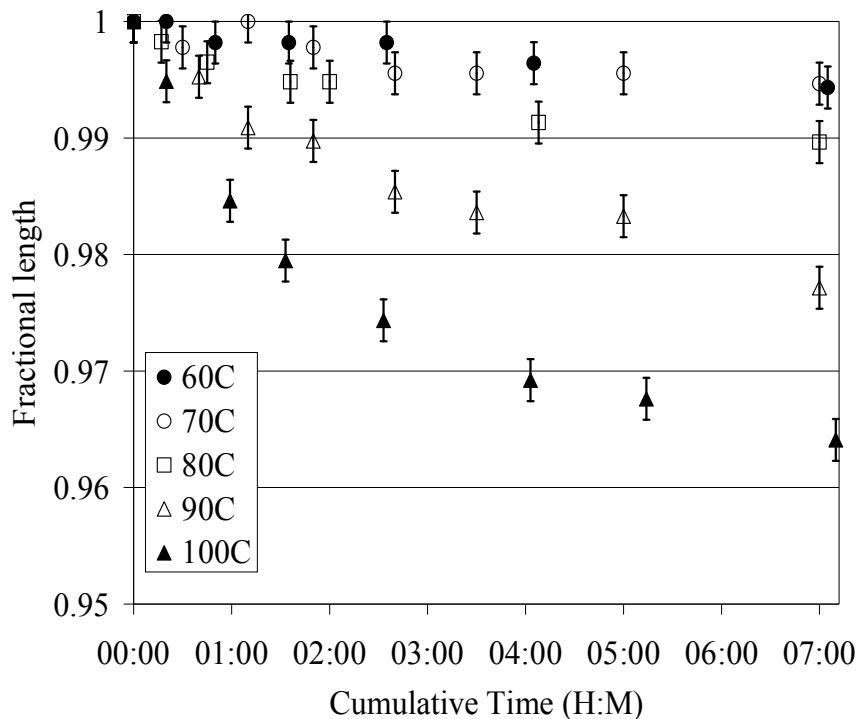
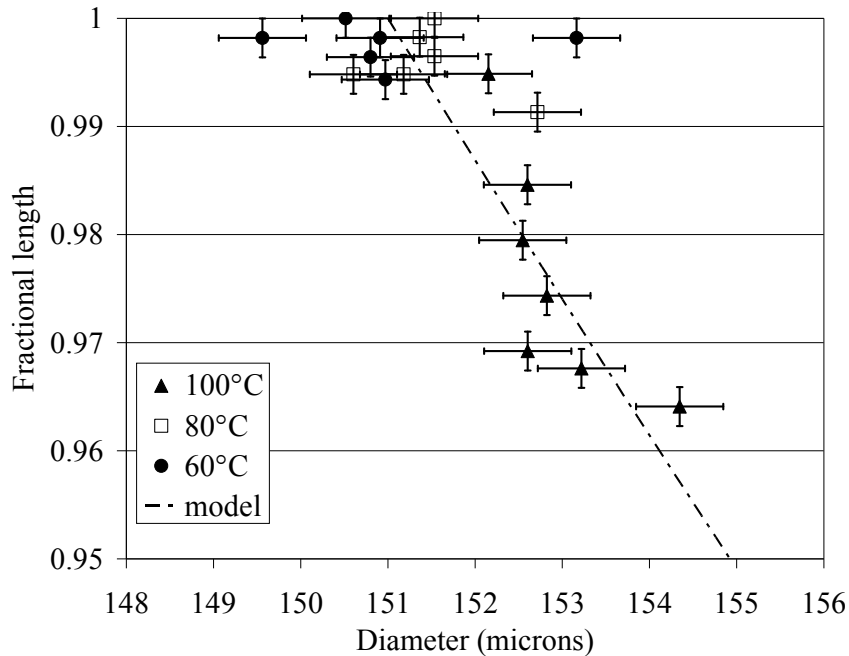


Figure 6- 12: Change in fibre length with time for different annealing temperatures.

The length and diameter results were combined in order to investigate whether there was likely to be any change in density of the fibre during shrinking. The results are shown in Figure 6-13 and indicate that there is no measurable change in density, and thus refractive index of the fibre during the annealing process. This result suggests that the most significant effect causing a permanent change in the grating wavelength during heating is the change in grating period due to shrinkage of the fibre, rather than any significant change in refractive index. This conclusion

## 6. Polymer Optical Fibre Bragg Grating Sensitivity Characterisation

also makes good agreement with the experimental results from Cariou et al, [10] who investigated the refractive index variations with temperature of PMMA and proved there is no such change when PMMA was heated below its glass transition temperature.



## 6. Polymer Optical Fibre Bragg Grating Sensitivity Characterisation

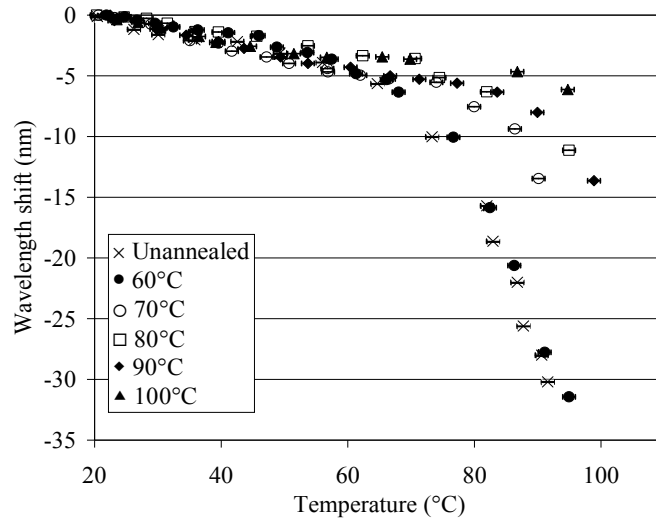


Figure 6- 14: Thermal response of gratings fabricated in preannealed fibre.

Figure 6-15 shows results from gratings fabricated in preannealed fibre and those fabricated in fibre annealed after inscription. There is good agreement between the results, with any small discrepancies due to the differences in annealing times (7 hours for the fibre before inscription, and 10 minutes per incremental temperature for the gratings annealed post inscription). This again suggests that the predominant effect in the permanent wavelength shift is that of fibre shrinkage.

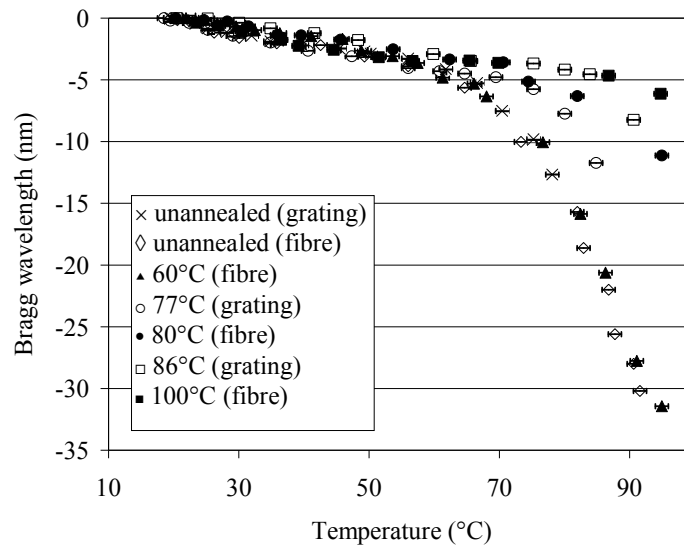


Figure 6- 15: Comparison between the thermal response of gratings fabricated in annealed fibre (fibre), and gratings made in unannealed fibre which were annealed after inscription (grating).

### 6.2.1.3 Thermal Properties of mPOFBGs in TOPAS

Similar measurements were carried out using the heating rig shown in Figure 6-9 for the FBGs inscribed in TOPAS fibre. In the experiment, the reachable maximum heating temperature was 28.4 °C, before the grating visibility became zero. The limitation of heating range is due to the shift of Bragg wavelength of the grating to the edge of the light source, of which the output power decreases dramatically, as already shown in Chapter 5. Typical results of the Bragg wavelength shift with temperature are shown in Figure 6-16, which reveals a positive temperature coefficient of  $250 \pm 0.5 \text{ pm}/^\circ\text{C}$ , when performing linear fit to the data – to the best of the authors' knowledge, this value is the highest temperature sensitivity of any FBG based device yet reported. Note that in PMMA, FBGs display a negative wavelength shift with rising temperature. [7]

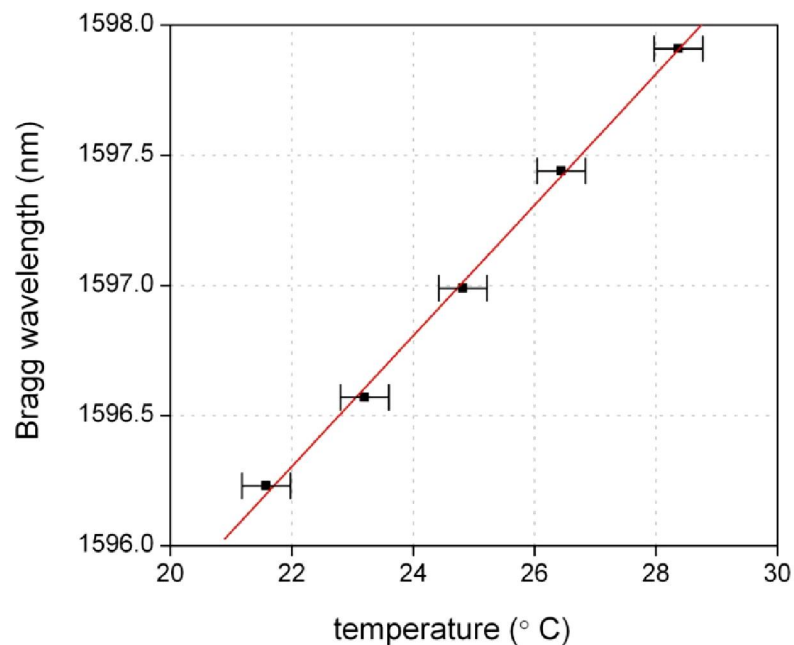


Figure 6- 16: Bragg wavelength shift with temperature of grating in TOPAS mPOF.

### 6.2.1.4 Discussion of Results

For PMMA mPOF, the temperature response results presented show a quasi-linear decrease of Bragg wavelength with increasing temperature below a transition temperature. This transition temperature is dependent on several factors. The thermal history of the fibre obviously affects the transition temperature, which has been proved in this chapter, as well as the fibre draw parameters [11] and UV exposure [12]. The exact mechanism associated with this transition is still not known, though it still can be largely explained by the fibre shrinking. As mentioned in Chapter 3, polymer optical fibres are pulled under tension, leading to residual strain in the fibre, as the polymer chains are axial orientated, while at a certain temperature, the axial orientated chains are thought to relax causing shrinkage of the fibre. [11] The temperature range of the transition region for non-annealed fibre coincides with that identified by Law as resulting in the best cleaves using a hot fibre/hot blade technique [13]. This shrinkage results in a permanent wavelength shift, which is dependent both on the maximum temperature to which the grating has been cycled, and the duration of heating. Thermal shrinkage tests on lengths of fibre without gratings indicate that there is no measurable change in density as a result of the shrinkage. Annealing of the fibre prior to grating inscription shifts this transition to a higher temperature dependent on the annealing temperature.

The equation describing the Bragg wavelength shift with temperature, as mentioned in Chapter 2 is as following [14]

$$\Delta\lambda_B = \lambda_B (\tilde{n}\alpha + \beta)\Delta T \quad (6.1)$$

## 6. Polymer Optical Fibre Bragg Grating Sensitivity Characterisation

where  $\Delta\lambda_B$  is the Bragg wavelength shift,  $\Delta T$  is the temperature change,  $\lambda_B$  is the wavelength of Bragg grating,  $\tilde{n}$  is the average effective core mode index in the grating area,  $\alpha$  is the thermal expansion coefficient,  $\beta$  is the thermo-optic coefficient. The reported thermo-optic coefficient for PMMA is around  $-1 \times 10^{-4} \text{K}^{-1}$  at room temperature but varies considerably with temperature, increasing in magnitude by about 40% over 40K [10]. Quoted values for  $\alpha$  vary between  $0.7 \times 10^{-4} \text{K}^{-1}$  and  $2.2 \times 10^{-4} \text{K}^{-1}$  [7,15-17]. By choosing different values above, we can get either a negative or a positive Bragg wavelength shift with temperature. However, to the authors' knowledge, no positive Bragg wavelength shift has yet been observed with PMMA. For the TOPAS material used in this study, the value of  $\beta$  ( $-10^{-4} \text{K}^{-1}$ ) [18] is also negative, but it is slightly smaller than  $\tilde{n}\alpha$  ( $1.53 \times 0.7 \times 10^{-4} \text{K}^{-1}$ ) [18] leading to a calculated positive Bragg wavelength shift of  $11 \text{ pm}/^\circ\text{C}$ , which is much smaller than the experimental result. It should be noted though that the values for the thermal expansion coefficient and thermo/optic coefficient obtained from reference [18] are only quoted to one significant figure, which leads to very large errors when the data are combined in equation 6.1 to calculate the thermal sensitivity. The data also refer to bulk material and the properties may well have been changed during the fibre drawing process. The discrepancy between the calculated and measured temperature sensitivities should be the subject of further work.

### 6.2.3 Thermal Response of Step-index POFBGs

When step-index single mode POF was humidity tested in the environmental chamber, as described in section 6.1.3, its thermal response was also investigated. With the humidity held constant at 45%, the temperature was

## 6. Polymer Optical Fibre Bragg Grating Sensitivity Characterisation

increased in the range of 18 °C to 39°C and at each step the temperature was held for 20 minutes to ensure the temperature equilibrium being built inside the huge volume of the chamber. The step-index POFBG exhibits a quasi linear thermal response, as shown in Figure 6-17 and the sensitivity determined to be  $-48.2 \pm 1 \text{ pm}/^\circ\text{C}$ . This sensitivity value is smaller than that of pure PMMA based mPOF, likely due to combination effect from the different drawing tension when producing these two kinds of fibres and also from the copolymers and photosensitive dopants doped into the step-index POF [19].

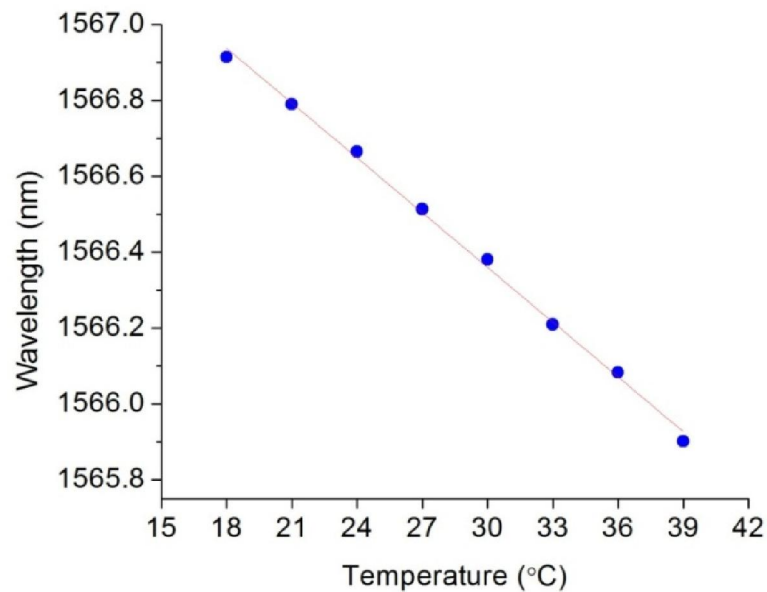


Figure 6- 17: Bragg wavelength shift with temperature of FBG in step-index single mode POF.

## 6.3 Strain Sensitivity of Step-index POFBGs

### 6.3.1 Introduction

The mechanical properties of PMMA based POFs have been discussed in Chapter 3. The fibre drawing history of the POFs can affect their mechanical

## 6. Polymer Optical Fibre Bragg Grating Sensitivity Characterisation

properties, like tensile strength, yield strain, failure strain, etc., and hence affect the strain sensing behaviour of POFBG. Furthermore, when POFBGs were applied to strain sensing, extra attention must be paid to the visco-elastic properties of the PMMA materials. Liu et al [20] have already reported that for tensile strains applied over relatively short time periods, reproducible, reversible and repeatable elastic behaviour of the POFBG has been confirmed for strains up to 22.2 m $\epsilon$  with a total tuning range of 32 nm which is much bigger than that of silica FBGs' few nanometres [21]. They also reported a strain sensitivity of 1.46 pm/ $\mu\epsilon$ , which is again better than that of silica FBGs' 1.2 pm/ $\mu\epsilon$ . In this section, the tensile strain tunability and sensitivity of fabricated doped PMMA based step-index POFBGs are characterized.

### 6.3.2 Experimental Arrangement

The strain tuning of polymer fibre Bragg gratings is investigated by the mechanical stretching, using the arrangement shown in Figure 6-18. To be noted here, the tensile behaviour of the pure PMMA mPOFBG was not able to investigated, due to the requirement of gluing the POF with Bragg grating to a silica optical fibre to form a device before testing.

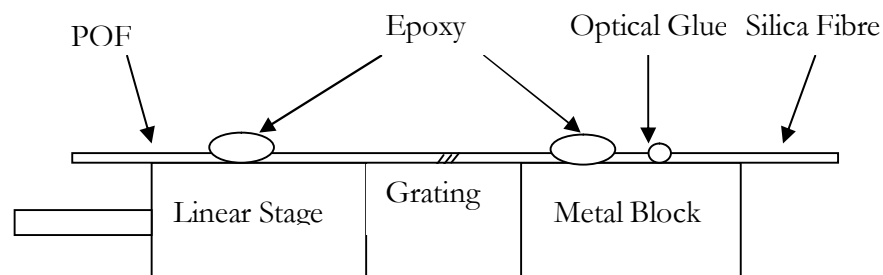


Figure 6- 18: Strain testing rig for step-index POFBGs.

## 6. Polymer Optical Fibre Bragg Grating Sensitivity Characterisation

During the test, the doped PMMA based step-index POFGBG device was fastened on the strain testing rig by Araldite epoxy adhesive, with one end on the metal block and the other on a linear stage with micropositioner (displacement accuracy = 0.01 mm), which can be moved longitudinally to apply axial tensile strain to the POF. The 6mm grating region is located in the middle of the 4 cm gap between the metal block and the linear stage. The axial strain values acting on POF are determined by dividing the longitudinal extension displacement of the POF by the  $4\pm 0.1$ cm. The axial strain is applied by manually moving the micropositioner with a speed of approximately  $1\text{m}\epsilon/\text{min}$ . During the whole process, the reflection spectra of the POFBG were recorded as the tensile strain is applied.

### 6.3.3 Strain Sensitivity and Tunability of Step-index POFBG

A loading-unloading experiment is designed to examine the strain tunability of the step-index POFBGs. In the loading process, the tensile strain is applied to the polymer fibre Bragg gratings in steps to certain value, which is 0.5%, 1%, 1.5%, 2% and 2.5% tensile strain respectively and then in the unloading process, the strain is gradually released to zero. During both processes, the reflection spectra of the POFBGs at each step are recorded by using the same broadband ASE light source and the optical spectrum analyser as in grating inscription.

The reflection spectrum of the same POFBG under different tensile strain is shown in Figure 6-19, which indicated that the Bragg wavelength of the grating shifted with the strain increased. It also gives the information of the variation of the reflection peak level at different tensile strains. Below the strain value of 2%, which corresponds to the Bragg wavelength tuning range of 26.6nm, the reflection peak level decreases continuously with increasing tensile strain. This is most

## 6. Polymer Optical Fibre Bragg Grating Sensitivity Characterisation

probably due to the decrease of the output power of the broadband ASE light source (refer to the output spectrum in Chapter 5), as the shape of the grating spectrum is almost constant and the grating spectrum can be restored to its original reflection peak level and the Bragg wavelength, when the stress to the POF is removed. Note when the grating spectrum shifts beyond 1590nm, its peak visibility is almost zero. For this reason, the strain behaviour of the FBGs with over 2% tensile strain applied is unable to be studied.

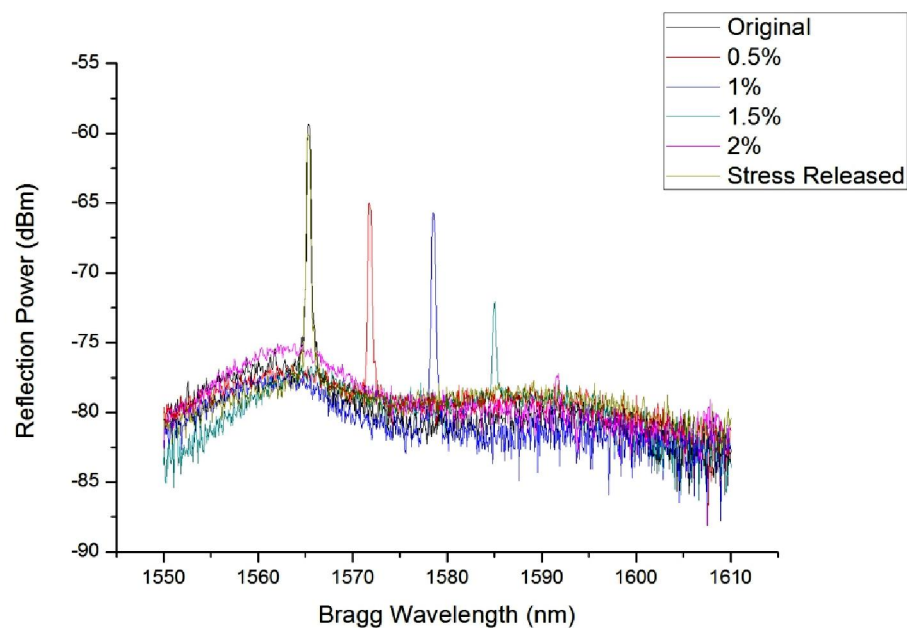
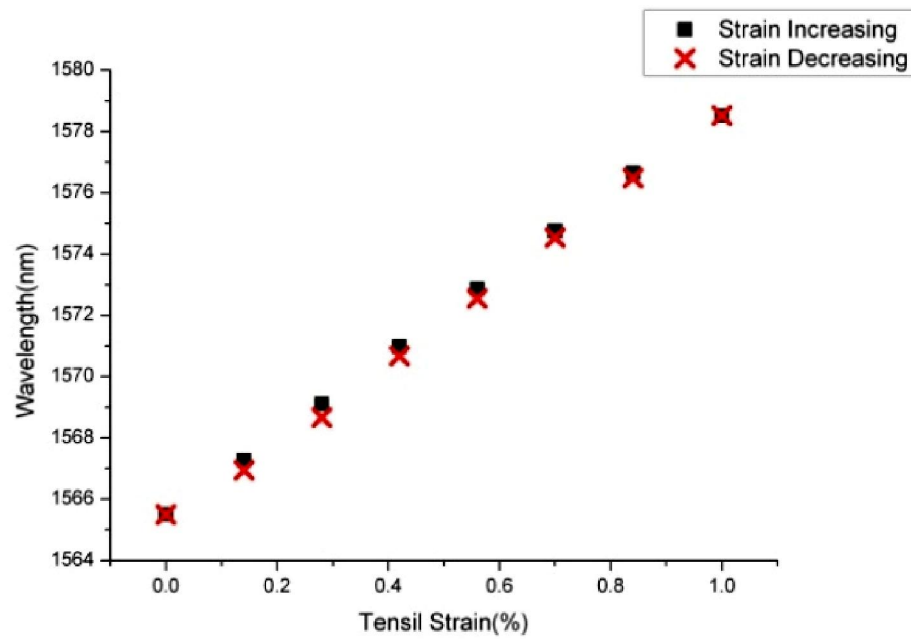
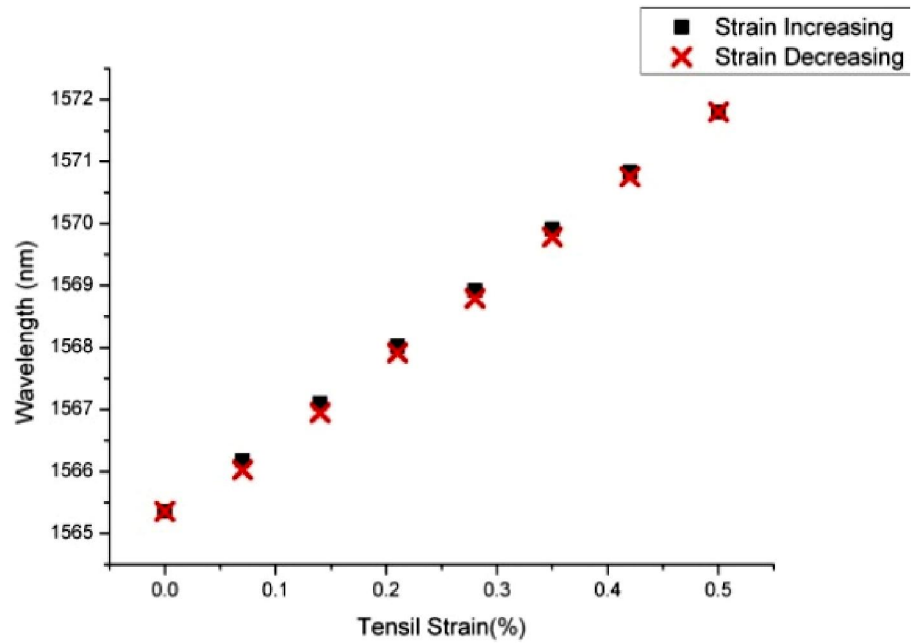


Figure 6-19: Reflection spectra of POFBG at four different tensile strain.

The cyclic loading–unloading test results in Figure 6-20 show that the step-index POFBGs have excellent reversibility and repeatability when the tuning strain is less than 2%. From the graph, the Bragg wavelength variation data obtained during the four different loading and unloading processes have good coincidence with each other, indicating that there is no hysteresis observed during the tensile strain tuning of POFBGs, thus the time-dependent viscoelastic effect was not

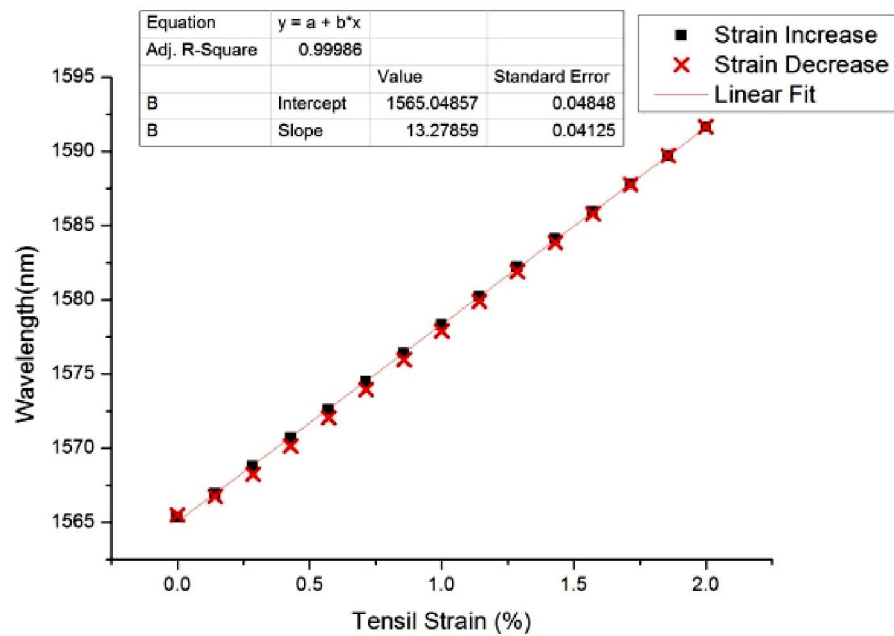
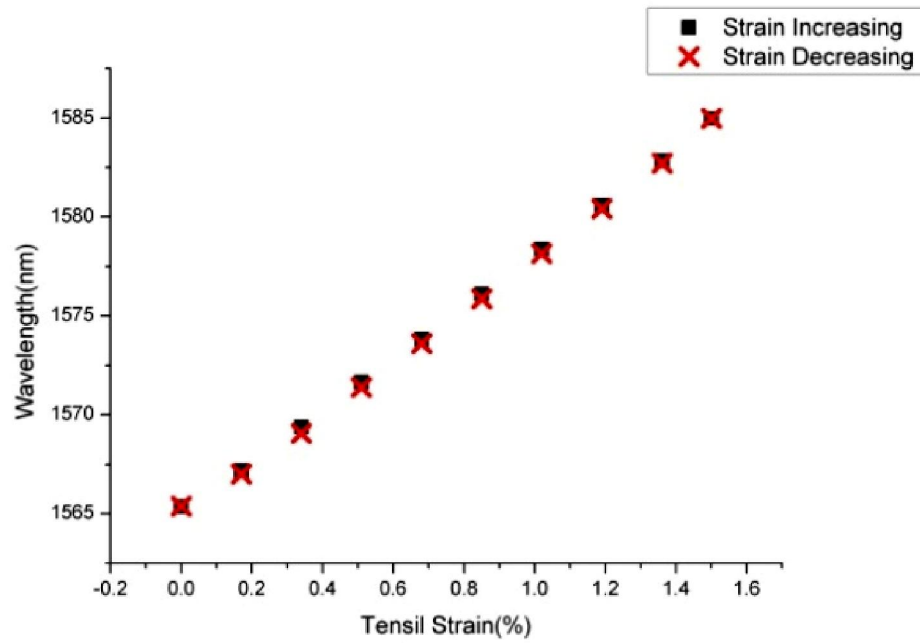
## 6. Polymer Optical Fibre Bragg Grating Sensitivity Characterisation

observed. From the data in graph 6-20(d), a strain sensitivity of  $1.33 \pm 0.04 \text{ pm}/\mu\epsilon$  can be calculated which is better than the sensitivity of silica FBGs.



(b)

## 6. Polymer Optical Fibre Bragg Grating Sensitivity Characterisation



(d)

Figure 6- 20: Bragg wavelength shift of POFBGs under reversible tensile strain test at the maximum strain of (a) 0.5% (b) 1% (c) 1.5% (d) 2%.

## 6. Polymer Optical Fibre Bragg Grating Sensitivity Characterisation

As mentioned in Chapter 3, the yielding strain of the PMMA based polymer fibre is about 6%, however, in this loading-unloading experiment, the applied strain to the step-index POF only reached 2%. For further investigation, the potential solution could be writing a grating at lower wavelength that will allow bigger strain tuning range of the step-index POFBGs.

### 6.4 Conclusion

In this chapter, the gluing coupling method between the single mode step-index POF and the single mode step-index silica fibre is developed and Norland 76&78 are proved to be the most suitable optical adhesive for this gluing task. However, the same method can not work on connecting microstructured POF and silica fibre.

Following the successful gluing method, the linear humidity sensitivity response of PMMA based POFBG is able to be obtained in an environmental chamber. The characterised humidity sensitivity is  $38.3 \pm 0.5$  pm per % RH and the repeatability of the sensitivity is verified to be good when the humidity cycles between 45% and 85% RH.

The wavelength to temperature response for various kinds of POFBG is also studied. Initially, the pure PMMA mPOFBG is heated up to 91.5°C in three heat-cool cycles. The Bragg wavelength shifts to lower wavelength region when mPOFBG is heated and the thermal response of the device is found to be non-linear in each cycle though a quasi-linear region always existing. The thermal sensitivity of the mPOFBG at quasi-linear region is varying between -97 pm/°C and

## 6. Polymer Optical Fibre Bragg Grating Sensitivity Characterisation

-71.8pm/°C. Furthermore, the permanent operational wavelength shift of the grating is observed, once the fibre is taken above a certain threshold temperature. The mechanism of the permanent change in the grating wavelength is investigated and is proved to be caused by the change in grating period due to shrinkage of the fibre, rather than any significant change in refractive index and it is also possible to shift this threshold temperature to higher temperatures by annealing the POF prior to grating inscription. In addition, the quasi-linear wavelength response to temperature is demonstrated to temperature up to 90°C by annealing the POF at 100°C after successive heating cycles that can be accounted for by fibre shrinkage.

The largest Bragg wavelength shift with temperature in transmission to date is observed in TOPAS mPOFBG. The measured temperature sensitivity is  $50 \pm 0.5 \text{ pm}/^\circ\text{C}$  when the device is heated from ambient temperature to 28.4 °C. The positive shift of the Bragg wavelength is different with the negative Bragg wavelength shift that was observed in PMMA mPOFBG. Some explanation to this phenomenon is given in this chapter but still have further works to be done.

A linear Bragg wavelength response to the relatively low temperature (18°C-39°C) is observed in step-index POFBG which reveals a thermal sensitivity of  $-48.2 \pm 1 \text{ pm}/^\circ\text{C}$ .

Finally, the strain sensitivity and tunability of step-index POFBG was investigated, which showed a reversible and repeatable elastic response up to 2% tensile strain for a strain rate of 1mε/min. The measured strain sensitivity of  $1.33 \pm 0.04 \text{ pm}/\mu\epsilon$  is better than that of silica FBGs.

## References

- [1] J.Brandrup, E.H.Immergut, and E.A.Grulke, eds., Polymer Handbook (Wiley, 1999). [2] D. T. Turner, "Polymethyl methacrylate plus water: sorption kinetics and volumetric changes," Polymer 23, 197–202 (1982).
- [3] N. G. Harbach, "Fiber bragg gratings in polymer optical fibers." PhD thesis Lausanne: EPFL, 2008.
- [4] SANYO Gallenkamp Product-Manual. SANYO E&E Europe BV.
- [5] T. Kaino, "Influence of water absorption on plastic optical fibers," Appl. Opt. 24, 4192–4195 (1985).
- [6] Y. Hida, Y. S. Imamura, "Influence of water sorption on acrylic polymer waveguide loss," IEEE Photon.Technol. Lett., 6, 845-847 (1994).
- [7] H.Y.Liu, G.D.Peng, and P.L.Chu, "Thermal tuning of polymer optical fiber bragg gratings," IEEE Photon.Technol. Lett. 13, 824 (2001).
- [8] H.B.Liu, H.Y.Liu, G.D.Peng, and P.L.Chu, "Strain and temperature sensor using a combination of polymer and silica fibre bragg gratings," Opt. Commun. 219, 139-142 (2003).
- [9] A. Othonos and K. Kalli, Fiber Bragg Gratings: Fundamentals and Applications in Telecommunications and Sensing. Artech House, Nordwood, MA, 1999.
- [10] J. M. Cariou, J. Dugas, L. Martin, and P. Michel, "Refractive-index variations with temperature of PMMA and polycarbonate," Appl. Opt. 25, 334-336 (1986).
- [11] T.Ishigure, M.Hirai, M.Sato, and Y.Koike, "Graded-index plastic optical fibre with high mechanical properties enabling easy network installations I" J. Appl. Polym. Sci. 91, 404-409 (2004).
- [12] E.E.Shafee, "Effect of photodegradation on the [beta]-relaxation in poly(methylmethacrylate)," Polym. Degrad. Stabil. 53, 57-61 (1996).

## 6. Polymer Optical Fibre Bragg Grating Sensitivity Characterisation

- [13] S.H.Law, M.A.van Eijkelenborg, G.W.Barton, C.Yan, R.Lwin, and J.Gan, "Cleaved end-face quality of microstructured polymer optical fibres," *Opt. Commun.* 265, 513-520 (2006).
- [14] A. Othonos and K. Kalli, *Fiber Bragg gratings: fundamentals and applications in telecommunications and sensing*, (Boston: Artech House, 1999) [15] A. Fender, M. Silva-López, W. N. MacPherson, J. S. Barton, J. D. C. Jones, D. Zhao, H. Dobb, D. J. Webb, L. Zhang, and I. Bennion, "Strain and temperature sensitivity of a single-mode polymer optical fibre," *Opt. Lett.* 30, 3129–3131 (2005).
- [16] Z.Y. Zhang, P. Zhao, P. Lin, F.G. Sun, "Thermo-optic coefficients of polymers for optical waveguide applications," *Polymer*, 47,14, 4893-4896 (2006).
- [17] S. H. Goods, R. M. Watson, and M. Yi, "Thermal Expansion and Hydration Behavior of PMMA Molding Materials for LIGA Applications, "SAND REPORT, SAND2003-8000, Sandia National Laboratories, 2003.
- [18] Topas® cyclic olefin copolymer Product Specification Document (Ticona Inc.).
- [19] T. Ishigure, M. Hirai, M. Sato, Y. Koike, "Graded-index plastic optical fiber with high mechanical properties enabling easy network installations. II," *J. Appl. Polym. Sci.* 91, 410-416 (2004).
- [20] H. Y. Liu, H. B. Liu, G. D. Peng, "Tensile strain characterization of polymer optical fibre Bragg gratings," *Opt. Commun.* 251, 37-43 (2005).
- [21] Andreas Othonos, "Fiber Bragg gratings," *Rev. Sci. Instrum.* 68, (1997).

# 7

## **Application of Polymer Optical Fibre Bragg Grating Sensors to Condition Monitoring of Textiles**

In this chapter, POF FBGs were used to measured strain in textile specimens. The quasi static tensile strain measurement of the specimen bonded with POF FBGs was carried out. Furthermore, the long term tensile strain test of the specimen was conducted in a temperature and humidity controllable environmental chamber. To be noted here, all the POF FBGs mentioned in this chapter were fabricated by the author at Aston University and the long term tensile test was finished by the author at Aston University. Under a collaboration with the mechanical engineering department of the University of Southampton, the quasi

static tensile experiment was executed with the help of Dr. Chenchun Ye from University of Southampton.

## **7.1 Introduction**

Tapestries are hand-woven textiles that are often large and heavy. Researchers have found the strain imposed by their own weight may be the key factor in their deterioration [1, 2]. Monitoring the stain, hence monitoring the deformations that occur in tapestries, is quite helpful to the textile conservation researchers. The FBG sensor was an attractive potential solution for monitoring the deformations that occur in tapestries [2]. However, in the previous research, only the trial with silica FBG was performed and it did not produce an effective strain transfer because the reinforcement introduced by the sensor attachment was significant [3]. The reason that causes this problem is that when the silica FBG sensor is used to monitor the material with low Young's modulus, the silica fiber itself can act to locally stiffen the material with applied stress, reducing the strain experienced in the region of the sensor. In contrast, POF can have much less of this effect, considering one of the significant advantages of POF: Young's modulus of PMMA POF is approximately 25 times smaller than that of a silica optical fibre [4], which is more compatible with the modulus of the textile, POF based FBG should provide an improved performance over silica fibres in applications to textiles. In this chapter, the POF based FBG will be used to measure the tensile strain applied to the textile.

## 7.2 The tensile Strain Measurement of Textile

### 7.2.1 Textile Specimen Preparation

The textile specimen used for experiments was 340mm long, 49 mm wide, 0.57 mm thick. Both the warp and weft yarns on the textile are wool with a spacing of 0.8 mm in the warp direction and 1.7 mm in the weft direction. Four FBGs, where two were silica optical fibre based FBG, two were POF based FBG, were bonded to the central part of the specimen, as shown in Figure 7-1.

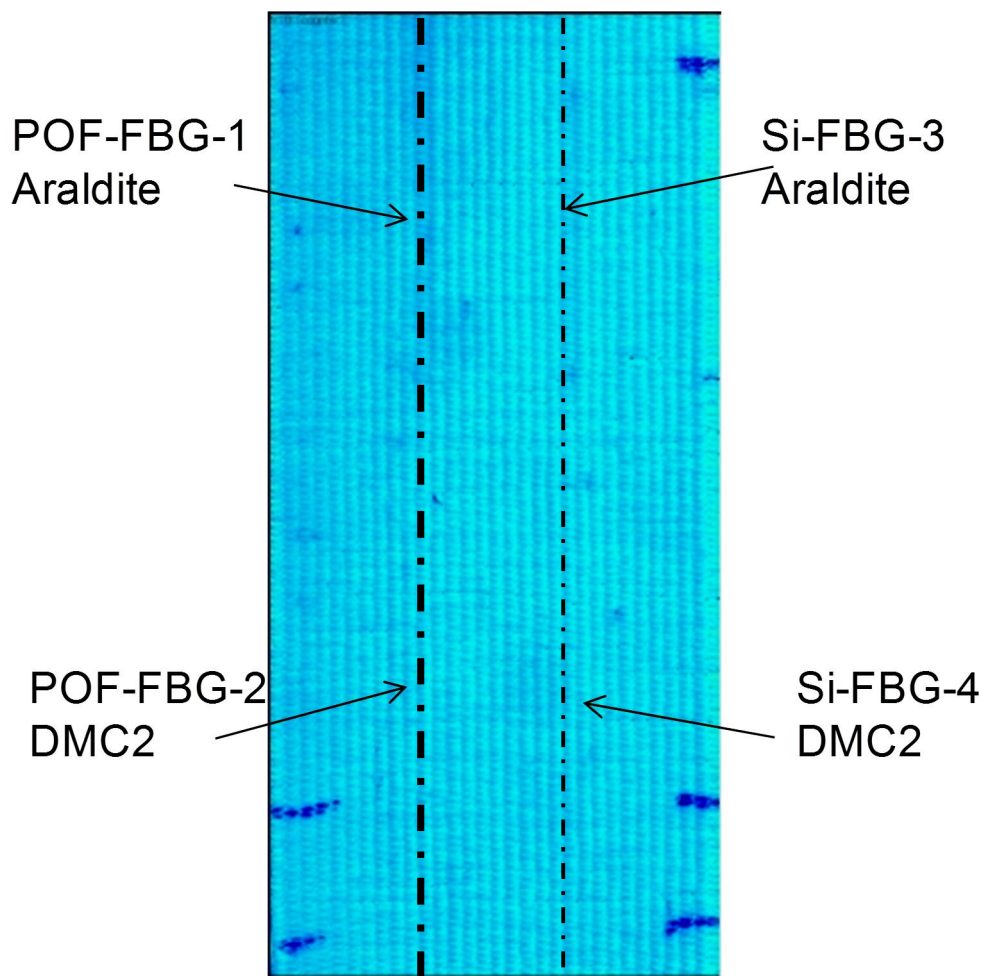


Figure 7- 1: Textile specimen with two POF FBGs and two silica FBGs bonded with different adhesives. (The image of the specimen was taken from the side without adhesives.) [data provided by C.C.Ye]

POF-FBG-1 and POF-FBG-2 were FBGs in POFs with a Bragg wavelength 1562 and 1565 nm respectively, which were fabricated following the method mentioned in Chapter 5. The length of each POF with Bragg grating was approximately 6cm and the grating length is 6mm. Each POF FBG was connected to a single mode silica optical fibre pigtail (with FC/APC) by the same gluing method as described in Chapter 5. The Si-FBG-3 and Si-FBG-4 were FBGs in silica optical fibres, with a Bragg wavelength 1542 and 1547 nm respectively, which are commercial product. To avoid the mixture of different grating's response to the strain, the Bragg wavelength of these gratings were separated. Si-FBG-3 and POF-FBG-1 were bonded to the textile surface with two part epoxy Araldite 2015, and Si-FBG-4 and POF-FBG-2 were fixed with the PVA based conservation adhesive Mowilith DMC2. The axes of the four FBGs were parallel to the weft yarns and the centres of the four FBGs were respectively on the corners of a rectangle, which is 16x50 mm. For each FBG, the area covered with adhesive was 3 mm wide, and up to 50 mm long. The thickness of adhesive was up to 0.4 mm. In addition, the mechanical strength of the connection between the POF and the silica fibre with an optical adhesive is weak and also, the section of silica fibre near the connection had coating stripped, which leads to this section being brittle. Both of these two parts make it very difficult to attach the POF FBG to the textile/tapestry appropriately. To make the test feasible, a short length of silica fibre with coating was bonded to the textile, as shown in Figure 7-2. The drawback for doing this is that the area with adhesive is comparatively long (~50 mm), although within acceptable limits, but also to avoid the breakage of the fibre connection, the maximum strain applied to the specimen is limited.

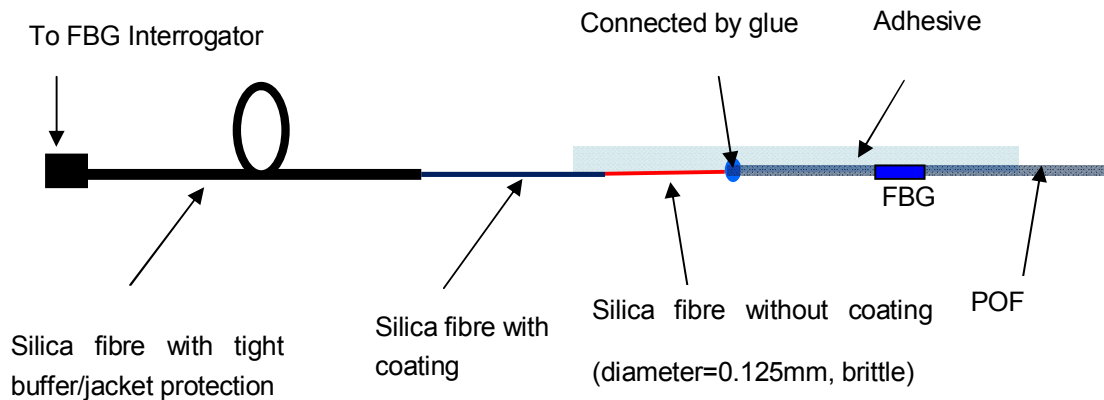


Figure 7- 2: Schematic of bonding POF based FBG to textile.

## 7.2.2 Quasi-static Tensile Test

### 7.2.2.1 Testing Setup

For carrying out the quasi-static tensile strain test to the textile specimen, an Instron 5569 test machine was used to apply load in the weft direction of the tapestry. The specimen was mounted in wedge grips of the test machine and the distance between the grips was 240mm. For quasi static tests, a constant displacement of 10 mm/minute was applied to the specimen. The deviation of the load was typically  $\pm 0.7\text{N}$ . The silica optical fibre pigtailed were connected to a swept laser integrated FBG Interrogator (FBG-SLI, Micron Optics) to monitor and record the Bragg wavelength shift, when the strain was applied to the textile specimen. The resolution of measured wavelength is 1pm, corresponding approximately to  $1\mu\epsilon$ . The wavelength range of the interrogator is from 1520 to 1570nm.

During the test, to provide a comparable independent measure of strain in a non-contact method [5], a LaVision digital image correlation (DIC) system [6] with

a single camera was used to obtain 2D full-field strain data of the specimen. Digital image correlation technique is based on an image-processing algorithm that uses grey-scale image patterns to track the 2D (with single camera) or 3D (with two cameras) surface displacement of a deformed object and then the displacement vector field is used to acquire the strain distribution. [7] Interrogation cells are the pixel arrays that were divided from the DIC image data, when the data is processed to produce deformation and strain behaviour. The size of interrogation cells is crucial to the spatial resolution and strain resolution. With the increasing of the interrogation cells, the spatial resolution is getting worse, while the strain resolution is getting better. In this work, when the strain was applied across the width of the specimen, the local strain variations from interrogation cell to cell in the section with adhesives and FBGs would be relatively quite different with that of the rest part of the sample, due to reinforcement. Hence, better spatial resolution in the strain from the DIC image processing is required. Therefore, the size of the interrogation window was chosen to be 32 x 32 pixels with 50% overlap, corresponding to 3 x 3 mm in the specimen. The small interrogation windows (32 x 32 pixels with 50% overlap) offer a minimum strain resolution of  $(0.1 \times 2) / 16 = 1.25\%$  [6]. The strain resolution is calculated by multiplying the precision of displacement vectors (With a 32 x 32 pixels interrogation window, at the worst contrast, the uncertainty is approximately 0.1 pixels) by a factor of 2 (There is two displacement vectors in the strain calculation), and dividing by 16 pixels, which is the gauge length. The strain resolution can be improved with good image contrast and by averaging over a number of interrogation windows. Figure 7-3 illustrates the typical strain distribution of the specimen under 20N load. It illustrates that the strain values in two areas covered by Araldite (POF-FBG-1 and Si-FBG-3) are

significantly lower than the rest of the sample and the strain in the area where a silica fibre Si-FBG-3 was bonded with DMC2 is also lower than the surrounding areas, while the strain difference induced by the bonding of POF-FBG-2 with DMC2 is smaller. Moreover, in the image, the patchiness of the strain distribution indicated typical errors in strain values obtained from DIC with this level of spatial resolution. Similar noise was also observed using a 3D two camera system for either metal or textile specimens, indicating it was an image processing error rather than an indication of the heterogeneity of the textile sample.

For the area away from the FBGs and adhesive, the uncertainty of the measured strain from DIC is reduced by averaging over a number of interrogation windows, and is estimated to be 0.06%. For the area with a FBG bonded, the strain measurement from DIC is virtually like an extensometer measurement [6] taken by correlating the interrogation cells which are overlapped the FBG at either end of the 20mm horizontal line of the image (Figure 7-3). The uncertainty for the measured strain is estimated to be  $0.2 \times 2/214 = 0.19\%$ .

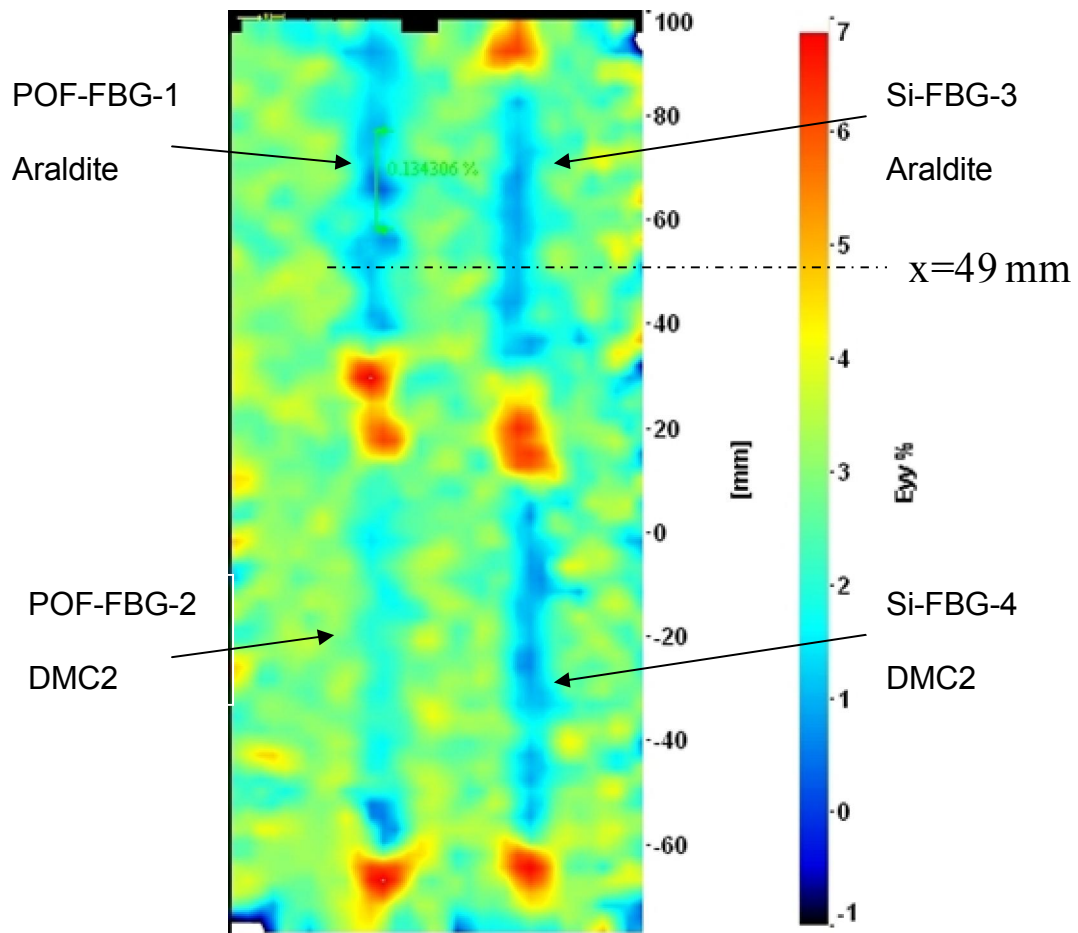


Figure 7- 3: The strain map obtained from DIC when the specimen was under a load of 20 N. [data provided by C.C.Ye]

The gratings are bonded to the textile using adhesive that covers the optical fibre and the adjacent area, which is in total approximately 3mm wide. As the interrogation cells cover an area of 3 mm then only one full interrogation cell can cover the area of the adhesive, this introduces more error. Furthermore, the reinforcement effects make the strain less in these areas introducing a more significant measurement error. To examine the strain map more clearly, the strain distributions along horizontal direction at  $x = 49\text{mm}$  (see Figure 7-3) for three different load levels of 1, 10 and 20N are given in Figure 7-4. In Figure 7-4 the half size of each interrogation cell (1.5 mm) can be seen.

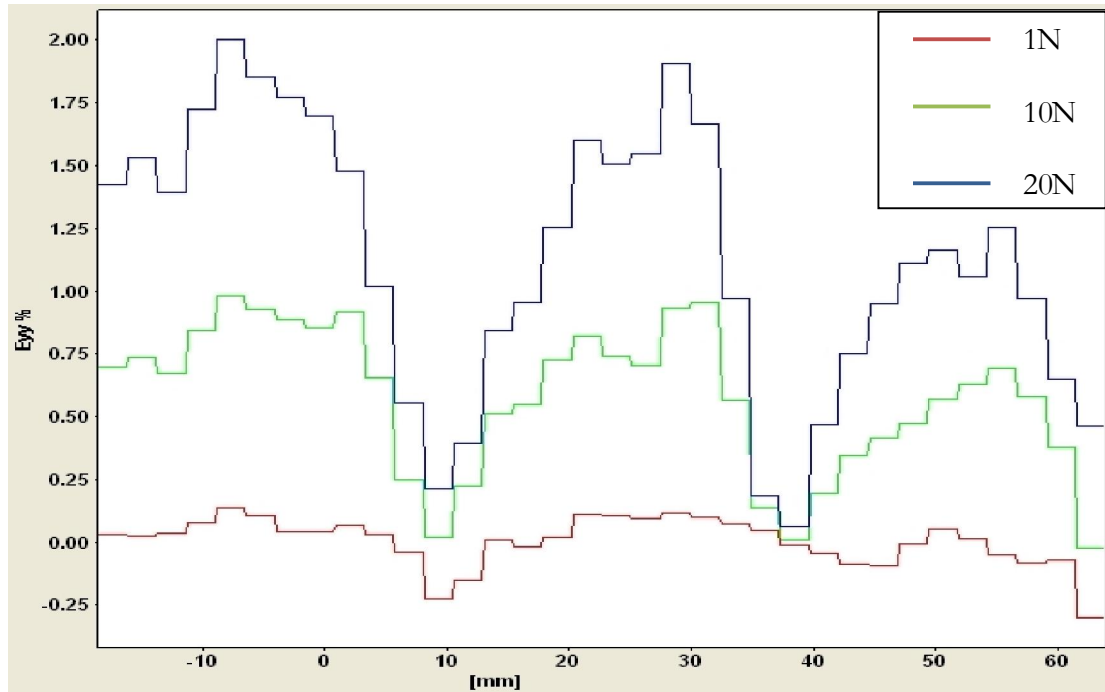


Figure 7- 4: Strain distributions along horizontal axis, at  $x = 49$  mm, for three different values of load up to 20 N (scale of the axis: 1.59:1) [data provided by C.C.Ye]

### 7.2.2.2 Experiment Results

#### 20N Load

The maximum load of 20N was applied to the specimen in an ambient condition. The recorded Bragg wavelength shifts of the four FBGs are given in Figure 7-5. To be noted here, for POF-FBG-2, parts of the data were missing, because its Bragg wavelength shifted out of the maximum measurement limit of FBG interrogation system. The maximum recorded wavelength was 1572nm

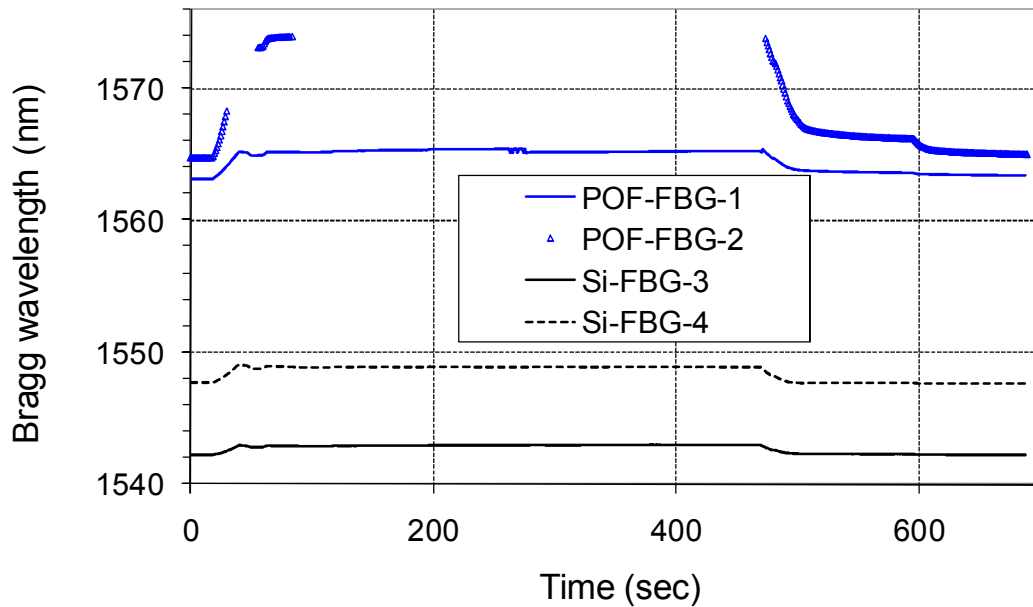


Figure 7- 5: Recorded Bragg wavelengths of the four FBGs (up to 20N load). [data provided by C.C.Ye]

Using a strain sensitivity of  $1.33 \text{ pm}/\mu\epsilon$  for POF FBGs (as measured in Chapter 6) and  $1.20 \text{ pm}/\mu\epsilon$  for silica fibre FBGs, the stress (total load divided by the area of cross section of the textile specimen) is plotted against strains from different FBGs and from DIC system for different locations in Figure 7-6. The recorded strain from POF FBG is greater than that from the silica FBG with the same adhesive and the recorded strain from each type of FBG with DMC2 is greater than that with Araldite 2015. The measured strains from DIC system for the areas where the two silica FBGs were bonded are quite noisy, and even became negative when the load was small. This indicates that the strain resolution of the DIC system is not high enough to measure accurately strains smaller than 0.2%. [3] The strains from the two POF FBGs almost match the corresponding strains from DIC, although the one bonded using the epoxy adhesive shows much more scatter.

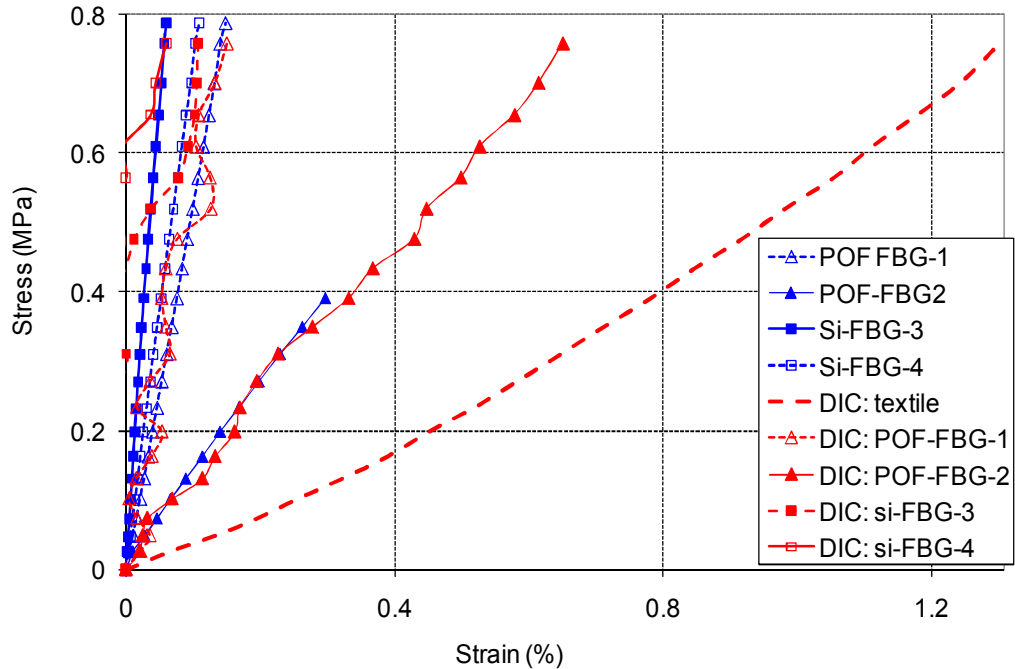


Figure 7- 6: Stress plotted against strains from FBGs and from DIC for different locations. [data provided by C.C.Ye]

Figure 7-7, which is the magnified part of Figure 7-6, shows the plots for both the strain obtained from Si-FBG-3 and Si-FBG-4 only, along with the DIC data taken local to the sensors. It is clearer that the strains from DIC local to the silica FBGs are subject to larger uncertainties. Ideally, the linear fit of the strain data from DIC system (black dash line and solid line) should correspond with the stress-strain gradients obtained from the FBGs, however, there actually exists large difference between them and only for the larger strains the correspondence is getting much better. This again indicates that at the strain resolution of the DIC system is not high enough to measure accurately strains smaller than 0.2%

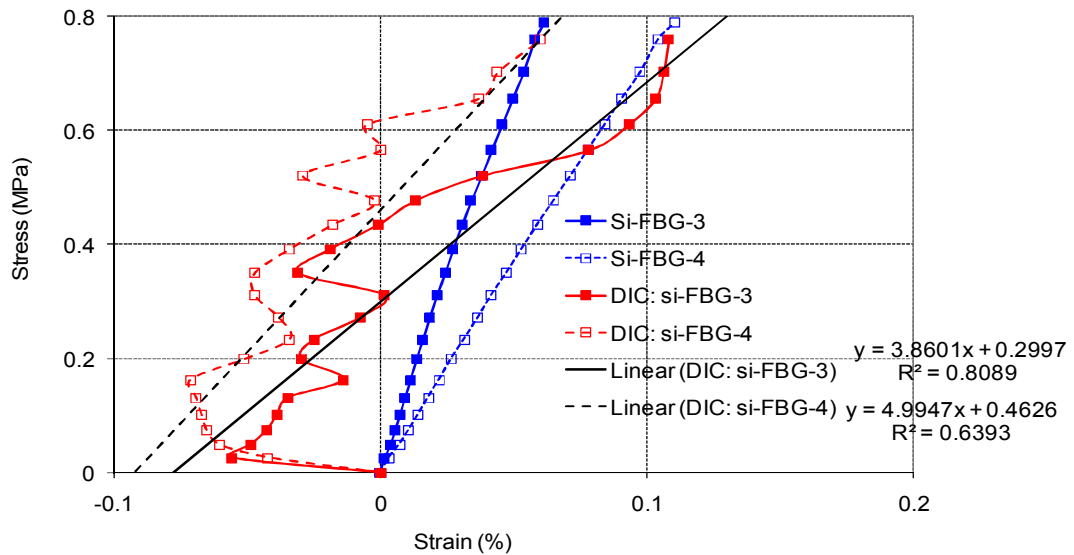


Figure 7- 7: Stress plotted against strains from FBGs and from DIC associated with silica FBGs.

[data provided by C.C.Ye]

### 10N Load

Since the Bragg wavelength shift of the POF FBG-2 exceeded the upper limit of the wavelength range of the FBG-interrogation system, when the load was greater than 10 N, the quasi-static test was done with the maximum load of 10N only in the ambient condition. The results are similar to that with 20N loading and are shown in Figures 7-8. The extra information given in Figure 7- 8 is the recorded Bragg wavelength shifts of four gratings when the load is released. It took much longer time for the Bragg wavelengths of POF FBGs to return to the original values, [8,9] comparing with silica FBGs. 37 minutes after the load was removed, the residual wavelength shift of POF-FBG-2 was still about 0.8 nm, however the Bragg wavelength of Silica-FBG-3 and Silica-FBG-4 had already shifted back to the original values.

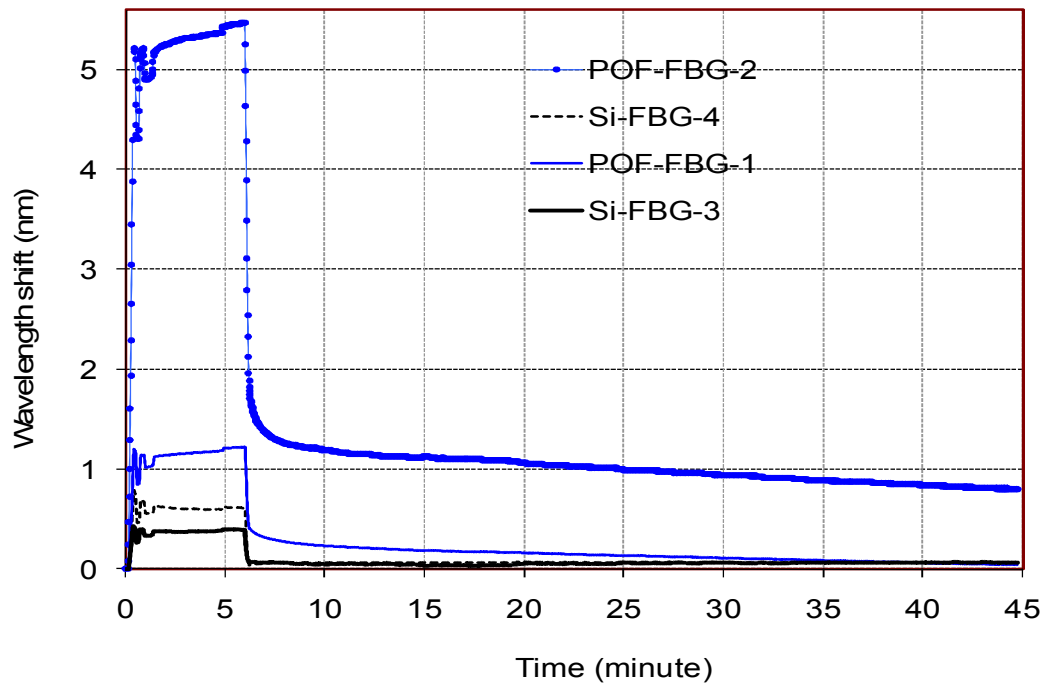


Figure 7- 8: The recorded Bragg wavelength shifts of the four FBGs during the 10N quasi static test.

[data provided by C.C.Ye]

The stress-strain curves for the four gratings obtained from two quasi-static tests with the maximum load of 10N and 20N, are shown in Figure 7-9. This demonstrates that the repeatabilities in both silica and POF sensors are reasonably good. The strain from POF-FBG-2 during 10N test was 0.02% approximately greater than that during 20N test for a given stress. This is likely due to the time between the two tests was too short for POF-FBG-2 or the textile to relax completely. Since it was observed that when the load applied to the specimen was removed, the Bragg wavelength of POF-FBG2 relaxed to original value much slower than other FBGs.

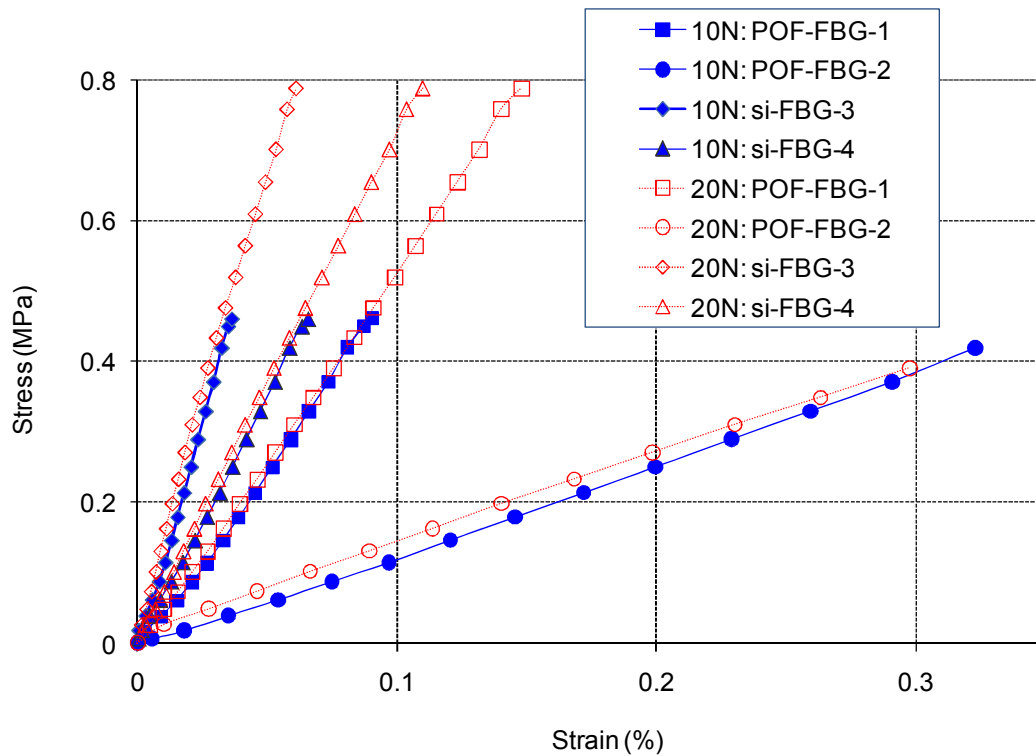


Figure 7- 9: Stress plotted against strains from FBGs for 10 N quasi-static test (solid markers and lines in blue colour); For each grating, the curve obtained from the previous 20 N quasi-static test is also shown in the figure (open markers and lines in red colour). [data provided by C.C.Ye]

### 7.2.2.3 Calculation and Discussion of Structural Reinforcement and Strain Transfer

By using the measured data given in Figure 7-6, the strain transfer coefficients and reinforcement coefficients can be calculated. The strain transfer coefficient is denoted as  $R_1$  and is the ratio of the strain measured from the FBGs divided by the strain measured from the DIC system in the area local to the sensor.

$$R_1 = \frac{\epsilon_{FBG}}{\epsilon_{DICL}} \quad (7.1)$$

The reinforcement coefficient is denoted as  $R_2$  and is denoted as the ratio of strain measured by the DIC local to the sensor to that away from the sensor.

$$R_2 = \frac{\epsilon_{DICL}}{\epsilon_{DICA}} \quad (7.2)$$

The two coefficients  $R_1$  and  $R_2$  and the strains  $\epsilon_{FBG}$ ,  $\epsilon_{DICL}$  and  $\epsilon_{DICA}$  for each sensor/adhesive combination are given in Table 6-1. Ideally,  $R_1$  should be close to unity and for the POFs this is the case. However for the Si-FBGs, it is different. The relative error in  $\epsilon_{DICL}$  local to the silica FBGs is a key consideration. In Table 6-1 the calculated theoretical value for  $R_1$  also provided using an analytical model [10] as follows:

$$R_1 = 1 - \frac{\sinh(kL)}{kL \cosh(kL)} \quad (7.3)$$

where  $k = \sqrt{\frac{1}{(1 + \nu_{ad})(E_f / E_{ad})r_f^2 \ln(t / r_f)}}$ ,  $E_{ad}$  and  $E_f$  are Young's moduli for the adhesive and the optical fibre, respectively.  $r_f$  is the radius of the optical fibre, and  $\nu_{ad}$  is the Poisson's ratio of the adhesive and is taken to be 0.4.

The parameters used in the calculation are as follows:  $E_f = 72$  GPa and  $r_f = 0.063$  mm for the Si-FBGs,  $E_f = 2.8$  GPa and  $r_f = 0.093$  mm for the POFs,  $E_{ad} = 1.5$  GPa for the epoxy adhesive,  $E_{ad} = 0.006$  GPa for the PVA adhesive. The bonded length of fibre is 40 mm for Si-FBG-3 and 50 mm for the other FBGs. It can be seen from Table 7-1 that the theory values have good agreement with actual values for the POFs, but for silica FBG, they have big difference, indicating the errors in the DIC system are the dominant cause. Although silica FBG with the DMC2 adhesive has a very low theoretical strain transfer coefficient, the actual experimental value indicates that the poor compatibility of the silica FBG with the

DMC2 PVA conservation adhesive. In contrast, the POFs have a much better compatibility with DMC2.

Table 7-1: Measured strain transfer and reinforcement ratio coefficients

FBG	Adhesive	Stress (MPa)	$\epsilon_{DICL}$ (%)	$\epsilon_{DICA}$ (%)	$\epsilon_{FBG}$ (%)	$R_1$	$R_1$ (theory)	$R_2$
POF-FBG-1	Araldite	0.79	0.151	1.303	0.140	0.93	0.99	0.12
POF-FBG-2	DMC2	0.39	0.332	0.783	0.298	0.90	0.85	0.42
Si-FBG-3	Araldite	0.79	0.108	1.303	0.058	0.53	0.97	0.08
Si-FBG-4	DMC2	0.79	0.06	1.303	0.104	1.7	0.66	0.05

In these tests the DIC measured strains for the areas with silica FBGs bonded are too small to be measured by the current DIC system. However the textile specimens have been tested with a silica FBG at a higher strain level [3] and  $R_1$  was obtained as ~23% and ~36% for DMC2 and Araldite, respectively, and still do not match the theoretical values.

The amount of reinforcement induced by bonding a fibre sensor can be quantified in terms of the ratio of strains  $R_2$ , when there is no reinforcement,  $R_2 = 1$ . The different reinforcement ratio  $R_2$  for the different adhesive/FBG combinations given in Table 7-1 can be explained in terms of the overall product of Young's modulus and cross section area of the bonded area. The overall product of  $E \cdot A$  is the sum of the products of the cured adhesive, optical fibre and the textile covered with adhesive, and can be written as follows:

$$E \cdot A = E_{ad} (w \cdot t - \pi \cdot r_f^2) + E_f \cdot \pi \cdot r_f^2 + E_t \cdot w \cdot t_i \quad (7.4)$$

where  $E_{ad}$ ,  $E_f$  and  $E_t$  are Young's moduli for the adhesive, optical fibre and textile respectively, respectively,  $r_f$  is the radius of the optical fibre,  $w$  and  $t$  is the width and length of cured adhesive, and  $t_i$  is the thickness of the textile.

Table 7-2: E·A values for different specimens.

Specimens	$E_{ad}$ (GPa)	$w$ (mm)	$t$ (mm)	$E \cdot A$ (GPa · mm <sup>2</sup> )
Si-FBG-Araldite	1.5	3.2	0.4	2.92
Si-FBG-DMC2	0.006	3.1	0.3	1.02
POF-FBG-Araldite	1.5	3	0.40	1.94
POF-FBG-DMC2	0.006	3	0.22	0.18
Textile only				0.11

The Young's modulus and thickness of the textile are  $E_t = 60$  MPa and  $t_i = 0.57$  mm. The measured  $E_{ad}$  values and the  $E \cdot A$  values for the three specimens are given in Table 7-2. The  $E \cdot A$  value for the specimen with Araldite is approximately 3 times greater than those with conservation adhesives, which is consistent with the difference in ratio  $R_2$ . This provides an adequate explanation for the reinforcement.

### **7.2.3 Long Term Tensile Test**

In the previous section, the strain condition of textile, applied with increasing load over a short period of time, was monitored by silica and POF FBG sensors. However, for tapestries, the common situation is that a constant stress is applied to the material at certain temperature and humidity conditions over a long period of time, due to their relatively large size and heavy weight. So the investigation of the long term strain condition monitoring of textile by using POF FBGs is necessary.

#### **7.2.3.1 Experiment Setup**

All of the tests in this section were carried out in environmental chamber (SANYO Gallenkamp plc) so that the environmental temperature and relative humidity during the tests can be controlled independently. To investigate the performance of POF FBG sensors bonded to the representative textile and their responses to environmental temperature and RH, a textile specimen with two POF FBGs bonded was prepared. To make sure the test could be conducted inside the chamber, a test rig was designed for placing into the chamber and applying load to the textile specimen, as shown in Figure 7-10. Both ends of the textile specimen were folded and secured to steel bars by stitching in place. One of the bars was clamped so that the textile specimen could hang freely and the other was loaded using deadweights via a weight hanger.

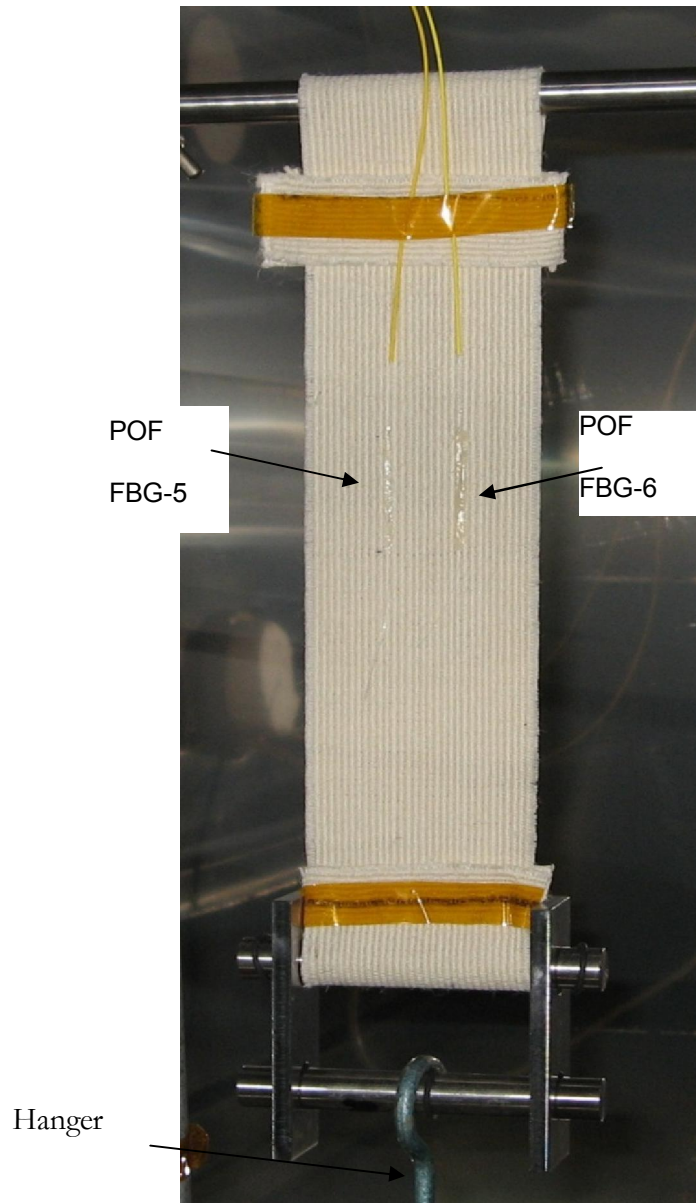


Figure 7- 10: The test rig inside the environmental chamber.

The textile is 50 mm wide, 0.57 mm thick and 275 mm long. Two POF FBGs (POF-FBG-5 and POF-FBG-6) were bonded parallel to the central part of the specimen, as shown in Figure 7-10. The Bragg wavelengths of the two FBGs were approximately 1564 nm. POF-FBG-5 was bonded to the textile surface with Araldite 2015, and POF-FBG-6 was with the conservation adhesive DMC2. For each FBG, the cured adhesive area was 3 mm wide and approximately 0.3 mm thick. The length of adhesive is around 34 mm, which is shorter than that of the

quasi static test, because the connection of the POF to the silica fibre was not covered with the adhesive, as shown in Figure 7-11. The advantage here is the magnitude of the strain applied to the textile is not limited by the weak connection. However, there is the danger of breaking the connection or the fragile section of silica fibre with the coating removed while installing the specimen.

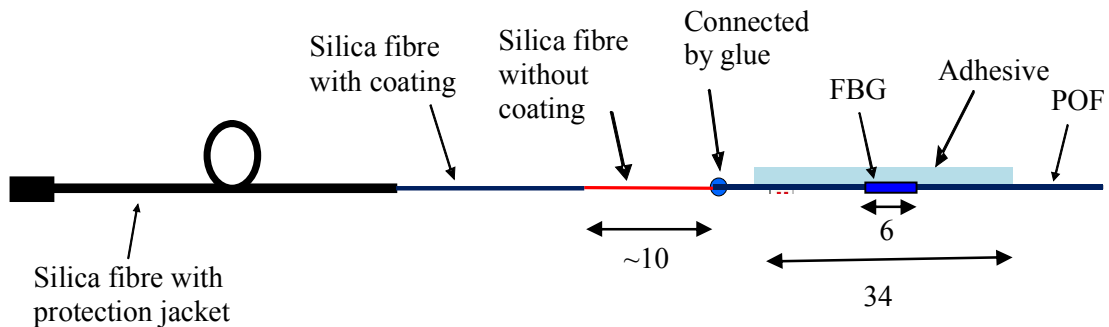


Figure 7- 11: Schematic of a POF FBG sensor bonded to textile. Unit: mm

To characterise the response of the adhesives to temperature and RH, two silica FBGs were also embedded in cured Araldite 2015 and DMC2, respectively. The Bragg wavelengths of the two FBGs were 1558 and 1546 nm, respectively. After pouring the adhesive (DMC2 or Araldite 2015) into a silicon mould, a FBG was embedded into the central part of the adhesive, then the adhesive was cured at room temperature. The cross section of the cured adhesive is schematically shown in Figure 7-12. The length of silica optical fibre containing the FBG embedded in the adhesive is 70 mm.

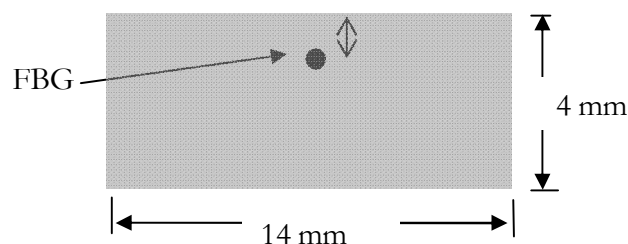


Figure 7- 12: Schematic of the cross section of the cured adhesive.

In all tests, although the chamber provides readings of the inside temperature and humidity itself, to enhance the accuracy of the experiment, the temperature and RH inside the chamber were recorded using a temperature/RH sensor (DLP-TH1) located nearby the specimens. Note that the values of temperature and RH given in this section are the readings of DLP-TH1 temperature/RH sensor, which are 1.1 °C, higher in temperature and 1.3% lower in RH than those from the chamber. For the tests on the textile, the reflection spectra of POF FBGs are monitored using an optical spectrum analyser with a resolution of 0.1 nm. For the tests with the two silica FBGs embedded in cured adhesives the Bragg wavelength changes are monitored by using a laser scanning FBG-interrogator (FBG-SLI, Micron Optics). For both specimen types the spectra data are recorded when the temperature and RH reached the set values and the thermal equilibrium had occurred inside the specimen.

### **7.2.3.2 Results and Discussion**

#### Calibration of the embedded sensors and adhesives

The textile specimen was lying flat inside the chamber. The two silica FBGs embedded in cured adhesives were also placed nearby the textile specimen. To begin with, RH was set constant at 48.7%. Responses of POF FBGs and silica FBGs were recorded while temperature varies from 23.1 to 41.3°C with an increment of 3°C. At each increment, 30 minutes was held to make sure the thermal equilibrium inside the adhesive. The recorded Bragg wavelengths of POF FBGs plotted against temperature are shown in Figure 7-13. In the figure, the black line is the linear fit of the measured data for POF FBG-6 with DMC2, while the blue line is 3rd order polynomial fit of the measured data for POF FBG-5 with

Araldite. For POF FBG-6 with DMC2, there is a relatively good linear dependence of the wavelength on temperature, indicating the temperature sensitivity of  $-48 \pm 0.8 \text{ pm}/^\circ\text{C}$ . Thus, the temperature sensitivity of the POF FBG bonded to textile is close to that of the bare POF FBGs mentioned in Chapter 5. For POF FBG-5 with Araldite, the wavelength initially increased with temperature raise, and then decreased with increasing temperature, indicating that the bonding of a POF FBG to textile with Araldite has complex effects on the thermal responses of the FBG. The sign of the thermal sensitivity of a POF FBG depend on competition between the thermo-optic effect (negative) and thermal expansion (positive). In bare POF, the thermo-optic effect is the dominant effect; while for embedded fibre, embedding could have increased the expansion coefficient, which could result in a small, possibly positive wavelength shift. When the temperature increased further, the adhesive became softer, leading to the bond between the POF and adhesive becoming weaker. As a result, the thermo-optic effect became dominant so that the wavelength decreased with increasing temperature.

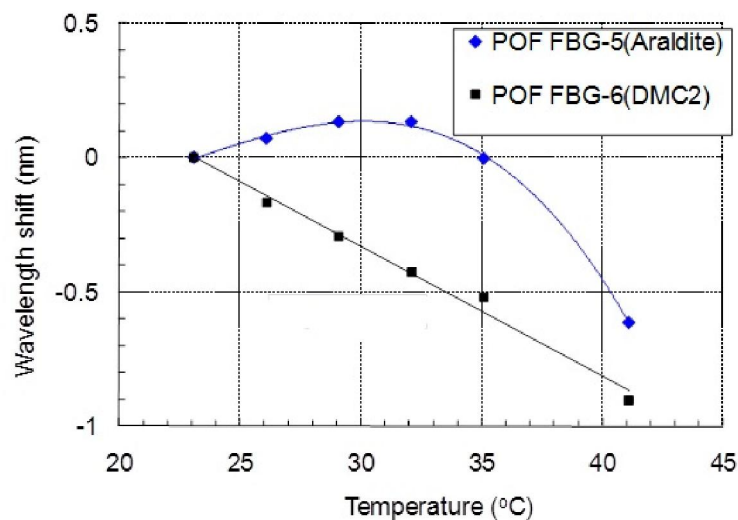


Figure 7- 13: The shifts of Bragg wavelengths of POF FBGs are plotted against temperature for RH = 48.7%.

The humidity response of the embedded sensor was also investigated. The temperature was set to 26.1°C, and RH varied from 43.7% to 68.7% with an increment of 5%. At each increment, the humidity was held 40 minutes to insure the humidity equilibrium inside the adhesive. During this process, the Bragg wavelengths shift of POF FBGs were recorded and plotted versus RH, as shown in Figure 7-14. Both of the lines in the figure are the trendlines of linear fit of the measured data. For both POF FBGs, the wavelength increased linearly with increasing RH. For POF-FBG-5 with Araldite, the humidity coefficient is  $40\pm 0.9\text{pm}/\%RH$ , which is almost the same as the measured value for the bare POF FBGs in Chapter 6. For POF FBG-6 with DMC2, the humidity coefficient is  $52\pm 0.3\text{ pm}/\%RH$ , slightly higher than that with Araldite.

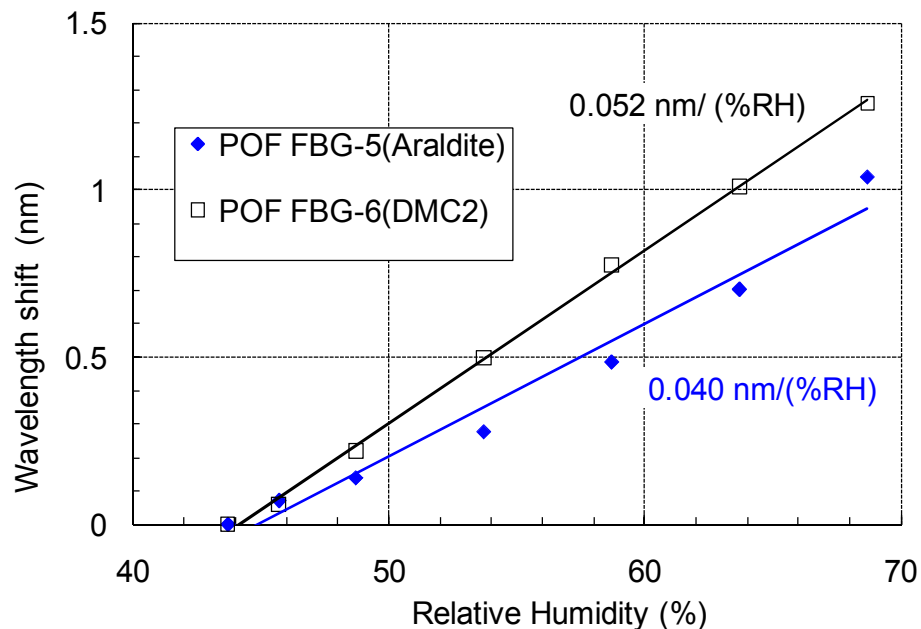


Figure 7- 14: Shifts of Bragg wavelengths of POF FBGs are plotted against RH for temperature = 26.1 °C.

The two tests of silica FBGs were conducted at the same time with the same temperature and RH as for the textile specimen with POF FBGs when all the

specimens were in the chamber. When the RH was constant at 48.7%, the wavelength shifts of silica FBGs were recorded and plotted against temperature, as shown in Figure 7-15. The lines are the trendlines of linear fit of the measured data. For both silica FBGs, there is a linear dependency of wavelength shift on temperature. The thermal sensitivity is  $9.2 \pm 0.1 \text{ pm}/^\circ\text{C}$  for the FBG in DMC2 and for the FBG in Araldite, it is  $116.8 \pm 0.1 \text{ pm}/^\circ\text{C}$ , which is 9 times greater than that of a free FBG in a standard silica optical fibre. The linear coefficient of thermal expansion (CTE) of Araldite can be estimated by using the measured data. The change in Bragg wavelength of a FBG due the changes of temperature and strain can be written as [11]

$$\frac{\Delta\lambda}{\lambda} = (1 - \rho_e) \frac{\Delta L}{L} + (\alpha + \xi) \cdot \Delta T \quad (6.5)$$

where  $\rho_e$  is the photo-elastic constant of the optical fibre,  $\alpha$  is the linear CTE,  $\xi$  is the thermo-optic coefficient and  $\Delta L/L$  is the relative change in grating length. For standard silica fibres at a wavelength of 1550 nm,  $\rho_e = 0.22$ ,  $\alpha + \xi = 8.39 \times 10^{-6}/^\circ\text{C}$ . Assuming the relative grating length change  $\Delta L/L$  is equal to the relative length change of cured Araldite when temperature increased, the CTE of Araldite can be calculated by

$$\alpha_{Araldite} = \frac{\Delta L}{L \cdot \Delta T} = \frac{1}{0.78} \left( \frac{\Delta\lambda}{\lambda \cdot \Delta T} - 8.39 \times 10^{-6} \right) = 85.6 \times 10^{-6} /^\circ\text{C}$$

This is around three times greater than that of epoxy ( $21\text{-}30 \times 10^{-6}/^\circ\text{C}$  [12]). Although the CTE of PVA based adhesives is around one order of magnitude greater than that of epoxy [13, 14], the response of the FBG embedded in DMC2 is not sensitive to the change in temperature, indicating that the strain transfer

from DMC2 to the silica fibre is small. Furthermore, the thermal sensitivity of the FBG in DMC2 which is conducted from the thermal test results of silica FBGs shown in Figure 7-15 is smaller than the published value of a free silica FBG ( $0.013\text{nm}/^\circ\text{C}$ ) [11]. We suspect due to the insufficient waiting time at each increment, the thermal equilibrium inside the adhesive specimens was not fully achieved.

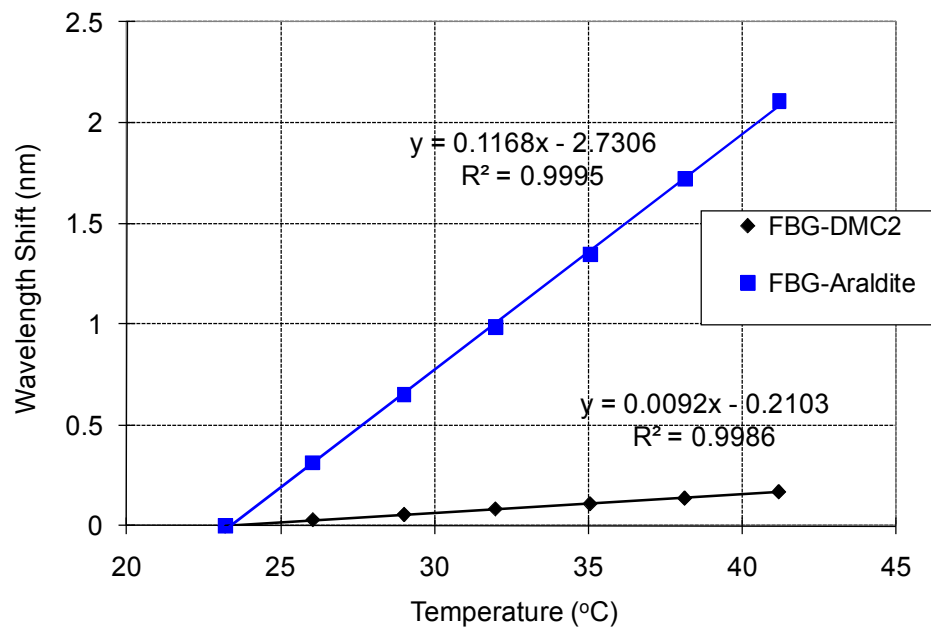


Figure 7- 15: The wavelength shifts are plotted against temperature for RH=48.7%.

The wavelength shifts of the FBGs plotted against RH for a constant temperature of  $26.1^\circ\text{C}$  are given in Figure 7-16. The lines are the trendlines of linear fit of the measured data. The responses of the FBGs to RH are small in both cases. As it is well known that the single FBG in a standard silica fibre is not sensitive to RH, the test data here show that the humidity response of Araldite is small. The sensitivity of DMC2 to RH could not be discussed since the strain transfer from DMC2 to the silica optical fibre is small.

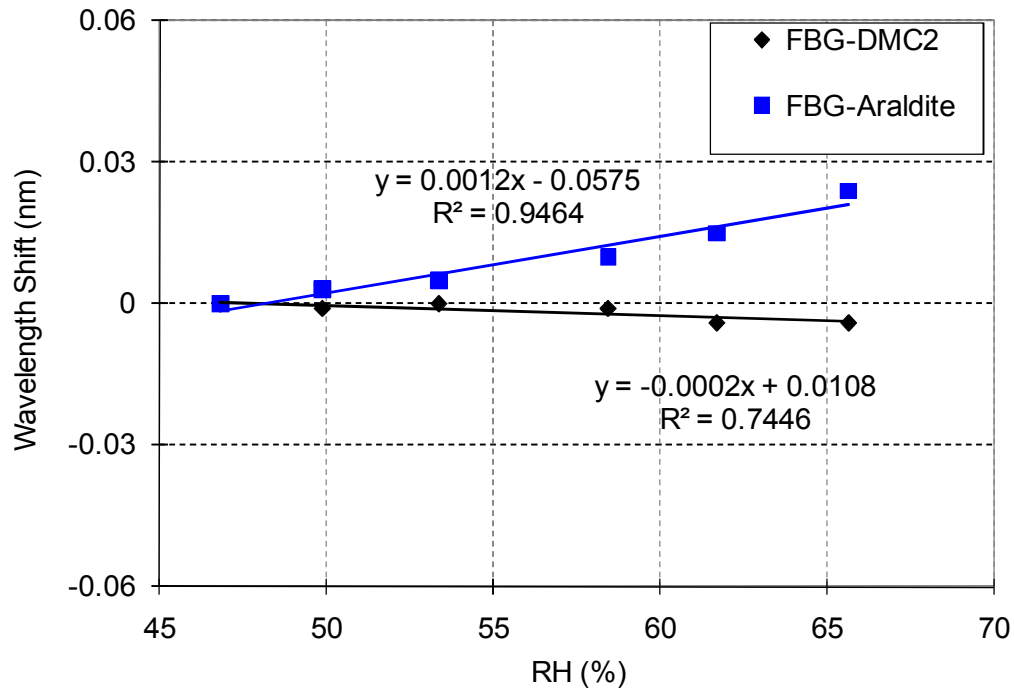


Figure 7- 16: The wavelength shifts vs. RH for temperature=26.1 °C.

### The long term tensile tests of textile specimen

To understand the long term strain behaviour of the textile specimen with bonded POF FBGS, the specimen was loaded using deadweight at a constant RH and temperature for more than 20 hours.

Firstly, The RH and temperature were set to be constant at 48.7% and 26.1°C. The recorded Bragg wavelengths of POF FBGs during the long term test are given in Figure 7-17. The applied load was 14 and 24N respectively. The problem is that in figure, the initial wavelengths of POF FBG-2 were almost the same for the two tests with different loads of 14 and 24N. It is likely that the problem was raised by the tape used to fix the fibre tail to protect the connection between silica optical fibre and POF (the top yellow tape, as shown in Figure 7-10). There should be extra length of fibre between the tape and the adhesive bonding section. However, in this case, this section of fibre was partially with protection tube, and

the fibre tail close to the adhesive may not be completely free. Therefore, when the textile was loaded with 14N, the strain applied to the grating could be affected by the extra force from the external fibre tail. After the test with 14N load, the tape was removed before the load was increased to 24N.

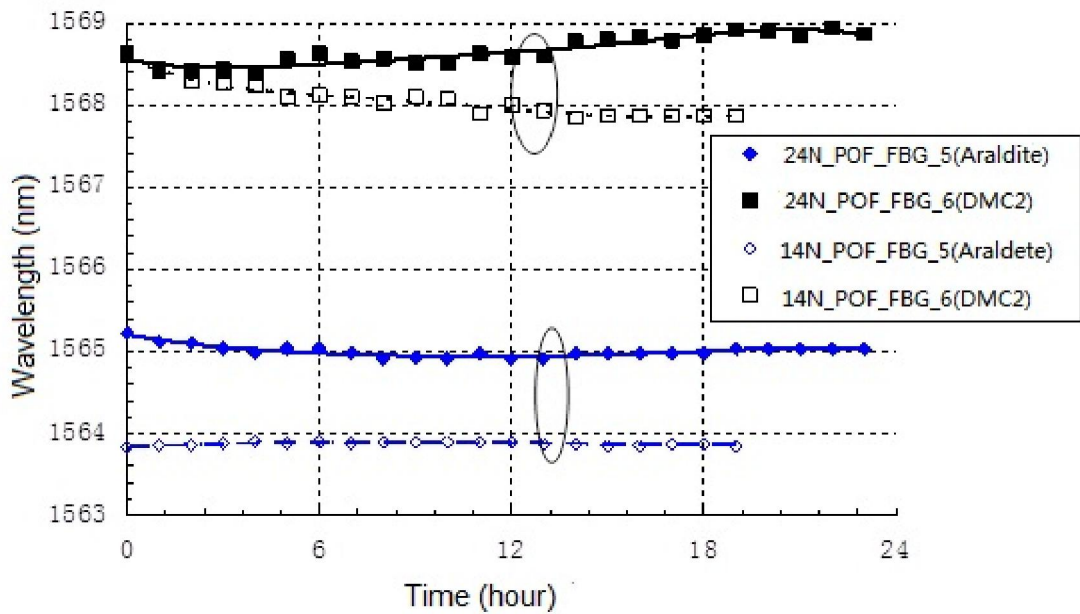


Figure 7- 17: The recorded Bragg wavelengths of POE FBGs during the long term test at intervals of 1 hour, for a constant RH of 48.7% and temperature 26.1 °C. The applied load was 14 and 24N respectively.

When the constant RH was increased to 58.7%, the same tests were repeated and results are given in Figure 7-18. The lines in these figures are the trendlines of polynomial fit of the measured data. .

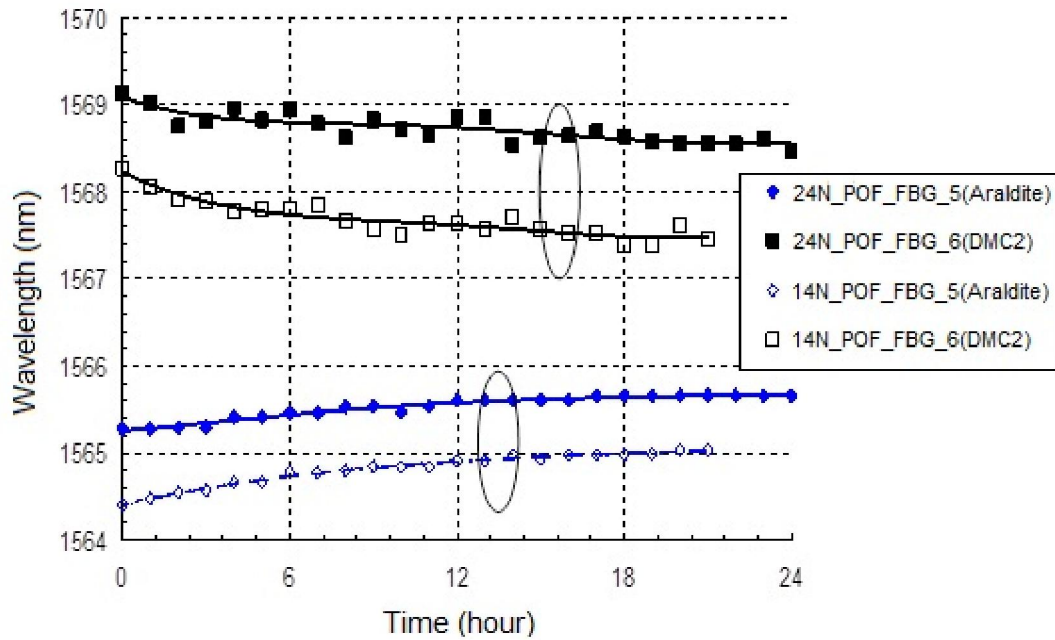


Figure 7- 18: The recorded Bragg wavelengths of POF FBGs during the long term test at intervals of 1 hour, for a constant RH of 58.7% and temperature 26.1 °C. The applied load was 14 and 24N respectively.

Both of the tests with different levels of load show that the conservation adhesive DMC2 is not strong enough to bond fibre sensors on textiles for long term strain monitoring, as the long term strain behaviours of the textile which is monitored by the DMC2 bonded fibre sensor is totally different with that of measured in tapestries by D. Khennouf etc. using digital image correlation technique [15], though in their experiment the temperature and humidity is not controlled, as shown in Figure 7-19. In contrast, the two-part epoxy adhesive can offer stable strain transfer between the textile and fibre, thus the obtained nonlinear long term strain behaviour of the textile has good agreement with the result in Figure 7-19.

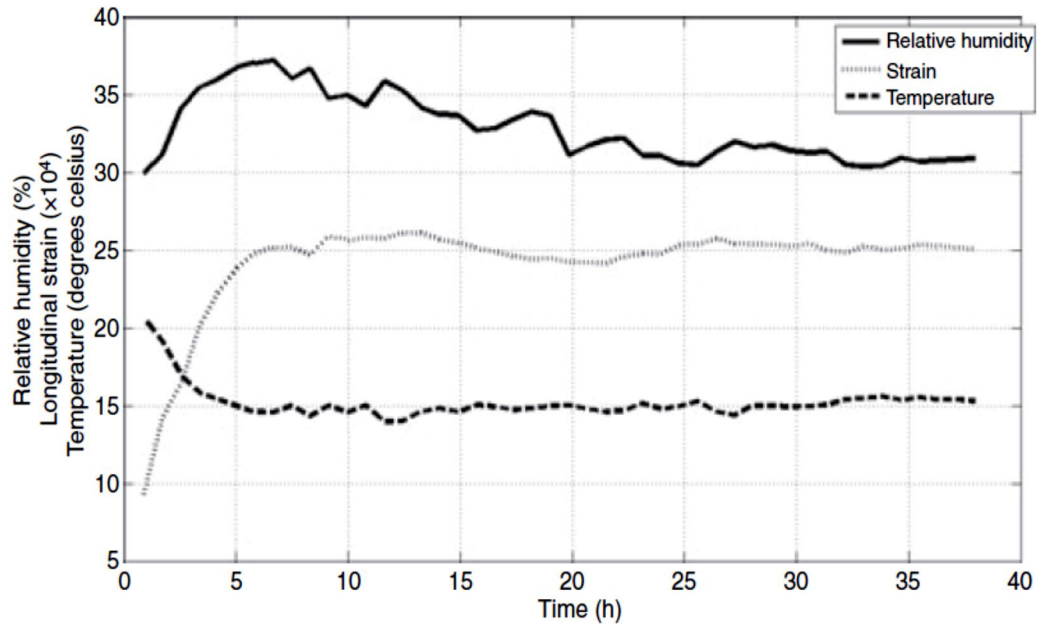


Figure 7- 19: The obtained Long term strain behaviour of the textile by using digital image correlation technique. [15]

### The long term tensile test of single POF FBG Sensor

One bare POF FBG was tested with a load of 0.6N. The load was applied to the POF using two silica fibres bonded to each end of the POF. One of the silica fibres was fixed to a bar and another was attached to a small deadweight. It failed in 2 minutes when the load had been applied. No further long term tensile tests of a single POF FBG have been conducted.

## 7.3 Conclusion

FBG devices have been considered as a potential solution of strain condition monitoring of ancient textiles. Both POF-based and silica-based FBGs have been bonded to a woven textile specimen with two part epoxy Araldite and PVA based conservation adhesive DMC2 and used to measure strain in the specimen. In

quasi-static test, it has been demonstrated that the POFs provide a favourable strain transfer coefficient and that the POFs bonded with PVA adhesive offer less structural reinforcement. The performance of POF-based and Silica-based FBGs in strain measurement is concluded in Table 7-3.

Table 7-3: Performance of FBGs in strain measurement.

FBG Device	POF-based-1	POF-based-2	Silica-based-1	Silica-based-2
Adhesive Type	Araldite	DMC2	Araldite	DMC2
Strain Transfer	Good	Good	Poor	Poor
Structural Reinforcement	High	Low	High	High

Before the long term tensile test of the textile specimen, the temperature and humidity responses of the embedded POF FBG are investigated, as illustrated in Table 7-4 and also the response of adhesives to the temperature and humidity is studied.

Table 7-4: Temperature and humidity responses of the embedded POF FBG.

FBG Device	POF-based-1	POF-based-2
Adhesive Type	Araldite	DMC2
Humidity Sensitivity (pm/ %RH)	40 ±0.9	52±0.3
Temperature Sensitivity (pm/°C)	Not available	-48±0.8

The long term tests are carried out with constant RH and temperature and with two different levels of load (14N and 24N) applied. The test results show that the two-part epoxy adhesive can offer much better and more stable strain transfer between the textile and polymer fibre than PVA adhesive.

To sum up, from the quasi-static and the long term test, we observe a conflict result: POFBGs bond with PVA adhesive have less structural reinforcement, while POFBGs bond with epoxy adhesive have better strain transfer. To solve this problem, further work should be conducted to find more suitable glue which can offer little structural reinforcement together with good strain transfer and perform the same tests as described in this chapter.

## References

- [1] Dulieu-Barton J.M., Sahin M., Lennard F.J., Eastop D.E. and Chambers A.R. "Assessing the feasibility of monitoring the condition of historic tapestries using engineering techniques", *Key Engineering Materials*, 347, 187-192 (2007).
- [2] Dulieu-Barton J.M., Ye C.C., Chambers A.R., Lennard F.J. and Eastop, D.E., "Optical fibre sensors for monitoring damage in historic tapestries", SEM XI International Congress on Experimental and Applied Mechanics, 2008, Orlando, Florida.
- [3] Ye C.C., Dulieu-Barton J.M., Chambers A.R., Lennard F.J., Eastop D. D., "Condition monitoring of textiles using optical techniques", DAMAS, 2009, Beijing, China.
- [4] Silva-Lopez M., Fender A., MacPherson W. N., Barton J. S., Jones J. D. C., Zhao, D., Dobb H., Webb D. J., Zhang L., Bennion, I., "Strain and temperature sensitivity of a single-mode polymer optical fiber", *Optics Letters*, 30, 3129-3131 (2005).
- [5] Chu T.C., Rason W.F., Sutton M.A. and Peters W.H., "Applications of digital image correlation techniques to experimental mechanics", *Experimental Mechanics*, 25, 232-244(1985).
- [6] LaVision DIC Product-Manual, StrainMaster 3D - Getting Started.
- [7] Vogel, J. and Lee, D. "An automated two-view method for determining strain distributions on deformed surfaces", *Materials Shaping Technology* 6, 205–216, (1989).
- [8] Yang DX, Yu J, Tao X, Tam H, Structural and mechanical properties of polymeric optical fiber, *Materials Science and Engineering*, A364, 256–259, (2004).
- [9] Liu HY, Liu HB, Peng GD, Tensile strain characterization of polymer optical fibre Bragg gratings, *Optics Communications* 251, 37-43 (2005).
- [10] Li D., Li H., Ren L., Song G. "Strain transferring analysis of fiber Bragg grating sensors", *Optical Engineering*, 45(2) 024402-1-8, (2006).

[11] M Majumder, "Fibre Bragg gratings in structural health monitoring—Present status and applications, *Sensors and Actuators A: Physical*, 147, 150–164 (2008).

[12] [www.matweb.com](http://www.matweb.com)

[13] Roland, C. M. and R. Casalini, "Temperature and Volume Effects on Local Segmental Relaxation in Poly(vinyl acetate)," *Macromolecules*, 36, 1361-1367, (2003).

[14] A. Nocke, M. Wolf, H. Budzier, K. Arndt and G. Gerlach, "Dielectrophoretic alignment of polymer compounds for thermal sensing," *Sensors and Actuators A: Physical*, 156, 164-170, 11 (2009).

[15] D. Khenouf, J. Dulieu-Barton, A. R. Chambers, F. J. Lennard and D. D. Eastop, " Assessing the Feasibility of Monitoring Strain in Historical Tapestries Using Digital Image Correlation," *Strain*, 46,19-32 (2010),.

# 8

## **Application of Polymer Optical Fibre Bragg Grating Sensors in Detecting Water**

In this chapter, two applications based on the water sensitivity of POFBG are demonstrated. A polymer optical fibre Bragg grating device is proved to be able to detect realistic levels of dispersed water in jet fuel; a compact silica and polymer FBG based sensor element shows well-conditioned response to humidity and temperature.

### 8.1 Detecting water in Jet Fuel

#### 8.1.1 Background Introduction

Water is a common impurity of jet fuel, and can exist in three forms: dissolved in the fuel, as a suspension and as a distinct layer at the bottom of the fuel tank. Water cannot practically be eliminated from fuel but must be kept to a minimum as large quantities can cause engine problems, particularly when frozen, as appears to have happened to the British Airways Boeing 777 that crashed at London Heathrow Airport, UK on 17 January 2008 [1] and the interface between water and fuel acts as a breeding ground for biological contaminants. The quantities of dissolved or suspended water are quite small, ranging from about 10 ppm to 150 ppm. This makes the measurement task difficult and there is currently a lack of a convenient, electrically passive system for water-in-fuel monitoring; instead the airlines rely on colorimetric spot tests or simply draining liquid from the bottom of fuel tanks. For all these reason, people have explored different ways to detect water in fuel [2, 3, 4], however all these approaches have problems, e.g. they may not be electrically passive or they may be sensitive to the refractive index of the fuel. Without the listed problems, POFBG is considered to be a well suitable sensing element to detect water in fuel, as POFBG was already proved to be sensitive to water in chapter 6 and also its promising humidity sensitivity was already calibrated. Therefore, an approach involving the use of a polymer optical fibre Bragg grating to detect small quantities of water in fuel was conducted.

### 8.1.2 Experiment Setup and Fuel Sample Preparation

The POFBG at the Bragg wavelength of 1565nm used in this experiment was inscribed in a 200 micron diameter single mode step index fibre with the same fabrication technique, as introduced in Chapter 5. A 7cm long POF containing the grating was then glued to a single mode silica optical fibre pigtail to form a device, as described in Chapter 6, which allowed us easily to monitor the Bragg wavelength change in reflection with broadband ASE light source and OSA.

Three fuel samples were prepared for the experiments. Dry jet fuel was prepared by taking 3.5g of molecular sieve 3A in a sample vial, which then had 10ml jet fuel added to it. The sample was then left for 24 hours for the sieve to remove the water. Wet fuel was prepared from a stock of dry fuel. 9.5ml of dry jet fuel was put into a sample vial and 0.5ml distilled water added (5% by volume). This sample vial was then shaken for 10minutes prior to running experiments to ensure that the water is mixed in with the fuel. Finally, a third fuel sample was obtained by taking fuel that had been exposed to ambient humidity for several days. For the proof of principal experiment, initially we had no means at hand to measure the dispersed water content of the three samples.

## 8. Application of Polymer Optical Fibre Bragg Grating Sensors in Detecting Water

### 8.1.3 Proof of Principal Experiment

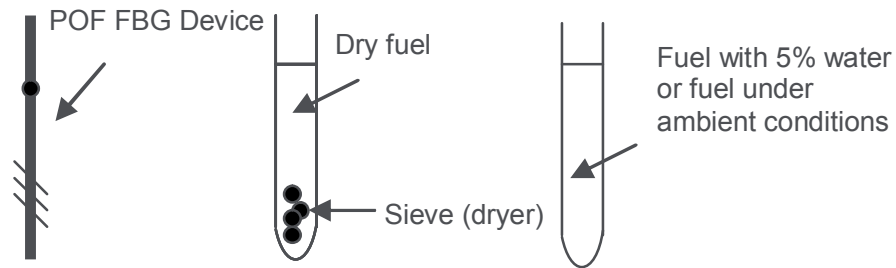


Figure 8- 1: Sketch of the experiment setup.

The sensor was put into one dry fuel tube for an hour to make sure that the device achieved equilibrium. Then the device was put into wet fuel for 40 minutes to allow the maximum water absorption and red wavelength shift to be observed. After that, the device was taken out and put into dry fuel again and the Bragg wavelength was observed to shift back to approximately the original place. This procedure was repeated three times to confirm the repeatability of the results. The nonlinear Bragg wavelength shift (around 1.4nm) trend of the whole experiment is shown in Figure 8-2.

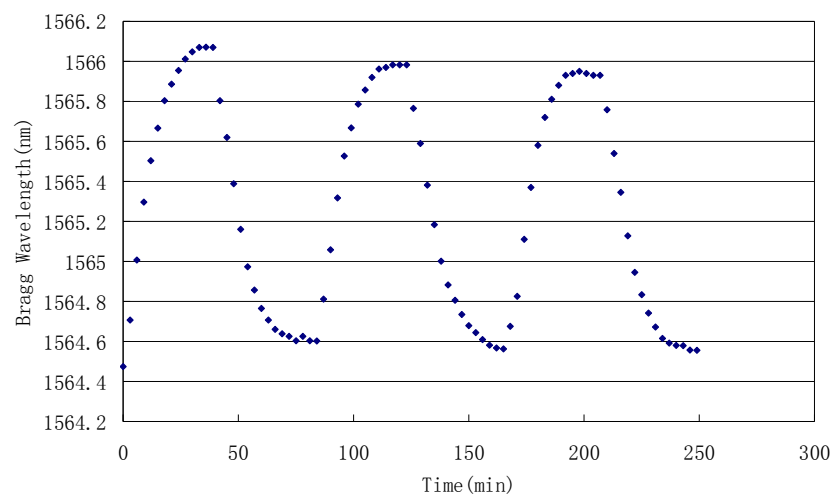


Figure 8- 2: Bragg wavelength shift when the sensor was swapped between wet and dry fuel at room temperature.

## 8. Application of Polymer Optical Fibre Bragg Grating Sensors in Detecting Water

As 5% water is quite a lot, a second experiment was carried out in a similar way but with the sensor being swapped between three fuel samples in the following order: dry, ambient, wet, ambient dry. The Bragg wavelength shift trend of this experiment is shown in Figure 8-3.

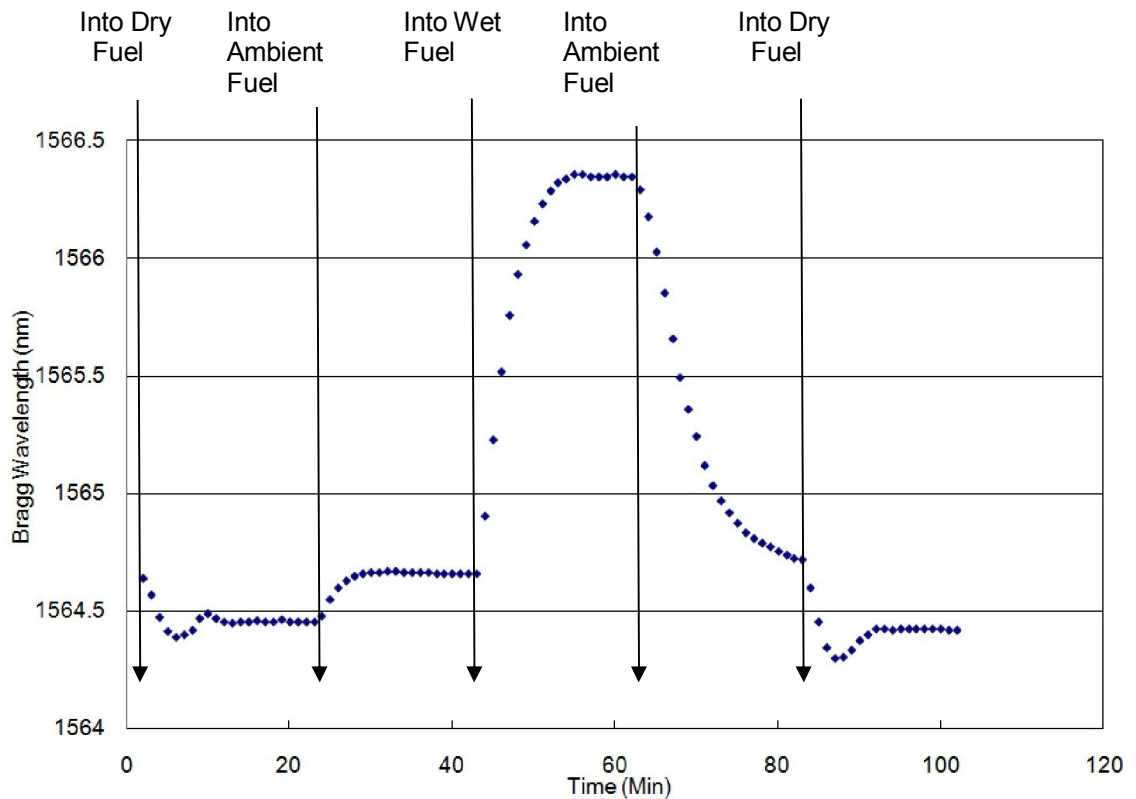


Figure 8- 3: Bragg wavelength shift when the test was swapped between dry fuel, ambient fuel and wet fuel at room temperature.

In addition, with help from the Gooch & Housego Plc, the water content of the fuel can be precisely measured and the sensor is tested in several different fuel samples, containing water from 17-148 ppm. It is again proved that the repeatability of the sensor is quite good and it can easily measure water content to less than 20 ppm, as shown in Figure 8-4.

## 8. Application of Polymer Optical Fibre Bragg Grating Sensors in Detecting Water

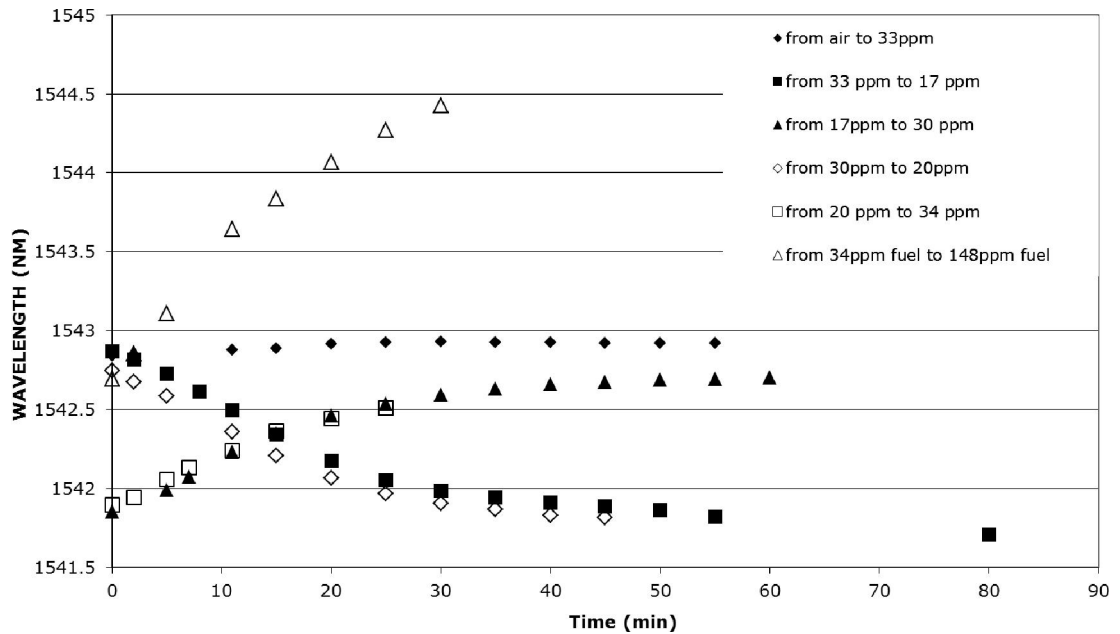


Figure 8- 4: Bragg wavelength shift when the test was swapped between dry fuel, ambient fuel and wet fuel at room temperature.

### 8.1.4 Discussion

The difference between dry and wet fuel is easily distinguishable in both experiments and even the change from dry to ambient samples is readily detected. In that regard the proof-of-concept experiments look to be very encouraging. There are however two points that need to be discussed. The first is the small but measurable differences observed in the Bragg wavelengths when the sensor returns to the same type of fuel. These differences show as a gradual decrease in the upper and lower Bragg wavelengths in Figure 8-2 and a lack of precise match in the initial and final dry fuel readings in Figure 8-3. These differences might actually be due to temperature changes of 1 or 2°C within the laboratory, which were not controlled for. The second issue is that the response time of tens of minutes limits the real-time applicability of the technology. The diameter of the

## 8. Application of Polymer Optical Fibre Bragg Grating Sensors in Detecting Water

fibre used was quite large, comparing with that of commercial single mode silica optical fibre (125nm), which will clearly have an adverse effect on the time taken for the water to diffuse into the core region, as already demonstrated in Chapter 5. Using the fibre with smaller diameter possibly coupled with lapping or etching the grating region of the fibre, might reduce the response time to a few minutes, which would open up the range of applications accessible.

## **8.2 Simultaneous Temperature and Humidity Sensor**

### **8.2.1 Introduction**

When POFBGs are applied to humidity or water-in-fuel sensing, an important issue is the cross-sensitivity to temperature, which affects the accuracy of the sensor. A dual parameter sensor was design to measure both temperature and humidity, comprising FBGs inscribed in both silica and polymer fibre which provides a well conditioned response to the two parameters.

### **8.2.2 Experiment and Result**

The dual parameter sensor was fabricated by attaching a 10cm length of 200 micron diameter single mode step index POF to single mode silica optical fibre down-lead using UV curable optical glue (Norland 76), as shown in Figure 8-5. The PMMA based POF contained a 5 mm long FBG. The initial Bragg wavelength of 1565 nm was reduced to 1542 nm by annealing the fibre. A second FBG had been inscribed 4 cm from the end of the silica fibre with 244 nm UV light from a

## 8. Application of Polymer Optical Fibre Bragg Grating Sensors in Detecting Water

frequency doubled CW Argon Ion laser, using the standard phase mask approach.

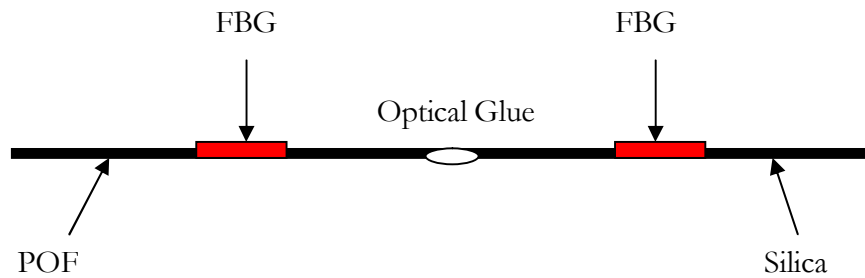


Figure 8- 5: Diagram of temperature and humidity sensor.

Due to the high attenuation of POF at the wavelengths used (around 1dB/cm), the silica FBG was fabricated with a reflectivity of about 4%, which allowed similar levels of signals to be obtained from the two gratings when they were illuminated with light from a broadband light source and observed in reflection using an IBSEN I-MON 400 wavelength interrogation system, see Figure 8-6.

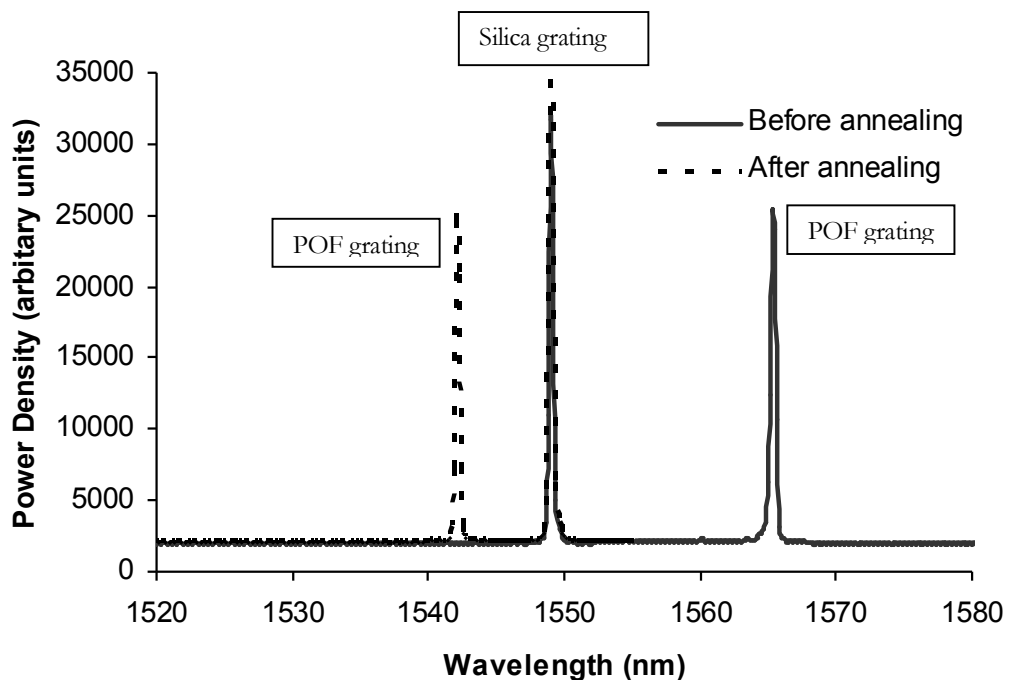


Figure 8- 6: Spectra returned from sensing gratings. In each case the POF FBG is at the longer wavelength.

## 8. Application of Polymer Optical Fibre Bragg Grating Sensors in Detecting Water

The sensor was placed inside an environmental chamber (Sanyo Gallenkamp) for characterisation. Previous research had shown that for this fibre, the diffusion time for water to reach the core was 30 minutes and so each reading was taken 30 minutes after the humidity was changed by 5%. Figure 8-7 shows the response at 25 °C of both sensors to humidity in the range 50-95%, where the environmental chamber had greatest stability. The humidity sensitivity of the POF appears to be linear over this range and linear regression (illustrated in the figure) returned a sensitivity of  $35.2 \pm 0.4$  pm/%. It may also be seen that the silica fibre showed some sensitivity to humidity, amounting to just  $0.28 \pm 0.01$  pm/%, probably as a result of the FBG being recoated with polymer following inscription.

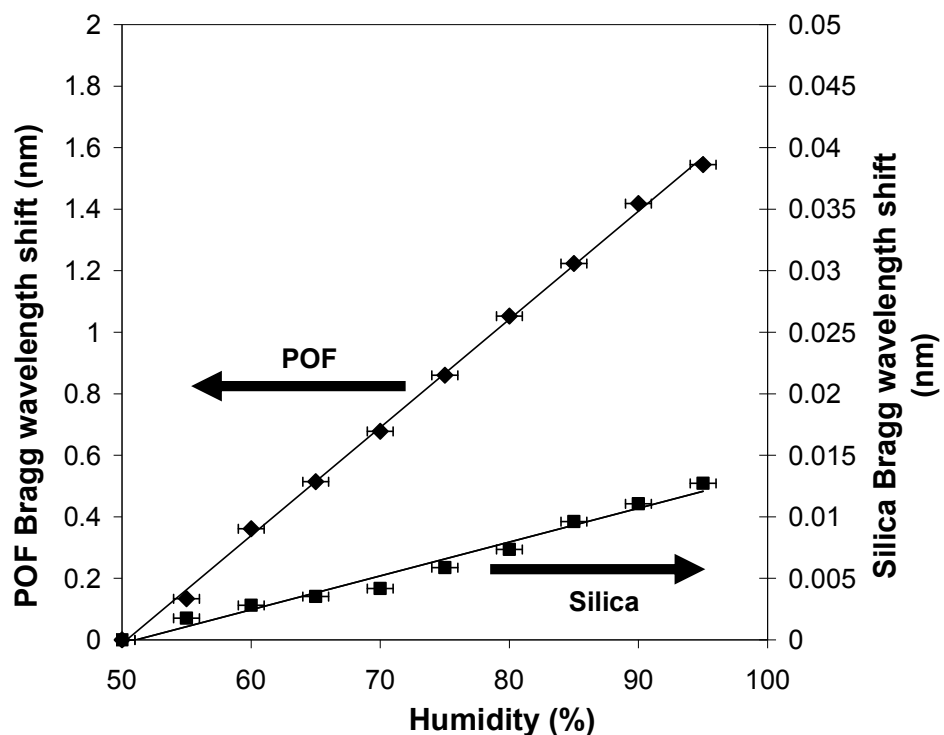


Figure 8- 7: Humidity response of the sensors. Note the very different scales on the ordinate axes.

The temperature response of the two sensors at a constant 50% humidity is shown in Figure 8-8. The sensitivities returned by linear regression are  $13.9 \pm 0.3$  pm/°C for the silica FBG and  $-55 \pm 3$  pm/°C for that in POF.

## 8. Application of Polymer Optical Fibre Bragg Grating Sensors in Detecting Water

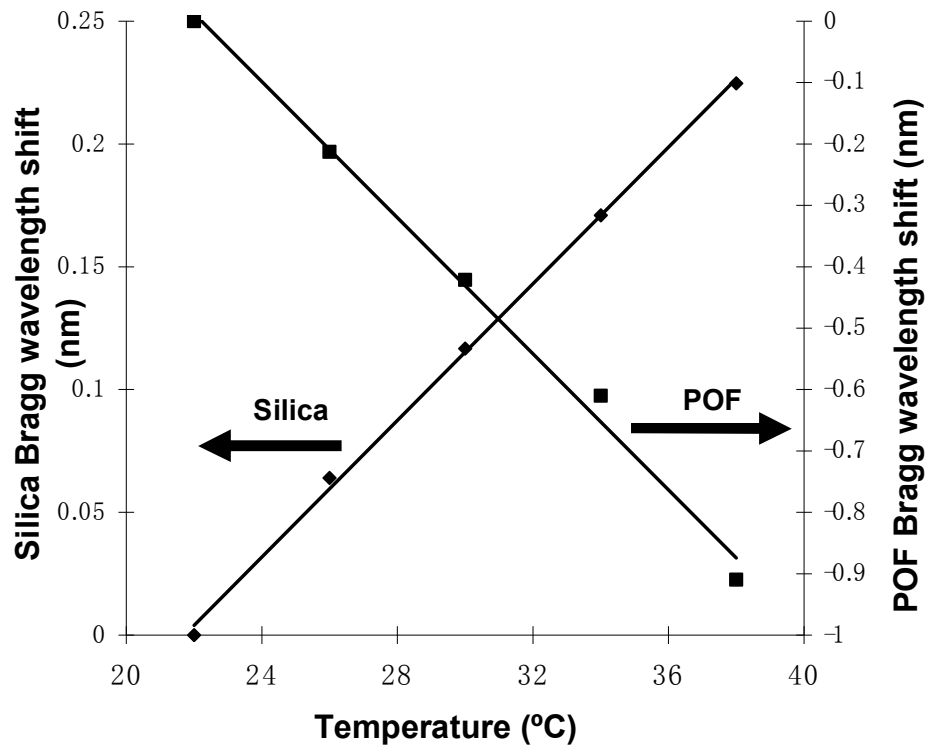


Figure 8- 8: Temperature response of the sensors.

### 8.2.3 Discussion

The parameters (Bragg wavelength shifts) vector  $\mathbf{L}$ , that can be measured are usually assumed to depend on the measurands (humidity and temperature) vector  $\mathbf{X}$  through a linear transform in matrix format as:

$$\mathbf{L} = \mathbf{KX} \quad (8.1) [5]$$

where  $\mathbf{L} = \begin{bmatrix} L_{POF} \\ L_{Silica} \end{bmatrix}$  is a two element column vector of the wavelength shifts

measured from the POF and silica gratings,  $\mathbf{X} = \begin{bmatrix} H \\ T \end{bmatrix}$  is a two element column

vector of the humidity (H) and temperature (T) variation experienced by the

## 8. Application of Polymer Optical Fibre Bragg Grating Sensors in Detecting Water

gratings and  $\mathbf{K} = \begin{bmatrix} 35.2 & -55 \\ 0.28 & 13.9 \end{bmatrix}$  is a 2x2 matrix containing both grating humidity

and temperature sensitivities measured earlier. Equation 8.1 can be inverted and humidity, temperature changes can be calculated as:

$$\mathbf{X} = \mathbf{K}^{-1}\mathbf{L} \quad (8.2)$$

where  $\mathbf{K}^{-1} = \begin{bmatrix} 0.0275 & 0.109 \\ -0.006 & 0.0697 \end{bmatrix}$  represents the inverse product of  $\mathbf{K}$ . Key to the

successful operation of the technique is the degree to which  $\mathbf{K}$  is well conditioned [5]. As may be anticipated from the matrix  $\mathbf{K}$  and  $\mathbf{K}^{-1}$ , this is a well conditioned problem with the condition number calculated from the 2-norm of  $\mathbf{K}$  being only 8.8. Such a low value for the condition number is reflected in the way in which errors in the measurements of the Bragg wavelength contribute to the uncertainty in the measurands. As an example, a very modest resolution of 10pm in the measurement of the Bragg wavelength of the silica grating would contribute an error of only 1.1% relative humidity or 0.7 °C.

### 8.3 Conclusion

The proofs of concept experiments are conducted to examine the ability of POF FBGs in detecting water in fuel. The POF FBGs show encouraging sensitivity to the fuel samples with different levels of water content, even the sample with water content of less than 20ppm. However, the response time of the device with 200 micron diameter usually takes 30-40 minutes, which is too long for practical applications. The response speed should be improved in further work, maybe by

## 8. Application of Polymer Optical Fibre Bragg Grating Sensors in Detecting Water

reducing the cladding thickness of the fibre for quicker water diffusion into the core region.

In this chapter, we have also characterised an optical fibre sensor system for humidity and temperature, as shown in Table 8-1, comprising two Bragg gratings recorded in silica and polymer fibre.

Table 8-1: Humidity and temperature sensitivity of POF FBG and Silica FBG.

FBG Device	POF	Silica
Humidity Sensitivity (pm / % RH)	35.2±0.4	0.28±0.01 pm/%
Temperature Sensitivity (pm/°C)	-55±3	13.9±0.3

The response of this system is very well conditioned (2-norm condition number = 8.8) and consequently uncertainties in wavelength measurement do not lead to large errors in the recovered humidity and temperature. Although the temperature measurement range of the system is limited by the working temperature of the optical glue, which is not as good as conventional electronic sensor (-40°C ~125°C) [6] and the temperature and humidity response time of the system is much slower than the electronic sensor (8s for humidity and 30s for temperature) [6], but the system do have better humidity measurement accuracy than that of electronic competitors (typically 2.0% relative humidity) [6] together with comparable good temperature accuracy.

## References

- [1] <http://news.bbc.co.uk/2/hi/8504734.stm>, A BBC webpage covering the official report of the British Airways plane crash at London Heathrow.
- [2] WJ Lewis, WATER DETECTION DEVICE FOR FUEL LINE, US Patent, 3,787,650 (1974).
- [3] Sean D. Pucketta and Gilbert E. Pacey, "Detection of water in jet fuel using layer-by-layer thin film coated long period grating sensor," *Talanta*, 78,1,300-304 (2009).
- [4] Kaida Khalid, Ionel Valeriu Grozescu, Lim Keng Tiong, Lee Teck Sim and Roslim Mohd, "Water detection in fuel tanks using the microwave reflection technique," *Meas. Sci. Technol.*,14,1905-1911 (2003).
- [5] Jin, W., Michie, W.C., Thursby,G., Konstantaki, M., and Culshaw,B. "Simultaneous measurement of strain and temperature: error analysis," *Opt. Eng.* 36, 598-609, (1997).
- [6] Siricon SHT1x series temperature and humidity sensor datasheet, available online at [http://www.sirion.com/en/pdf/product\\_information/Datasheet-humidity-sensor-SHT1x.pdf](http://www.sirion.com/en/pdf/product_information/Datasheet-humidity-sensor-SHT1x.pdf).

# 9

## Thesis Conclusion

This thesis has been concerned in investigating the potential application of polymer optical fibre Bragg grating in sensing areas. The background knowledge relating to fibre Bragg gratings, polymer optical fibres and polymer photosensitivity mechanisms is introduced respectively at the first few chapters of the thesis. The rest chapters are related to the original experimental works including polymer optical fibre Bragg grating fabrication, sensitivity characterisation and potential applications development. The outcomes and further works of these experimental works are concluded in following sub-topics.

### Bragg Grating Inscription in Polymer Optical Fibre

*Achievements:*

1. A Bragg grating inscription set-up based on 325nm CW UV laser and phase mask technique has been developed for fabricating Bragg gratings in polymer optical fibres
2. Bragg gratings are successfully written in different kinds of polymer optical fibres, including PMMA based single mode microstructured polymer optical fibre, TOPAS cyclic olefin copolymer based few moded microstructured polymer optical fibre and PMMA based photosensitive single mode step-index polymer optical fibre

*Further works:*

1. The fabricated PMMA based POF FBGs in this thesis are all working in the wavelength region where PMMA exhibits high attenuation and this significantly limits the length of the fibre used in grating fabrication, hence the application areas of the polymer optical fibre Bragg grating sensors, as in many sensing applications, especially in building sensing networks, long length of the fibre is required. The further improvement should be concentrated on writing POF FBGs in lower wavelength regions by using other phase masks and the ideal region could be the visible wavelength region, where PMMA fibres have much lower attenuation than in near infrared, though finding a suitable light source could be an issue. In addition, the improvement of the quality, especially the transparency of the polymer optical fibre could also be very helpful. Currently, the polymer optical fibres used in this thesis are all fabricated in the lab condition at low quality by different research groups and have attenuation as high as 0.8~1dB/cm.

## Polymer Optical Fibre Bragg Grating Sensitivity Characterisation

### *Achievements:*

1. Thermal sensitivity of pure PMMA based microstructured polymer optical fibre Bragg grating: To discover the thermal response of the fabricated Bragg gratings in microstructured polymer optical fibres, a special rig for heating the Bragg gratings was built. During thermal testing experiment, the PMMA mPOFBG was heated up to 91.5°C in three heating-cooling cycles and the Bragg wavelength of the grating shifts non-linearly to the lower wavelength region with increasing of temperature. Furthermore, in each cycle, a quasi-linear region always exists and the thermal sensitivity of the mPOFBG at this region is varying between -97pm/°C and -71.8pm/°C. When performing the thermal test of mPOFBG, the permanent operational wavelength shift of the grating is also observed, once the fibre is taken above a certain threshold temperature, which is able to be shifted to higher value by annealing the POF before grating inscription. The mechanism of the permanent change in the grating wavelength is proved to be caused by the change in grating period due to shrinkage of the fibre. In addition, the quasi-linear wavelength response to temperature is demonstrated to temperature up to 90°C by annealing the POF at 100°C after successive heating cycles that can be accounted for by fibre shrinkage.
2. Thermal sensitivity of TOPAS based microstructured polymer optical fibre Bragg grating: The largest Bragg wavelength shift with temperature in transmission to date is observed in TOPAS mPOFBG and the positive shift of

the Bragg wavelength with temperature increasing is different with the negative Bragg wavelength shift that was observed in PMMA mPOFBG. The measured temperature sensitivity is  $250 \pm 0.5 \text{ pm}/^\circ\text{C}$ , when the device is heated from ambient temperature to  $28.4^\circ\text{C}$ .

3. A stable gluing coupling method for connecting the single mode step-index POF and the single mode step-index silica optical fibre is successfully developed, which let the sensitivities of PMMA based step-index polymer optical fibre Bragg grating to be characterised inside an environmental chamber and supplies the mobility to the polymer optical fibre Bragg grating outside the optical bench.
4. Unlike silica fibre Bragg gratings, the PMMA based step-index polymer optical fibre Bragg grating appears to be sensitive to water. The linear humidity (45% - 85% RH) sensitivity response of step-index POFBG is obtained and the characterised humidity sensitivity is  $38.3 \pm 0.5 \text{ pm}$  per % RH. A linear Bragg wavelength response to the temperature ( $18^\circ\text{C}$ - $39^\circ\text{C}$ ) is observed in step-index POFBG which reveals a thermal sensitivity of  $-48.2 \pm 1 \text{ pm}/^\circ\text{C}$ . The step-index POFBG also shows a reversible and repeatable elastic response to up to 2% tensile strain for a strain rate of  $1 \text{ m}\epsilon/\text{min}$  and the strain sensitivity is  $1.33 \pm 0.04 \text{ pm}/\mu\epsilon$ , which is better than that of silica FBGs.

*Further works:*

1. The stable coupling for connecting microstructured polymer optical fibre Bragg grating and silica optical fibre need to be developed, so that the sensitivities other than to temperature can be characterised.

2. The connection between step-index POF and silica optical fibre needs to be further improved to extend the working temperature range. The solution could be looking for other optical adhesive with large working temperature range or trying to protect the connection point away from the temperature variation.
3. In order to expand the potential sensing applications of polymer optical fibre Bragg grating, we should measure some other sensitivity responses of polymer fibre Bragg gratings, i.e. bending and pressure.

### The Application of Polymer Optical Fibre Bragg Grating

#### *Achievements:*

Several attempts have been made for the investigation in the application of the step index polymer optical fibre Bragg grating:

1. The PMMA based step-index polymer optical fibre Bragg grating is proposed as a potential solution of strain condition monitoring of heavy ancient textiles. When both the POFBGs and the silica FBGs are bonded to a woven textile specimen with two part epoxy and PVA based conservation adhesive to measure strain in the specimen, the POFBGs can provide better strain transfer and offer less structural reinforcement than the silica counter parts in quasi-static test. To further verify the effects of the adhesives to the strain measurement, the long term strain test of the POFBGs bonded textile specimen is conducted in a constant RH and temperature environment and the results show that the adhesive is essential to strain measurement result:

POFBGs bond with PVA adhesive have less structural reinforcement, while POFBGs bond with epoxy adhesive offer better strain transfer.

2. The PMMA based step-index polymer optical fibres show the ability of detecting water in fuel. In proof of concept experiments, the POFBGs exhibit good sensitivity to the fuel samples with different levels of water content, even the sample with water content of less than 20ppm. The response time of 200 micron diameter POFBG is 30-40 minutes.
3. An optical fibre Bragg grating sensor system for measuring humidity and temperature simultaneously is built, by comprising two Bragg gratings respectively recorded in step-index single mode silica optical fibre and PMMA based step-index single mode polymer optical fibre. The response of this system is very well conditioned and consequently uncertainties in wavelength measurement do not lead to large errors in the recovered humidity and temperature. The sensor system has better humidity measurement accuracy (1.1%) than that of electronic competitors (2.0%) together with comparable good temperature accuracy, though the temperature measurement range is shorter and the response time is slower than the electronic sensor.

*Further works:*

1. For textile strain condition monitoring applications, further work should be conducted to the adhesive selection, which can offer little structural reinforcement and good strain transfer. The adhesives together with the POFBGs should perform the same test as described in Chapter 8.
2. For water detecting applications, the response time of the current POFBG device is too long for practical applications. The response speed should be

improved in further work, maybe by reducing the cladding thickness of the fibre either in chemical way (etching) or mechanical way (polishing) for quicker water diffusion into the core region.

3. The potential applications of polymer optical fibre Bragg gratings is far more beyond that has mentioned in this thesis, for example, embedding the polymer optical fibre Bragg grating into elastomers, like silicone rubbers to form a sensor system, could be used to measure the pressure together with the shear force applied to such a system, hence, may be applied into structure health monitoring applications.

Finally, polymer optical fibre Bragg gratings have shown great advantage and potential in sensing applications, though there is still a lot of work to be done in this challenging research area.

# Publication List

## Journal Papers:

- Karen E. Carroll, **Chi Zhang**, David J. Webb, Kyriacos Kalli, Alexander Argyros, and Maryanne C. Large, "Thermal response of Bragg gratings in PMMA microstructured optical fibers," *Optics Express*, Vol. 15, Issue 14, pp. 8844-8850, 2007.
- **C. Zhang**, W. Zhang, D.J. Webb, G.-D. Peng, "Optical fibre temperature and humidity sensor," *Electronic Letters*, 46(9), pp.643 – 644, 2010
- X. Chen, **C. Zhang**, D. J. Webb, K. Kalli, and G. D. Peng, "Highly sensitive bend sensor based on Bragg grating in eccentric core polymer fibre", *IEEE Photon. Technol. Lett.*, 22(11), pp.850 – 852, 2010.
- X. Chen, C. Zhang, D. J. Webb, G. D. Peng, and K. Kalli, "Bragg grating in polymer optical fibre for strain, bend and temperature sensing", *Meas. Sci. Technol.* 21 094005, 2010

## Conference Papers:

- K. Kalli, D. J. Webb, K. Carroll, **C. Zhang**, Alex Argyros, Maryanne Large, and Martijn van Eijkelenborg, "Non-linear temperature response of Bragg gratings in doped and un-doped holey polymer optical fibre," *Proc. SPIE 6588*, 65880E (2007)
- **C. Zhang**, D.J. Webb, G. Emiliyanov, O. Bang, E.M. Kjaer, K. Kalli, "Bragg grating inscription in TOPAS microstructured polymer optical fibre," *Proceedings of the 16th International Conference on Plastic Optical Fibers(2007)*
- David J. Webb, Kyriacos Kalli, Karen Carroll, **Chi Zhang**, Michalis Komodromos, Alex Argyros, Maryanne Large, Grigoriy Emiliyanov, Ole Bang, and Eric Kjaer, "Recent developments of Bragg gratings in PMMA and TOPAS polymer optical fibers," *Proc. SPIE Vol. 6830*, 683002 (Nov. 26, 2007) (invited paper)
- David J. Webb, Kyriacos Kalli, **Chi Zhang**, Michael Komodromos, Alexander Argyros, Maryanne C. Large, Grigoriy A. Emiliyanov, Ole Bang, and Erik Kjaer, "Temperature sensitivity of Bragg gratings in PMMA and TOPAS

microstructured polymer optical fibres,” Proc. SPIE Vol. 6990, 69900L (Apr. 21, 2008)

- **Chi Zhang**, Karen Carroll, David Webb, Aston Grigoriy A. Emiliyanov, Ole Bang, Erik M. Kjaer,, Kyriacos Kalli, Gangding Peng, “Recent progress in polymer optical fibre gratings,” (Oral presentation) Proc. SPIE 7004, 7004194 (2008)
- **C. Zhang**, X. Chen, D. J. Webb, and G.-D. Peng, “Water detection in jet fuel using a polymer optical fibre Bragg grating”, 20th International Conference on Optical Fibre Sensors (OFS-2009) (Post deadline), Edinburgh, United Kingdom, Proc. of SPIE Vol. 7503750380, Oct. 2009
- X. Chen, **C. Zhang**, D. J. Webb, R. Suo, G. D. Peng, and K. Kalli, “Optical bend sensor for vector curvature measurement based on Bragg grating in eccentric core polymer optical fibre”, 20th International Conference on Optical Fibre Sensors (OFS-2009), Edinburgh, United Kingdom, Proc. of SPIE Vol. 7503 750327, Oct. 2009
- C. C. Ye; J. M. Dulieu-Barton; D. J. Webb; **C. Zhang**; G.-D. Peng; A. R. Chambers; F. J. Lennard; D. D. Eastop, “Applications of polymer optical fibre grating sensors to condition monitoring of textiles”, Edinburgh, United Kingdom, Proc. of SPIE Vol. 7503 75030M, Oct. 2009
- X. Chen, **C. Zhang**, B. Van Hoe, D. J. Webb, K. Kalli, G. Van Steenberge, and G.-D. Peng, “Photonic Skin for pressure and strain sensing”, SPIE Photonics Europe 2010, SPIE Vol. 7726-3, Brussels, Belgium, 12 - 16 April 2010